รายงานวิจัยฉบับสมบูรณ์

โครงการ: (ภาษาไทย) การศึกษากลไกการดื้อยาปฏิชีวนะผ่านช่องพอรินของแบคทีเรียก่อโรคเมลิออยโดสีส *Burkholderia pseudomallei*

(English) A study of antibiotic-resistant mechanism through a porin channel of the melioidosis bacterium *Burkholderi pseudomallei*

โดย

รองศาตราจารย์ ดร. วิภา สุจินต์

สาขาวิชาชีวเคมี สำนักวิชาวิทยาศาสตร์
มหาวิทยาลัยเทคโนโลยีสุรนารี
จังหวัดนครราชสีมา

13 สิงหาคม พ.ศ. 2556

สัญญาเลขที่ RMU5380055

รายงานวิจัยฉบับสมบูรณ์

โครงการ: (ภาษาไทย) การศึกษากลไกการดื้อยาปฏิชีวนะผ่านช่องพอรินของแบคทีเรียก่อโรคเมลิออยโดสีส *Burkholderia pseudomallei*

(English) A study of antibiotic-resistant mechanism through a porin channel of the melioidosis bacterium *Burkholderi pseudomallei*

โดย

รองศาตราจารย์ ดร. วิภา สุจินต์

สาขาวิชาชีวเคมี สำนักวิชาวิทยาศาสตร์
มหาวิทยาลัยเทคโนโลยีสุรนารี
จังหวัดนครราชสีมา

สนับสนุนโดยสำนักงานกองทุนสนับสนุนการวิจัย และ
สำนักงานคณะกรรมการการอุดมศึกษา
(ความเห็นในรายงานนี้เป็นของผู้วิจัย สกว. ไม่จำเป็นต้องเห็นด้วยเสมอไป)

กิตติกรรมประกาศ

ขอขอบคุณสำนักงานกองทุนส่งเสริมงานวิจัยแห่งชาติ (สกว) และสำนักงานคณะกรรมการอุดมศึกษาแห่งชาติ (สกอ) ที่ได้สนับสนุนงบประมาณในงานวิจัยชิ้นนี้ตลอดระยะเวลา 3 ปี และขอขอบคุณ Professr Dr. Mathias Winterhalter, Biophysics Laboratory, School of Science and Engineering, Jacobs University Bremen, Dortmund, Germany ที่ให้ความร่วมมือในการใช้เครื่องมือ high-resolution electrophysiology setup เป็นอย่างดียิ่ง

สุดท้ายนี้ขอขอบคุณมหาวิทยาลัยเทคโนโลยีสุรนารีที่ให้ทุนสนับสนุนร่วมตลอดโครงการวิจัยและอุปกรณ์เครื่องมือในห้องปฏิบัติการชีวเคมี ทำให้งานวิจัยสำเร็จลุล่วงไปด้วยดี

รองศาสตราจารย์ ดร. วิภา สุจินต์
อาจารย์สาขาวิชาชีวเคมี สำนักวิทยาศาสตร์
มหาวิทยาลัยเทคโนโลยีสุรนารี

บทคัดย่อ

Burkholderia pseudomallei (Bps) เป็นแบคทีเรียชนิดแกรมลบที่ก่อโรคเมลิออยโดซีสซึ่งเป็นโรคติดเชื้อร้ายแรงในคนและสัตว์ พบอุบัติการณ์ของโรคสูงในแถบภาคเหนือและภาคตะวันออกเฉียงเหนือของประเทศไทย โอกาสการรักษาโรคให้ได้ผลสำเร็จทำได้ยากสาเหตุมาจากการดื้อต่อยาปฏิชีวนะเกือบทุกชนิดของเชื้อ Bps ได้มีการศึกษาพบว่าการดื้อยาของเชื้อ Bps อาจเกิดจากการที่เชื้อมีความสามารถในการต้านการนำเข้ายาปฏิชีวนะเนื่องจากมีช่องพอรินที่เยื่อเซลล์ด้านนอกที่มีคุณสมบัติในการนำเข้าของสารต่ำ ในงานวิจัยก่อนหน้านี้ ผู้วิจัยได้ทำการแยกโปรตีนขนาด 38 kDa จากเยื่อเซลล์ด้านนอกของ Bps โดยให้ชื่อโปรตีนนี้ว่า 'BpsOmp38' จากโครงสร้างทำนายและการศึกษาอัตราการนำเข้าโดยวิธี liposome-swelling assay พบว่าโปรตีน BpsOmp38 ประกอบด้วยโครงสร้างแบบ β-barrel ทำหน้าที่เป็นช่องพอรินแบบ 'general-diffusion porin' การศึกษาครั้งนี้ใช้เทคนิค planar black lipid membrane (BLM) reconstitution ในการแสดงคุณสมบัติการสร้างช่องเดี่ยวของ BpsOmp38 การวิเคราะห์แบบ high-time resolution BLM measurements แสดงให้เห็นว่าขณะที่โมเลกุลของยาปฏิชีวนะผ่านเข้าสู่ช่อง BpsOmp38 จะเกิดการลดระดับของกระแสการไหลของอิออนอันเนื่องมาจากการขัดขวางการผ่านของอิออนเข้าช่องโปรตีน โดยระดับของการขัดขวางการผ่านของอิออนขึ้นกับความเข้มข้นของสารปฏิชีวนะแต่ละชนิดที่ไม่เท่ากัน โดยค่า on-rate (k_{on}) ของการผ่านของยาเป็นไปตามลำดับดังนี้ norfloxacin >> ertapenem > ceftazidime > cefepime > imipenem > meropenem >> penicillin G ส่วน dwell time ของยาปฏิชีวนะที่เลือกนำมาศึกษาต่อคือ ertapenem มีค่าลดลงแบบชี้กำลังเมื่ออุณหภูมิขณะเกิดการส่งผ่านเพิ่มขึ้น การคำนวณจากกราฟ Arrhenius ให้ค่าพลังงานก่อกัมมันต์ของการเข้าจับของ ertapenem ที่ตำแหน่งจับมีค่าเป็น 12 kT ขณะที่ค่าพลังงานของการหลุดออกของยาจากตำแหน่งจับมีค่า 13 kT ที่ membrane potential ในการวัดเป็น +100 mV จากโครงสร้างทำนายพบว่ากรดอะมิโน Tyr-119 ที่อยู่ที่กลางของช่องพอรินน่าจะมีคุณสมบัติในการกำหนดขนาดและชนิดสารที่มีขั้วในการผ่านเข้าช่อง *Bps*Omp38 การทดสอบระดับการดื้อยาโดยเทคนิค antibiotic susceptibility assay พบว่า Omp-deficient *E. coli* ที่ผลิตพอรินกลายพันธุ์ BpsOmp38Y119A และ BpsOmp38Y119F มีความไวต่อยา meropenem และ ceftazidime มากกว่า แต่มีความไวต่อยา doripenem น้อยกว่าเชื้อ *E. coli* ที่ผลิตโปรตีน BpsOmp38 ดั้งเดิม การศึกษาเปรียบเทียบโดยเทคนิค liposome swelling assay พบว่าอัตราการแพร่ผ่านของน้ำตาลเข้าช่อง *Bps*Omp38 ดั้งเดิมและกลายพันธุ์มีความคล้ายกันคือมีอัตราลดลงเมื่อน้ำหนักโมเลกุลของน้ำตาลเพิ่มขึ้น แต่อัตราการผ่านของยาปฏิชีวนะไม่ขึ้นกับน้ำหนักโมเลกุลโดยตรง ผลการทดลองแสดงให้เห็นว่าการผ่านเข้าของยาปฏิชีวนะไม่ขึ้นกับขนาดของโมเลกุลเพียงอย่างเดียว แต่อันตรกิริยาระหว่างโมเลกุลของยาและกรดอะมิโนที่เป็นองค์ประกอบด้านในของช่องพอริน *Bps*Omp38 ก็มีความสำคัญอย่างมากต่อการผ่านเข้าของยาปฏิชีวนะด้วย

ABSTRACT

Burkholderia pseudomallei (Bps) is a Gram-negative bacterium that causes melioidosis, an infectious disease of animals and humans. This disease has high incidence in northern and north-eastern parts of Thailand. Successful treatment of melioidosis is difficult due to high intrinsic resistance of Bps to most antibacterial agents. It has been studied that the antimicrobial resistance of this organism may result from poor permeability of the active compounds through porin channels located in the outer membrane (OM) of the bacterium. In previous work, a 38-kDa protein, namely "BpsOmp38", was isolated from the OM of Bps. A topology prediction and liposome-swelling assay suggested that BpsOmp38 comprises a β-barrel structure and acts as a general diffusion porin. The present study employed planar black lipid membrane (BLM) reconstitution to demonstrate the single-channel conductance of the trimeric BpsOmp38. High-time resolution BLM measurements displayed ion current blockages of each antimicrobial agent in a concentration-dependent manner with the translocation on-rate (k_{on}) following the order: norfloxacin>> ertapenem > ceftazidime > cefepime > imipenem > meropenem >> penicillin G. The dwell time of a selected antimicrobial agent (ertapenem) decayed exponentially with increasing temperature. The energy barrier for the ertapenem binding to the affinity site inside the BpsOmp38 channel was estimated from the Arrhenius plot to be 12 kT and for the ertapenem release to be 13 kT at +100 mV. Topology prediction suggested that Tyr-119, located in the middle of the pore, may act as a pore-constricting residue that controls the permeability of hydrophilic species through *Bps*Omp38. Antibiotic susceptibility assay showed that the Omp-deficient *E. coli* expressing BpsOmp38Y119A and Y119F mutants were more susceptible to meropenem and ceftazidime, but less susceptible to doripenem when compared with the susceptibility of *E. coli* expressing BpsOmp38 wild-type. Liposome-swelling assay suggested that the permeability rate of neutral sugars through the *Bps*Omp38 variants increased as the molecular weight of the sugar decreased. However, the permeation of antibiotics through the *Bps*Omp38 porins showed modest correlation between the molecular weight and the diffusion rates. The result suggested that not only the pore diameter, but the interactions between the antibiotic and the residues lining the pore interior also play an important role in the molecular uptake through *Bps*Omp38.

สัญญาเลขที่ RMU5380055

ชื่อโครงการ (ไทย) การศึกษากลไกการดื้อยาปฏิชีวนะผ่านช่องพอรินของแบคทีเรียก่อโรคเมลิออยโดสีส *Burkholderia pseudomallei*

(English) A study of antibiotic-resistant mechanism through a porin channel of the melioidosis bacterium *Burkholderia pseudomallei*

หน้าสรุปโครงการ (Executive Summary)

==========

ชื่อหัวหน้าโครงการ รองศาสตราจารย์ ดร. วิภา สุจินต์

หน่วยงานที่สังกัด สาขาวิชาชีวเคมี สำนักวิชาวิทยาศาสตร์ มหาวิทยาลัยเทคโนโลยีสุรนารี อ.เมือง จ. นครราชสีมา 30000 โทร 044 22 3968 แฟกซ์ 044 22 4193/044 22 4185

สาขาวิชาที่ทำการวิจัย สาขาชีวเคมีทางการแพทย์

คำสำคัญ Outer membrane porins, *Burkholderia pseudomallei*, antibiotic resistance, melioidosis

งบประมาณรวมทั้งโครงการ 1,2000,000.- บาท

ระยะเวลาดำเนินงาน 3 ปี

1. ความสำคัญและที่มาของปัญหา

Black Lipid Membrane (BLM) studies have been published on the functional characterization of various bacterial porins, however, to the best knowledge of the applicant there is nothing available yet on porins that come from the bacterium that causes melioidosis. With the clinical relevance of this disease, the high antibiotic resistance of *Burkholderia pseudomallei* (Bps) strains, and the risk for an abuse of the Bps microorganism as biological weapon, an assessment of the basic structural and functional properties of the Bps porin and an evaluation of their role in the establishment of antibiotic resistance are certainly of importance to health science and pharmaceutical industry.

2. วัตถุประสงค์ของโครงการ

1. Cloning, expression, and generation of relevant mutants of *Bps* porin.
2. BLM measurements with both the native and mutated BpsOmp38 porin.
3. Thorough analysis of the outcome of BLM measurements and examination of the effects of point mutations on the functional characteristics of Bps porins in terms of e.g. the permeability for relevant ions, sugars, and antibiotics.
4. Investigation of the important residues that are responsible for the molecular uptake through *Bps* channels.

3. ระเบียบวิธีวิจัย

The research will be carried out as follows:

1. Literature review and database search
2. Recombinant expression in *E. coli* and purification of BpsOmp38
3. Refolding of BpsOmp38 in the presence of appropriate detergent and further purification
4. BLM measurements of ion transport through BpsOmp38 porin
5. BLM measurements of sugar transport through BpsOmp38 porin
6. BLM measurements of antibiotic transport through BpsOmp38 porin
7. Point mutations of BpsOmp38 porin
8. Confirmation of correct mutation by DNA sequencing and recombinant expression of the mutated Omp porins
9. BLM measurements of ion/sugar/antibiotic transports through mutated *Bps*Omp38 porin
10. Data analysis and preparation of manuscripts and final report

เนื้อหางานวิจัย

1. ความสำคัญและที่มาของปัญหา

Burkholderia pseudomallei (Bps) is a Gram-negative bacterium and pathogen that triggers melioidosis, an infectious disease that is primarily a problem in tropical and subtropical regions, especially southeast Asia and northern Australia, and reason for significant counts of fatalities [1,2]. *B. thailandensis* (Bth) is a homologue of Bps but not infectious. As all Gram-negative bacteria, both Bps and Bth are delimited by an outer lipid bilayer membrane (OM) that is at the same time cell wall and effective barrier against the free diffusional exchange of hydrophilic solutes between the cytosol of the microorganisms and their surroundings. In- and outward movements of e.g. ions, sugar nutrients or amino acid metabolites through the outer membrane of a bacterium is, however, essential for the maintenance of a balanced intracellular environment and typically controlled by passive diffusion through transmembrane protein channels (porins) or by means of active pump-like transporter proteins. Bacterial porins are, in general, made of ß-barrel proteins that insert as trimers into the OM to form water-filled channels through which molecules can diffuse [3-4,5]. Representing the first gateway for substances into bacterial cells, porins fulfill a number of modulatory physiological functions and thus are intensively studied for fundamental reasons to get a better understanding of this type of membrane trafficking and for practical applications in pharmaceutical research to explore opportunities for optimal drug delivery to intracellular target sites.

In an earlier work, two 38 kDa integral outer membrane proteins of Bps and Bth, in the following named BpsOmp38 and BthOmp38, were isolated and purified in non-denatured and entirely functional conformation from whole-cell lysates [6,7]. As well, the genes encoding for BpsOmp38 and BthOmp38 were cloned and sequenced with their nucleotide sequences discovered to be 99.7% identical. MALDI-TOF (**M**atrix-**A**ssisted **L**aser-**D**esorption **I**onization-**T**ime **o**f **F**light) and ESI (**E**lectro**S**pray **I**onization) mass spectrometry on the two purified *Burkholderia* proteins showed a broad sequence similarity to the OpcP1 porin from *Burkholderia cepacia*. By means of secondary structure analysis via FTIR (**F**ourier-**T**ransform **I**nfra**R**ed) spectroscopy it was furthermore possible to resolve the typical ß-sheet structure of bacterial porins for both BpsOmp38 and BthOmp38 proteins. With proteoliposomes reconstituted from BpsOmp38 and BthOmp38 (native or refolded) in common phospholipids, it was demonstrated via the conventional liposome swelling assay that both proteins showed fairly similar permeability for a set of small saccharides (molecular masses, M_r, between about 180 and 660) and antibiotics (M_r between about 380 and 780), with the rate of diffusion linearly decreasing with increasing M_r of the diffusing species. The latter finding provided a further hint that the refolded trimers of BpsOmp38 and BthOmp38 proteins were porins. Finally, a topology prediction and molecular modelling strongly suggested that the newly-isolated and cloned porins most likely fold as a 16-

stranded ß-barrel with eight loops and eight turns, expressing closest structural similarity to an anion-selective porin from *Comamonas acidovorans* [8].

Successful medical treatment of melioidosis has been demonstrated difficult owing to the well recognized high resistance of *Bps* to a variety of antibiotics, including ß-lactams, aminoglycosides, macrolides, and polymyxins [9-11]. It has been suggested for *Bps* and other bacterial species that their antibiotic resistance may be induced by a limitation of the permeability of the active compounds through the porin channels in the outer membrane of the bacterium [12-15]. Although liposome-swelling assay [16] is frequently used for permeability studies with porins, a more suited technique to obtain structural and functional information is electrophysiology, as this technique allows channel properties, including pore size, ion selectivity and gating to be measured more accurately. More recently, high resolution electrophysiology known as black lipid membrane (BLM) measurements had been applied to investigate in detail the permeation of single molecules through the porin channel [17] and a similar method could also be used to quantify the permeation of antibiotic molecules.

First BLM measurements in an own-newly established experimental setup in the laboratory at the Suranaree University of Technology have been successfully conducted with an outer membrane porin (VhOmp) from *Vibrio harveyi*, a pathogenic bacterium that causes fatal *Vibriosis* in marine animals [18]. Later, the preliminary BLM measurements confirmed the porin nature of the refolded trimers of BpsOmp38 and BthOmp38 and proved the inserted units functional as ion channels. Figure 1 is displaying representative fractions of typical BLM recordings (I vs. t traces) with the two porins. The ionic currents through Bps and Bth channels appeared in the high-resolution electrophysiology measurements about equal in amplitude but multiple times smaller than the ones that are measured under same conditions with for instance the well-studied bacterial OmpF porins. Also in contrast to the OmpF porins, the Bps and Bth channels did not remain open long but fluctuated rapidly between the open and closed states. A comparison of the behavior of the Bps and Bth porins suggested that the Bps variant in average displayed a higher ratio topen/tclosed of the opening to closing times. The observed channel characteristic may be sign of the distinct character of Bps and Bth porins, however, more intense studies and a thorough statistics are needed for proper validation.

2. วิธีการทดลอง

2.1. Cloning and site-directed mutagenesis

The genes encoding full-length BpsOmp38 was isolated from genomic DNA of B. pseudomallei and cloned into the pGEM-T easy vector as described previously [7]. Since the BpsOmp38 expressed from prvious work was not solubilized and it was tedius to obtain the functional protein by the refolding protocol. Therefore, in this study we set out a new cloning strategy by including a signal peptide sequence at the 5'-end of the *BpsOmp38* DNA so that the expressed BpsOmp38 could readily insert in the cell wall of the *E. coli* expression host. This protein was also engineered to have hexahistidine residues tagged at the C-terminus to aid purification. To do so, the

recombinant plasmids, designated pGEM-T-BpsOmp38, was used as templates for PCR amplification of the BpsOmp38 fragments. The forward primer included the initiation codon ATG following an NcoI restriction site and the nucleotides that encode BpsOmp38 has a signal peptide fragment. The reverse primer included an XhoI restriction site following the nucleotides that encodes BpsOmp38 having six histidine residues attached to its C-terminal end. The primer sequence are: NcoI (sequence underlined) forward primer, 5'-TACCATGGCAAATAAGACTGATTGTTG-3'; XhoI (sequence underlined) reverse primer, 5'-TACTCGAGGAAACGTGACGCAGACC-3'. Gene amplication was carried out with P*f*u DNA polymerase in a GeneAmp® PCR System 9700 termocycler (PE Applied Biosystems, Foster City, CA, U.S.A.). The PCR product of expected size (1.1 kb) was purified using PureLinkTM Genomic DNA Kits (Invitrogen, Gibthai Company Ltd., Bangkok, Thailand), then digested with the corresponding restriction enzymes to generate cohesive ends. The 1.1-kb DNA fragment was re-extracted from an 1% agarose gel. The purified DNA fragment was subsequently ligated to the plasmid pET23d(+) previously digested with the same restriction endonucleases and transformed into *E. coli* host strain DH5α, according to the standard protocol.

For site-directed mutagenesis, the pET23d(+) plasmid harboring the *BpsOmp38/His*$_6$ DNA fragment was used as DNA template. Mutations of the desired nucleotides were carried out using the PCR-based strategy. For BpsOmp38 mutant Y119A, the mutagenic primers are 5'-CTGGGCCGTCAGGCCGACGCAACCCAAGAC-3' (forward primer) and 5'-GCTTTGGGTTGCGTCGGCCTGACGGCCCAG-3' (reverse primer). For BpsOmp38 mutant Y119F, the forward primer is 5'-GGGCCGTCAGTTCGACGCAACCCAAG-3' and the reverse primer is 5'-CTTGGGTTGCGTCGAACTGACGGCCC-3'. Sequences underlines represent the mutated codons. The PCR product was digested with DpnI to remove the non-mutated parental DNA strand. The DpnI-treated DNA was transformed into *E. coli* XL1-Blue supercompetent cells. The recombinant plasmids obtained from positive colonies were extracted, using Qiagen Plasmid Miniprep kit (QIAGEN, Germany). The recombinant plasmid, designated pET23d(+)/BpsOmp38Y119A and pET23d(+)/BpsOmp38Y119F, were re-transformed into *E. coli* DH5α cells. To verify correct mutation, the nucleotide sequences of sense an anti-sense strands of the PCR fragments were determined by automated sequencing (First BASE Laboratories Sdn Bhn, Selangor Darul Ehsan, Malaysia).

2.2. BpsOmp38 expression and purification

The *E. coli* strain BL21 (DE3) Omp8 Rosetta was a gift from Ralf Koebnik, Laboratoire Génome et Développement des Plantes, Universit é de Perpignan via Domitia, Montpellier, France. This strain of *E. coli* does not express major outer membrane proteins: LamB, OmpA, OmpC and OmpF [19]. The cells were transformed with the recombinant plasmid pET23d/BpsOmp38. Purification of the recombinant BpsOmp38 followed a modified version of protocols described by Garavito and Rosenbusch [20] and Rosenbusch [21]. In brief, transformed cells were grown at 37°C in Luria-Bertani (LB) liquid medium containing 100 µg/ml ampicillin. At an OD_{600} reading of 0.5, IPTG (isopropyl β-D-thiogalactoside) was added to a final concentration of 0.4 mM. Cell growth was continued for a further

6 h and then cells were harvested by centrifugation at 2,948 xg for 10 min. The cell pellet was resuspended in buffer containing 20 mM Tris-HCl, pH 8.0, 2.5 mM $MgCl_2$, 0.1 mM $CaCl_2$, 10 µg/ml DNase I and 10 µg/ml RNase A and then disrupted using a high-pressure homogenizer (EmulsiFlex-C3, Avestin Europe, Mannheim, Germany). The recombinant BpsOmp38 was further extracted from the peptidoglycan layer using sodium dodecyl sulfate (SDS)-containing solutions based on a procedure reported by Lugtenberg and Alphen [22]. Briefly, SDS was added to the cell suspension to a final concentration of 2% (v/v) and incubation carried out for 1 h at 60°C with gentle shaking. The crude extract was then centrifuged at 40,000 xg for 60 min at 4°C. The pellet, which at this stage included the cell envelopes, was re-suspended in 20 mM phosphate buffer, pH 7.4 (PBS), containing 0.125% (v/v) octyl-POE (n-octyl-polyoxyethylene; ALEXIS Biochemicals, Lausanne, Switzerland). The suspension was incubated at 37°C with gentle shaking for 60 min and then centrifuged at 100,000 xg at 4°C for 40 min. The new pellet, now rich in outer membranes, was re-suspended in 20 mM phosphate buffer, pH 7.4 containing 3% (v/v) octyl-POE and the suspension incubated at 37°C with shaking at 250 rpm for 1h to solubilize the porin. Insoluble material was removed by centrifugation at 100,000 xg at 20°C for 40 min and the porin-rich supernatant concentrated using Amicon Ultra-15 centrifugal filter devices with a nominal MW limit of 30 kDa (Millipore, Schwalbach, Germany). Amicon centrifugal filters were also used to exchange the original preparation buffer with 20 mM PBS, containing 1% (v/v) octyl-POE. Aliquots of the final protein sample were used for absorbance measurement at 280 nm for the determination of protein concentration using NanoDrop-T 1000 Spectrophotometer (Thermo Fisher Scientific, Wilmington, DE, U.S.A) and for SDS-polyacrylamide gel electrophoresis (SDS-PAGE) for the assessment of sample purity.

2.3. Lipid bilayers measurements and single channel analysis

The following chemicals were used: NaCl, KCl, MES, n-pentane, hexadecane (Sigma-Aldrich, Hamburg, Germany); ceftazidime, norfloxacin, penicillin G, (Sigma-Aldrich); cefepime, imipenem, meropenem and ertapenem (Basilea Pharmaceutica Ltd, Basel, Switzerland); 1, 2-diphytanoyl-sn-glycero-3-phosphatidylcholine (DPhPC) (Avanti Polar Lipids, Alabaster, AL, U.S.A). Double distilled and deionised water was used to prepare chemical reagents and the freshly-made solutions passed through a 0.4-µm filter. The drug stock solutions for translocation experiments were prepared with 1 M KCl in electrolyte buffer (20 mM phosphate buffer, pH 7.0 or in 20 mM HEPES, pH 8.0). Lipid bilayer measurements and single channel analysis were performed as described elsewhere [23,24]. Briefly, a cell with a 40-60 µm diameter aperture in a 15 µm-thick Teflon partition provided a two-compartment black lipid membrane (BLM) chamber and two silver-silver chloride electrodes at either side of the dividing wall allowed voltage control of solvent-free planar lipid bilayers that were formed using a solution of DPhPC in pentane. Low levels of the study BpsOmp38 channel were introduced to the cis- or trans side of the bilayers by adding the protein stock solution of about 1-2 ng/ml containing 1% (v/v) octyl-POE (Alexis, Switzerland). In the trials addressing the temperature dependence of drug

translocation, a peltier element (Dagan Corporation, Minneapolis, MN, U.S.A) was used for accurate temperature regulation of the BLM chamber. At an applied transmembrane voltage of ± 200 mV, spontaneous channel insertion was usually obtained within a few minutes after adding the protein solution. Conductance measurements were performed using an Axopatch 200B amplifier (Molecular Devices, Sunnywale., CA, U.S.A.) in the voltage clamp mode and the internal filter at 10 kHz. Amplitude, probability, and single channel analyses were performed using pClamp v.10.0 software (Molecular Devices). Control experiments (refer to Supplementary S3, upper left recording) showed no dependence of the BpsOmp38 conductance and open channel noise on the presence of the buffer alone.

Black lipid bilayer measurements with BpsOmp38 from an earlier preparation with mass spectrometry (MS) identification established that the single-channel conductance of the targeted reconstituted protein channel is about 2.7 nS ± 0.3 nS in 1M KCl. A channel of identical conductance also routinely appeared when freshly formed solvent-free DPhPC bilayer membranes were exposed to the protein prepared by the procedure described in the preceding section. Accordingly, translocation of drug molecules was analyzed in recordings of this particular channel. Another channel that frequently incorporated during the BLM experiments was not used for the translocation studies after its small conductance (0.3 nS in 1 M KCl) and MS data suggested it was a maltoporin.

2.4. Porin homology modelling

The structural model of recombinant BpsOmp38 was built based upon the Modeller suite of programs [25]. Initially, several iterations of the PSI-BLAST protein sequence search program in the pdb database were performed to allow detection of remote homologues of the BpsOmp38 porin. Only the templates with non-redundant structures were kept and further used for building the homology model. Such templates included the pdb codes 3K1B (OmpF), 2IXX (OmpC), 1E54 (Omp32), 1OSM (Ompk36) and 3A2R (PorB). A multiple-sequence alignment revealed a complete coverage of the homology sequence, although only about 24% sequence identity was observed between the BpsOmp38 and the template amino acid residues. Fifty structural models of the BpsOmp38 trimers were further generated by the Modeller program, from which the “representative model”, was defined as the one that minimized both the overall ‘Modeller objective function’ and the ‘Dope score evaluation function’. Finally, the “final best model” was assessed with the energetic based validation suite ProQ [26] and the geometric based PROCHECK, with the latter showing only 2.8% of Ramachandran disallowed regions, and absence of close (or "bad") contacts.

2.5. Liposome swelling assay

Trimeric BpsOmp38 channel was reconstituted into liposomes as described previously [27,28]. *E. coli* total lipid extract was used to form liposomes and 15% (w/v) dextran (M_r 40,000) was entrapped in the liposomes. The size of the formed liposomes was checked using a Nano-ZS ZEN3600 zetasizer. The isotonic solute concentration was determined with different concentrations of raffinose solution

(prepared in 20 mM HEPES buffer, pH 7.5) added into the protoliposome suspension. The value obtained for isotonic concentration of raffinose was used as an approximation to facilitate the adjustment of isotonic concentrations for different solutes. Twenty microliters of liposome or proteoliposome solution was diluted into 500 µL of the isotonic test solution in a 1-mL cuvette and mixed manually. The initial swelling rate upon addition of the isotonic sugar solutions was monitored using a UV-Vis spectrophotometer with the wavelength set at 500 nm. The absorbance change over the first 60 sec was used to estimate the swelling rate (s^{-1}) following the equation: $\Phi = (1/A_i)dA/dt$, in which Φ is the swelling rate, A_i the initial absorbance, and dA/dt the rate of absorbance absorbance change during the first 60 s. The swelling rate of each sugar was normalized by setting the rate of arabinose (Mr 150.1) to 100%. The values shown are averages obtained from four to six determinations. Protein-free liposomes and proteoliposomes without sugars were used as negative controls.The tested sugars included L-arabinose (M_r 150), D-glucose (M_r 180), D-mannose (M_r 180), D-galactose (M_r 180), GlcNAc (N-acetylglucosamine; M_r 221), D-sucrose (M_r 342), D-melezitose (M_r 522) and D-stachyose (M_r 667). Antibiotics that are potentially used for melioidosis treatment included gentamicin (M_r 709), ceftazidime (M_r 637), cefepime (M_r 572), cefotaxime (M_r 477) and meropenem (M_r 383).

2.6. Antibiotic susceptibility tests

MIC values were determined in triplicate by a standard 2-fold broth dilution method using Mueller-Hinton (MH) broth according to the CLSI (Clinical and Laboratory Standards Institute) guidelines. Bacterial growth in the presence of varied concentrations of antibiotics were evaluated after 24 hr of incubation at 37 °C and classified according to the Antibiogram Committee of the French Society for Microbiology [29]. Different clasess of antibiotics were tested, included penicillin, dicloxacillin, cefoxitin, cefpime, doripenem, ciprofoxatin, enrofloxacin, meropenem, imipenem, amoxycillin, ceftazidime, co-trimoxazole, gentamicin, kanamycin and norfloxacin. MIC values were determined in the presence and absence of phenylarginine-β-naphthylamide (PAβN), a well-known efflux pump inhibitor acting on members of the RND efflux pump family of Gram-negative bacteria. Recombinant plasmids were transformed into *E. coli* BL21 (DE3) Omp8 Rosetta strain. *B. pseudomallei* and *B. thailandensis* were streaked on LB agar plate and incubated at 37°C for 16 hr. Single colonies of bacteria were grown in 5 ml of MH (Mueller Hinton) medium and incubated at 37°C for 16 hr. The starter cultures were diluted to OD_{600} of approximately 0.08-0.1 (104-105 CFU/ml) in MH broth. After that, 10 µl of cells were pipetted into 100 µl of the diluted antibiotic and incubated at 37°C for 24 hr. The growth of overnight culture was monitored by OD_{600}.

3. ผลการวิจัยและอภิปราย

3.1. Channel properties of BpsOmp38

We previously reported the recombinant expression of the BpsOmp38 gene in *E. coli* BL21 Origami (DE3) cells. The recombinant BpsOmp38 protein, which was in form of inclusion bodies, was further refolded into trimeric form using 10% (w/v) Zwittergent^{TM} 3-14. In the present study, the *Bps*Omp38 gene, including a 20-amino acid signal peptide fragment, was subcloned into a pET23d(+) vector so it could be incorporated and fully expressed as a fully functional trimeric protein in the cell wall of the *E. coli* BL21(DE3) Omp8 mutant strain. After extraction by 2% (w/v) SDS and solubilisation in 1% (v/v) octyl-POE, SDS-PAGE analysis demonstrated migration of the extracted porin as a protein band with an apparent MW 100 kDa (Fig. 1, lane 2). This was assumed to be the trimeric form of BpsOmp38. Upon heat treatment at 100°C for 10 min, the presumed trimer was denatured and a new band with apparent MW of 35 kDa appeared as expected for the *Bps*Omp38 monomer (Fig. 1, lane 3).

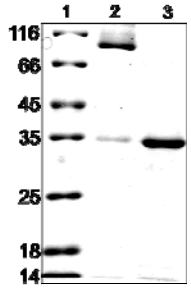

Fig. 1 SDS-PAGE analysis of recombinant BpsOmp38.

Track 1: low molecular weight protein markers (PageRuler, Fermentas Inc., U.S.A); Track 2: intact *Bps*Omp38 trimers under non-denaturing conditions; Track 3: *Bps*Omp38 subunit after denaturing at 100°C for 10 min.

When BpsOmp38 was reconstituted in stable DPhPC lipid bilayers, the study protein (porin) behaved like an ion channel and allowed a specific current flow under controlled voltage application. Using the solvent-free BLM recordings, single trimeric BpsOmp38 units in the bilayer membrane showed a characteristic conductance of 2.7±0.3 nS in 1M KCl/20 mM HEPES, pH 8.0 but the channels were prone to close at high transmembrane potentials (above ±100 mV). A typical membrane current recording that was obtained for a single trimeric BpsOmp38 channel at an elevated transmembrane potential of +150 mV is shown in Fig 2.

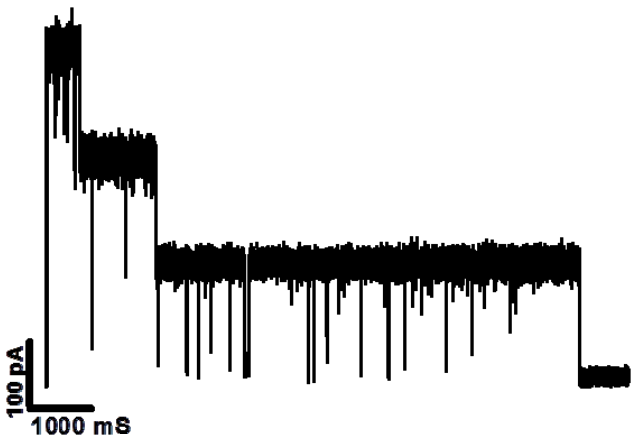

Fig. 2 Trimeric BpsOmp38 porin from *Burkholderia pseudomallei*.

A single channel recording of the BpsOmp38 reconstituted in solvent-free DPhPc membranes. A three-step closure was induced by increasing the applied voltage to +150 mV.

Within the time-span of a few seconds, the fully open BpsOmp38 channel changed sequentially by a three-step process into the fully closed state. This process appeared as a three-stage decrease in conductance signal and confirmed once again the trimeric channel organization that had already been suggested by the SDS-PAGE gel analysis (Fig. 1). The biological relevance of the successive closure of the individual units of multimeric bacterial porins is poorly understood, bearing in mind that, *in vivo*, the potential difference across the bacterial outer membrane is usually negligible. On the other hand, parameters such as pH, ion composition of the internal and external cell milieu and pressure influence, to a certain extent, the membrane potential and response to variations of these factors may contribute to the physiological significance of channel closing.

To study the translocation of drug molecules through the isolated porin, a potential was applied across the incorporating lipid membranes at which reconstituted BpsOmp38 channels predominantly existed in their fully open state. Ion current blockages through the open channels were then analyzed after applying the selected antimicrobial agent to either the cis or trans side of the bilayer. Drug translocation trials were performed with a set of antimicrobial agents including three ß-lactam antibiotics (penicillin G, meropenem, imipenem), two cephalosporins (cefepime, ceftazidime), one fluoroquinolone (norfloxacin) and one carbapenem (ertapenem) (Fig.3).

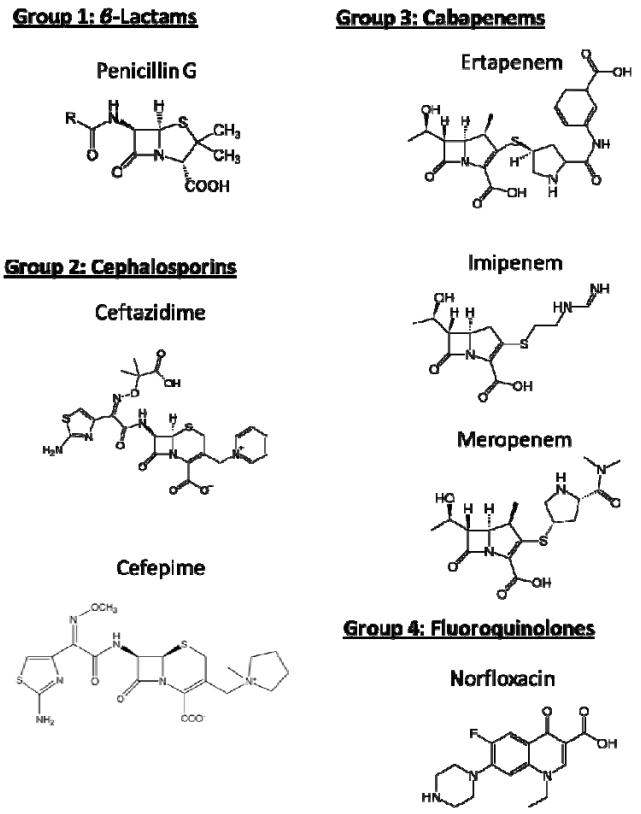

Fig. 3 Chemical structures of seven antimicrobial agents used in this study.

With the exception of penicillin G, all the test antimicrobial agents interacted with the BpsOmp38 channel in such a way that spontaneous fast fluctuations of the BLM membrane current were induced (Fig. 4). Overall, the number of current deflections in the recording of certain length varied linearly with concentrations that were independent of the type of antibiotic tested.

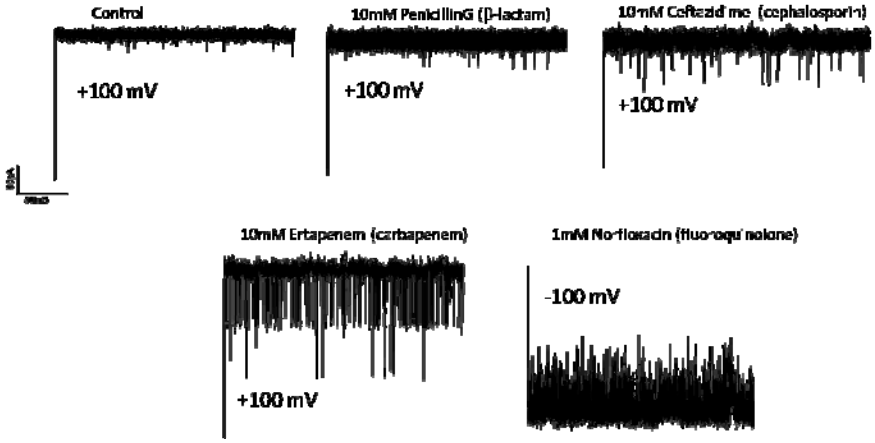

Fig. 4 Antibiotic translocation through BpsOmp38.

The blockages of ion currents through BpsOmp38in the presence of various antibiotics. One compound per class of antibiotics is presented. Direction: cis to trans Electrolyte: 1 M KCl/20 mM HEPES, pH 8.0

The rates of channel entry and exit are critical factors in the net flux of an antibiotic through a bacterial Omp pore. The BLM-based observation of the molecular interaction of ertapenem with the BpsOmp38 channel at various temperatures and concentrations allowed calculation of: i) the drug binding kinetics and the second-order on-rate constant k_{on} ($M^{-1}s^{-1}$), ii) the first-order off-rate constant k_{off} (s^{-1}), and iii) the equilibrium binding constant K (the ratio of k_{on}/k_{off}; M-1). Table 1 gives a comprehensive list of the three parameters k_{on}, k_{off} and K for all seven antimicrobial agents whose translocation through the *Bps*Omp38 channel was investigated in the present study (blockage characteristics of the ion flow through *Bps*Omp38 by representatives of each class of the antimicrobial agents).

Table1. Kinetics of antibiotic translocation through *Bps*Omp38

Antibiotic	$k_{on(cis)}$ ($s^{-1}M^{-1}$)	$k_{off(cis)}$ (s^{-1})
Penicillin G	n.d.[a]	n.d.
Meropenem	250	6,700
Cefepime	420	5,500
Imipenem	830	6,700
Ceftazidime	4,200	7,000
Ertapenem	22,000	5,500
Norfloxacin	300,000	20,000

Note that ion blockage by ertapenem applied to the cis side of the lipid membrane at a transmembrane potential +100 mV occurred with k_{on} = 8,200 $M^{-1}s^{-1}$ and a binding constant of about 1.2 M^{-1}. These values reasonably agree with those for the interaction of ertapenem with the major *Enterobacter aerogenes* Omp36. Furthermore, the off-rates did not vary significantly for this panel of antimicrobial agents, while a ranking of k_{on} and *K* saw the three ß-lactam antibiotics with rather low values that were clearly at the bottom end, the two cephalosporin drugs in the middle, and carbapenem and fluoroquinolone antibiotics in top positions. Greater values of k_{on} and *K* indicated that translocation of the newer class of drugs through the *Bps*Omp38 pore took place more rapidly.

Effects of temperature on the translation rate of the selected antibiotic (ertapenem) were investigated. For a given concentration of ertapenem, additions to the trans side led to about a two-fold higher number of blocking events than to the cis side. BLM measurements between 5°C and 45°C in the presence and absence of the antibiotic demonstrated that temperature had a strong impact on the rate of ertapenem permeation through the *Bps*Omp38 channel (Fig. 5).

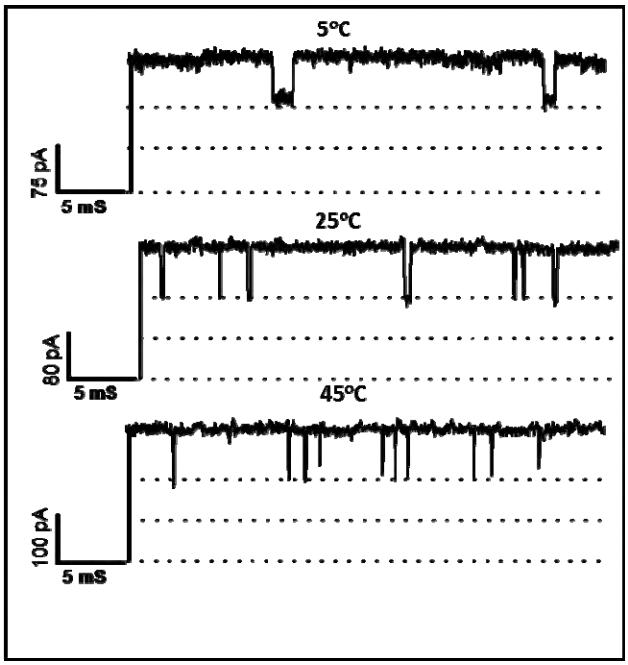

Fig. 5 Effect of temperature.

An increased number of blockage events was observed upon increases in temperature from 5, 10, 15, 20, 25, 30, 35, 40, and 45 °C. On the other hand, the dwell time of ertapenem translocation decreased exponentially with increasing temperatures. Here, only the BLM recordings at 5, 25 and 45 °C are presented. The single channel recordings were recorded at +100 mV.

At non-physiologically low temperature of 5 °C, relatively few membrane current blockages with rather long blocking times of over 1 ms were observed. Increasing the temperature to 45 °C increased the frequency of current deflections and at the same time lessened the dwell time (τ) of the penetrating molecules. Average dwell time (τ) values for defined conditions in terms of temperature and concentration were obtained through a statistical analysis of raw BLM data and a single-exponential fitting of blockage time histograms as exemplified in Fig. 6 for the ertapenem interaction with BpsOmp38 measured at 25 °C.

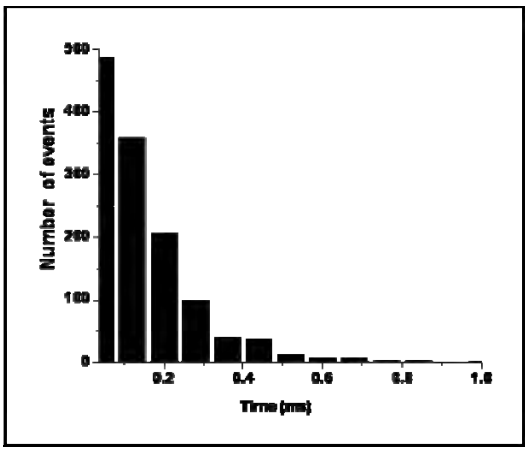

Fig. 6 Dwell time histogram.

Ertapenem (10 mM) was added on the cis side of the lipid membranes. The average dwell time was obtained when the data was fitted using the standard exponential curve fit available in pClampfit v10.0.

The average dwell time of ertapenem molecules inside of *Bps*Omp38 channel decreased exponentially with increasing temperature and did not depend on the actual concentration of the applied antibiotic; nor was it influenced by the side of the antibiotic addition. The latter two properties support the existence of a single affinity site for the ertapenem molecules in the *Bps*Omp38 channel. Temperature dependence measurements were used to calculate the free energy profile of transporin antibiotic permeation. For ertapenem, the effective energy barriers (E) to reach and cross the internal binding site of a *Bps*Omp38 channel from the cis (E_{on},cis) or trans (E_{on},trans) side of the bilayer were estimated from the typical Arrhenius plots (Fig 7A).

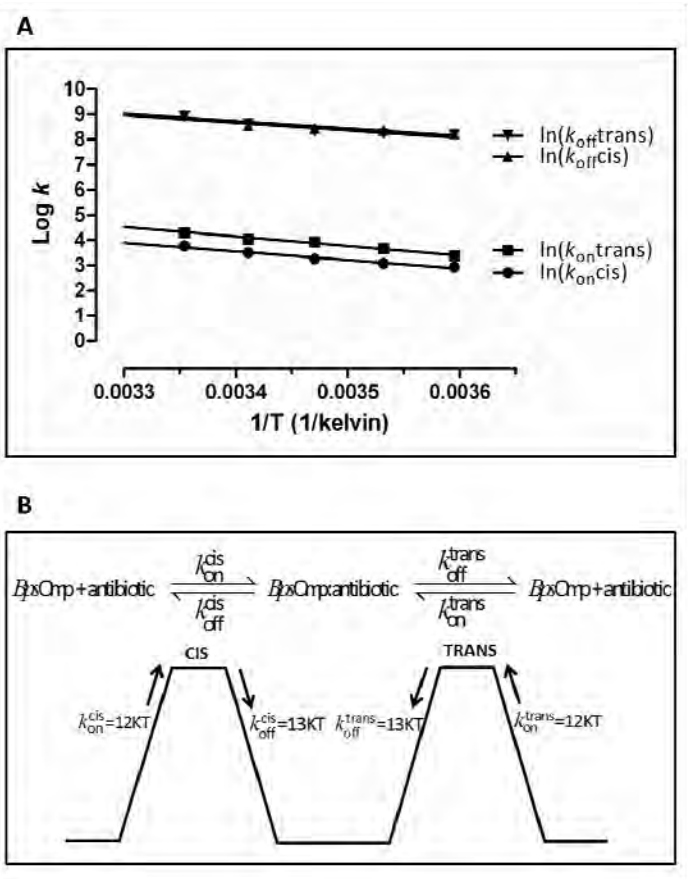

Fig. 7 Arrhenius plots for the ertapenem translocation through BpsOmp38 protein pores.

A. The logarithmic values of the on-rate and off-rate constants obtained from both cis and trans sides were plotted as a function of temperature.

B. A diagram representing symmetrical values of the energy barriers required for ertapenem binding and releasing from most likely the identical affinity site localized within the BpsOmp38 pore.

The analysis of the relevant plots revealed effective energy barriers Eon,cis and Eon,trans, representing the binding of ertapenem to the affinity site of a *Bps*Omp38 protein pore at +100 mV transmembrane voltage were estimated to be 12 kT. The Arrhenius plots for the off rates allowed

calculation of the effective energy barriers E_{off},cis and E_{off},trans for the ertapenem release from the affinity site of the BpsOmp38 channel at +100 mV, were 13 kT (Fig. 7B). Estimation of symmetrical values of the energy barriers required for ertapenem binding and release from cis-to-trans side and from trans-to-cis side further supports a single affinity site inside the *Bps*Omp38 channel as earlier on suggested.

3.2. Structural modeling

The homology model of the porin BpsOmp38 was built based on five different templates obtained from homologous Gram-negative bacterial porins with non-redundant structures (refer to Materials and Methods). Despite an observed low-sequence identity (~24%), the overall fold of the generated BpsOmp38 trimers was found to be conserved. The alignment in Fig. 4A shows that the target sequence is completely covered by the different templates and that a few insertions and deletions are all found in the extracellular loops except for the small protrusion of a four-residue loop in the middle of the second strand of each monomer (Fig.8B). This small protrusion was also reported in the previously-characterized Omp32 [30].

The BpsOmp38 model was compared with the structure of the porin OmpF, for which the structure-function relationship of antibiotic translocation has been extensively studied [34]. Compared with OmpF, however, the amino acid sequences of various regions that participate in pore-forming properties were found to be different. These include the L3 loop that forms the constriction region of the channel, the arginine residues at the mouth of the OmpF channel, and the basic cluster in the anti-L3 side. In case of the BpsOmp38 channel, more acidic residues are observed instead in such regions. Within the known key residues of OmpF that were aligned with BpsOmp38, segments with conserved or amino acid substitutions are highlighted (Fig. 8A).

Fig. 8B is a graphic representation of the modelled BpsOmp38 trimeric structure, when incorporated into phospholipid bilayer membranes. Highlights indicate an obstructing internal protrusion, as well as the polar to acidic character of certain channel wall residues that point towards the lumen of the pore. It is predictable that the substitutions from OmpF to BpsOmp38 of the residues: K16V29, V20D31, K80F108, D113S130, F118W135, R167N187, and R168N188 may have an effect on drug transport through the BpsOmp38 porin (see Fig.4B). However, this hypothesis has to be confirmed by a combined approach, including microbiological assays, site-directed mutations and biophysical measurements, together with molecular dynamic simulations of antibiotic transport as previously described for OmpF [8,31].

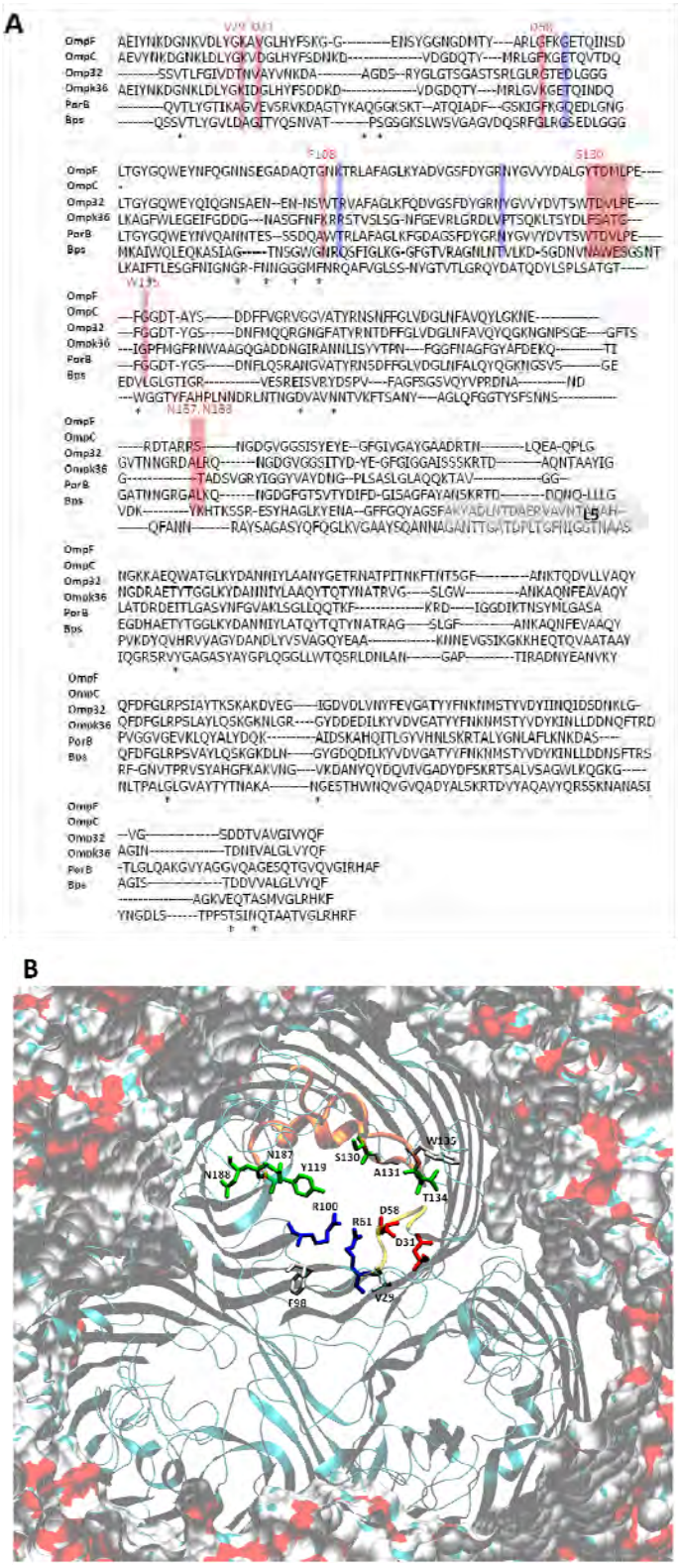

Fig. 8 The modelled structure of BpsOmp38 based on multiple templates.

A. A multiple alignment of the BpsOmp38 sequence was performed by SALIGN from the Modeller suite of programs. The pdb codes used as the homology templates are: 3K1B (OmpF); 2IXX (OmpC), 1E54 (Omp32); 1OSM (Ompk36); 3A2R (PorB), and the modelled structure of BpsOmp38 (Bps). Highlights are the conserved residues important for antimicrobial agent translocation of OmpF or OmpC (blue) and the substituted ones (red). Numbering of the BpsOmp38 residues follows the complete sequence containing the 20-aa signal peptide (not included here) (GenBank accession no: AY312416).

B. A snapshot of the homology model of BpsOmp38 (top view). The lipid bilayer membrane inserted around the porin is illustrated by its molecular surface properties. Differences in the known key residues of OmpF compared to the BpsOmp38 (corresponding to the alignment in Fig.8A) are highlighted with the residues in “sticks” representation and colored green for polar, blue for positively-charged, and red for negatively charged. The backbone of the BpsOmp38 porin is displayed in cartoons in order to highlight its secondary-structure elements with the loop L3 colored in orange.

3.3. Mutations and ion channel activities of mutated BpsOmp38

The *Bps*Omp38 model showed that the cluster of positively and negatively charged residues are located on short and long loop of the BpsOmp38 protein The tyrosine at position 119 of BpsOmp38 are observed in middle of the pore (Fig. 9A). This residue was substituted by alanine (Fig. 9B), and phenylalanine (Fig. 9C), respectively.

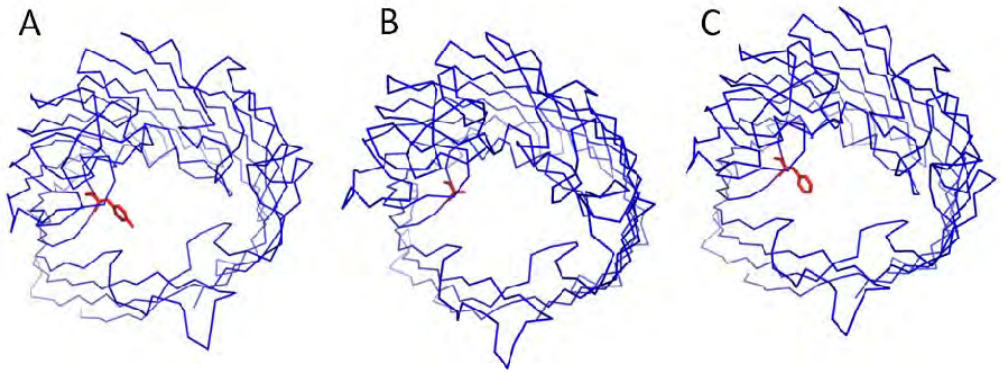

Fig. 9 The homology structure of BpsOmp38.

A. *Bps*Omp38 wild type showing Tyr at position 119. B. Tyr at position 119 was mutated to Alanine. C. Tyr at position 119 was mutated to Phe.

BpsOmp38 wild-type and mutants were successfully expressed in the *E. coli* DE3 (Omp8) knockout strain. When the three porins were inserted into artificial membrane, all could form multiple channels in a step-wise manner as seen in Fig. 10. Using the solvent-containing BLM, statistical estimation of the pore conductance obtained from several hundred insertions showed that BpsOmp38Y119A mutant had slightly larger conductance (1.9 ±0.2 nS) than the wild-type porin (1.6 ±0.03 ns). On the other hand, mutant BpsOmp38Y119F had lower conductance (1.5 ±0.05 nS) than wild-type’s conductance.

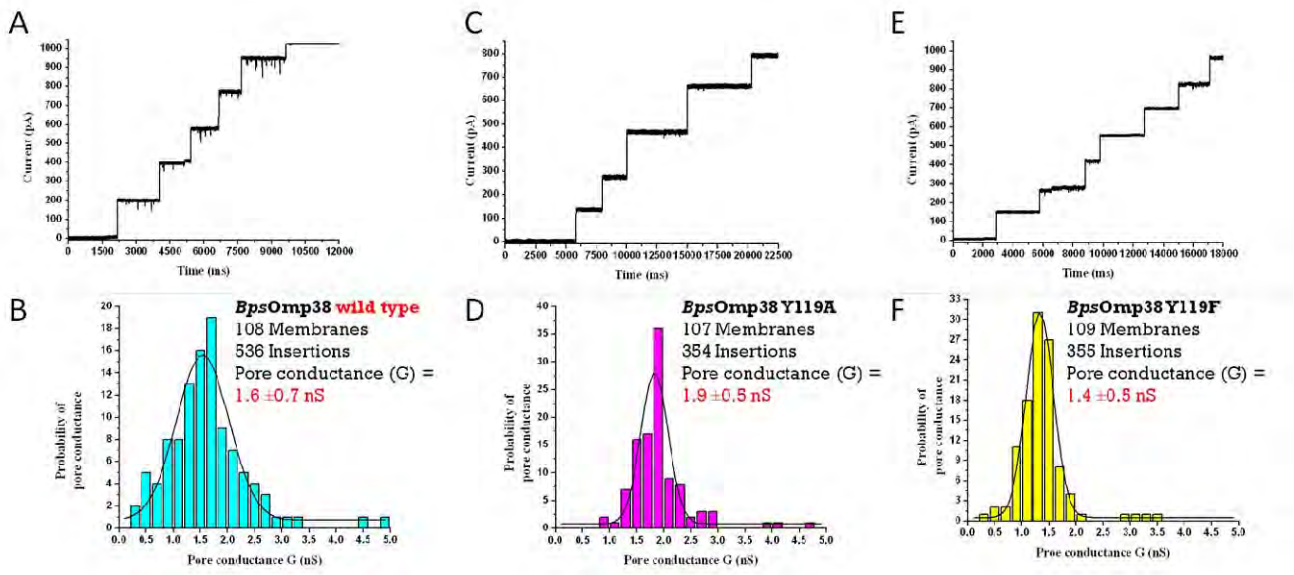

Fig. 10. Conductance properties of BpsOmp38 wild-type and Tyr119 mutants.

Measurement of BpsOmp38 pore conductances in 1 M KCl. Successive insertion events and histogram of BpsOmp38 wild-type (A,B), mutant BpsOmp38Y119A (C,D), and mutant BpsOmp38Y119F (E,F) into an azolectin bilayer at a transmembrane potential of +100 mV were recorded. Lipid bilayers were painted with a solution of 50 mg azolectin in 1 ml n-hexane and bathed on either side with 1 M KCl. BpsOmp38 (1 µg) was added to the 1-ml electrolyte on the cis side to trigger pore insertions.

3.4. Permeability of BpsOmp38 by liposome swelling assay

Diffusion rates of sugars through BpsOmp38 channels were determined by proteoliposome swelling assay, which indicated the influx of solutes through the proteoliposomes. Liposome swelling was visualized by recording changes in the scattering signal of the liposome solution, using a spectrophotometer. Under isotonic condition, the scattering remains constant throughout the measuring time, indicating neither swelling nor shrinking of the proteoliposomes. Here, we used raffinose, a branched sugar (M_r 504.42) that is unable to diffuse through the porins and arabinose, a small sugar that always permeates through the channel, for comparison. The relative permeation rates of neutral sugars are shown in Fig. 11A and B. For BpsOmp38 wildtype, the relative diffusion rate of the studied sugars was found to decrease as the size of the sugar increased as follows: arabinose (M_r 150.1) > galactose (M_r 180.1) ≅ glucose (M_r 180.1) ≅ mannose (M_r 180.1) > GlcNAc (M_r 221.2) > sucrose (M_r 342.3) ≅ maltose (M_r 342.3) > melezeitose (M_r 504.4) > raffinose (M_r 594.5). The size exclusion limit of the Bps*O*mp38 pores was estimated to be MW < 600. Similar results were observed with the two mutants. BpsOmp38Y119A mutant was shown to have increased permeation rate due to its small side chain as compared to the tyrosine side-chain. On the other hand mutant Y119F showed similar rates due to its indistinguishable side chain to tyrosine. The result of mutant Y119F someway

indicated that changes in hydrophilicity in the side chain did not affect the permeability of the sugar through BpsOmp38.

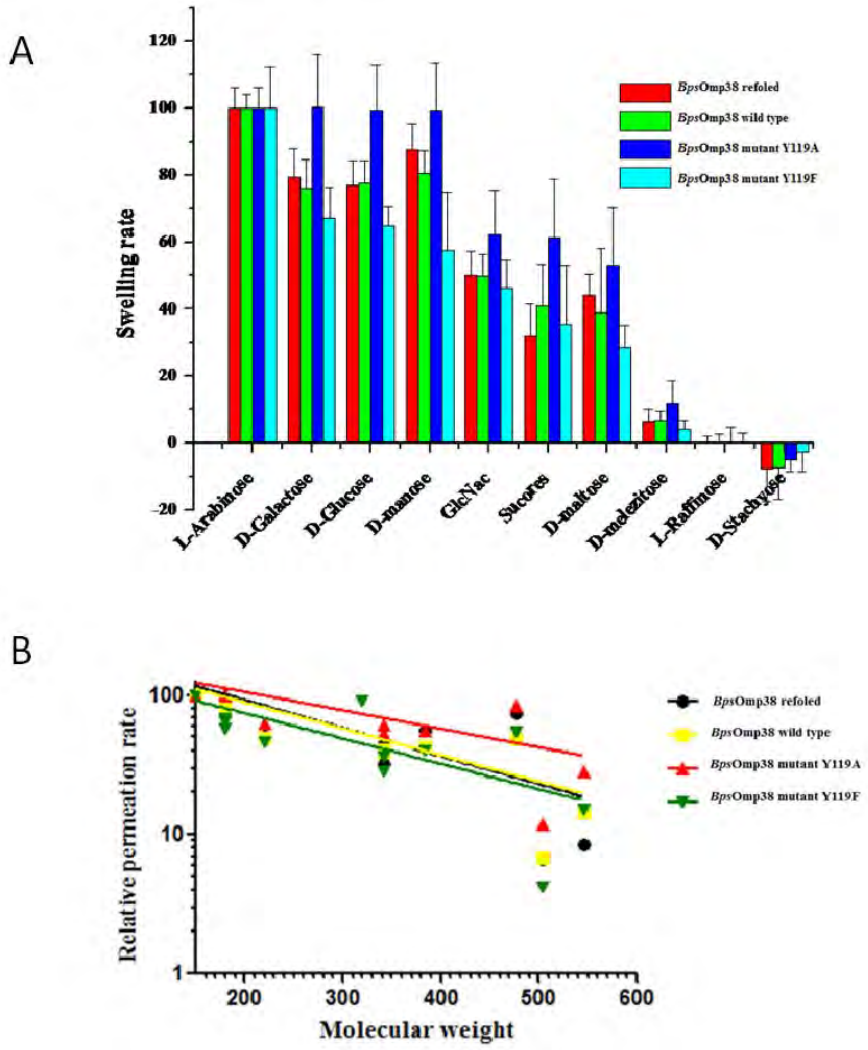

Fig. 11. Liposome swelling assay of *Bps*Omp38 induced by neutral sugars.

Multilamellar liposomes were reconstituted with purified *Bps*Omp38 (200 ng). The isotonic concentration was defined as the concentration of raffinose added into the proteoliposome suspension that did not caus change in absorbance at 500 nm for a period of 60 s. Permeation of different types of sugars through BpsOmp38 reconstituted liposomes were then tested. (A) The swelling rate was normalized, with the rate of swelling of arabinose set to 100%. Values presented are averages of 4-6 independent experiments. (B) Relative permeation rates of sugar through liposomes reconstituted with BpsOmp38 wild type and mutants. The values are normalized to the permeation rate of L-arabinose and plotted on a logarithmic scale.

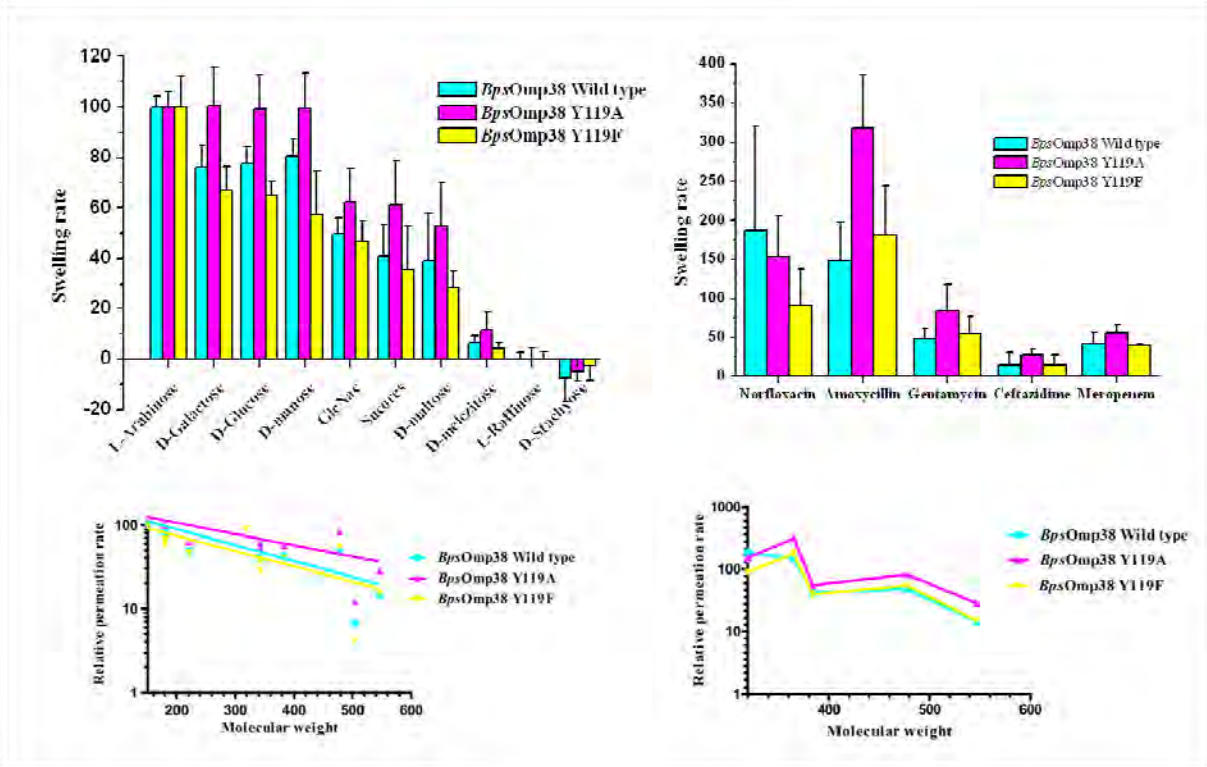

Fig. 12 Liposome swelling assay of BpsOmp38 induced by antibiotics.

Multilamellar liposomes were reconstituted with purified *Bps*Omp38 (200 ng). The isotonic concentration was defined as the concentration of raffinose added into the proteoliposome suspension that did not caus change in absorbance at 500 nm for a period of 60 s. Permeation of different types of antibiotics through *Bps*Omp38 reconstituted liposomes were then tested. (A) The swelling rate was normalized, with the rate of swelling in arabinose set to 100%. Values presented are averages of 6 independent experiments. (B) Relative permeation rates of antibiotic through liposomes reconstituted with *Bps*Omp38 wild type and mutants. The values are normalized to the permeation rate of L-arabinose and plotted on a logarithmic scale.

We also compare the permeation of antibitotics through BpsOmp38 variants (Fig.12). The relative rates of diffusion and molecular weight of antibiotic was not significantly correlated. The diffusion rate was increased following the order: amoxicillin (M_r 365.4) > norfloxacin (M_r 319.3) > gentamycin (M_r 477.6) > meropenem (M_r 383.5) > ceftazidime (M_r 546.6). The result suggested that not only the pore diameter, but the molecular interactions between the antibiotic and the residues lining the pore interior also play an important role in the molecular uptake through BpsOmp38.

3.5. Antimicrobial agent susceptibility

Antibiotic susceptibility of *B. pseudomallei* ATCC 23343 and *B. thailandensis* ATCC 700388 were carried out using Microdilution method as shown in Table 1. In general, the MIC values of all antibiotics tested with *B. thailandensis* were higher than that of *B. pseudomallei*. Both strains were categorized as resistant to all antibiotics, as the values compared with breakpoint for resistance suggested from the CASFM and EUCAST standard. The only exception is *B. speudomallei*, its MIC

value for meropenem (4 µg/ml) and ceftazidime (2 µg/ml) gave an indication that this Bps strain was sensitive to such antibiotics (breakpoints for sensitive, meropenem ≤ 4 µg/ml; ceftazidime ≤ 4 µg/ml).

Table 1. Antibiotic susceptibility of Bps native strains by micro-dilution method.

	Breakpoint for resistance		MIC (µg/ml)			
			B. pseudomallei		*B. thailandensis*	
	S ≤	R >	-	+ PAβN	-	+ PAβN
Penicillins						
Penicillin G	≤ 0.25	> 16[a]	1024	1024	2048	2048
Amoxycillin	≤ 4	> 16[a]	256	256	2048	2048
Dicloxacillin	IE	IE	1024	1024	2048	2048
Cephalosporins						
Ceftazidime	≤ 4	> 32[a]	2	2	512	512
Cefoxitin	≤ 8	> 32[a]	1024	1024	1024	1024
Cefepime	≤ 4	> 32[b]	512	512	1024	1024
Carbapenems						
Meropenem	≤ 4	> 8[a]	4	4	16	16
Imipenem	≤ 4	> 8[a]	8	8	16	16
Doripenem	≤ 1	> 4[b]	>2048	>2048	>2048	>2048
Fluoroquinolones						
Norfloxacin	≤ 1	> 2[a]	8	8	256	256
Ciprofoxacin	≤ 1	> 2[a]	4	4	128	128
Quinolone carboxylic acid						
Enrofloxacin	≤ 0.008	> 0.03[b]	4	4	128	128
Sulfonamide-Trimethoprim						
Cotrimoxazol	≤ 2/38	> 8/152[a]	128	128	512	512
Aminoglycosides						
Kanamycin	≤ 8	> 16[a]	16	16	128	128
Gentamicin	≤ 4	> 8[a]	32	32	256	256

[a]Breakpoints defined in the general recommendations of the 'Comite de l' Antibiogramme de la Societe Francaise de Microbiologie' (CASFM)

[b]Breakpoints defined in the general recommendations of the European Committee on Antimicrobial Susceptibility Teasting (EUCAST)

IE indicates that susceptibility testing is not recommrnded as the species is a poor target for therapy with the drug

R, Resistant; S, Sensitive

As shown in Table 1, MICs were also determined in the presence of phenylarginine-β-naphthylamide (PAβN), a well-known efflux pump inhibitor acting on members of the RND efflux pump family of Gram-negative bacteria. The results showed no significant difference in the MIC values as observed in the presence of PAβN, suggesting that the efflux pump does not play a role in the level of antibiotic susceptibility of *B. pseudomallei* and *B. thailandensis*.

Role of *Bps*Omp38 in antibiotic susceptibility was also tested using Microdilution method (Table 2). The Omp-deficient *E. coli* strain BL21 (DE3) Omp8 Rosetta was used to express BpsOmp38

wild type, BpsOmp38 mutant Y119A and BpsOmp38 Y119F. The results showed that expression of BpsOmp38 porin in the Omp-deficient *E. coli* strain increased the susceptibility towards some antibiotics such as doripenem, kanamycin and gentamycin.

Table 2. Antibiotic susceptibility of recombinant plasmid (pET23d(+) vector) in *E. coli* Omp8 Rosetta by micro-dilution method.

	MIC (µg/ml)							
	Without insert		**Insert *Bps*Omp38 Wild type**		**Insert *Bps*Omp38 Y119A**		**Insert *Bps*Omp38 Y119F**	
	-	**+ PAβN**	**-**	**+ PAβN**	**-**	**+ PAβN**	**-**	**+PAβN**
Penicillins								
Penicillin G	>2048	>2048	>2048	>2048	>2048	>2048	>2048	>2048
Amoxycillin	>2048	>2048	>2048	>2048	>2048	>2048	>2048	>2048
Dicloxacillin	512	256	512	256	512	256	512	256
Cephalosporins								
Ceftazidime	0.5	0.5	0.5	1	0.5	0.5	0.5	0.5
Cefoxitin	8	2	8	4	8	4	8	4
Cefepime	0.5	0.125	0.5	0.25	0.5	0.25	0.5	0.125
Carbapenems								
Meropenem	0.25	0.25	0.5	0.5	0.25	0.25	0.125	0.25
Imipenem	4	4	4	4	4	2	4	2
Doripenem	512	128	512	256	512	512	1024	512
Fluoroquinolones								
Norfloxacin	0.125	0.0625	0.125	0.125	0.125	0.125	0.125	0.125
	≤	≤	≤		≤	≤	≤	
Ciprofoxacin	0.03125	0.03125	0.03125	≤ 0.03125	0.03125	0.03125	0.03125	≤ 0.03125
Quinolone carboxylic acid								
	≤	≤	≤		≤	≤	≤	
Enrofloxacin	0.03125	0.03125	0.03125	≤ 0.03125	0.03125	0.03125	0.03125	≤ 0.03125
Sulfonamide-Trimethoprim								
Cotrimoxazol	2	1	2	2	2	2	**4**	1
Aminoglycosides								
Kanamycin	128	256	512	512	256	512	256	256
Gentamicin	0.25	0.25	1	2	1	1	0.5	0.5

The MIC values increase follows the tendency: mutant Y119F ≥ wild type **>** mutant Y119A ≥ E. coli without BpsOmp38 expressed. The MIC values suggested a significant contribution of the mutant Y119F to the antibiotic susceptibility of the *E. coli* strain. Moreover, BpsOmp38 mutant Y119F was found to exhibit greater resistant to co-trimoxazol (4 µg/ml) when compared with the MIC breakpoint of CASFM standard (sensitive ≤ 2 µg/ml, resistant **>** 8 µg/ml).

4. สรุปผลการทดลอง

In this study, we cloned the gene encoding outer membrane protein, namely BpsOmp38, of *Burkholderia pseudomallei*. A topology prediction and liposome-swelling assay suggested that recombinant BpsOmp38 comprises a β-barrel structure and acts as a general diffusion porin. Single channel recordings using planar black lipid membrane (BLM) reconstitution demonstrated that BpsOmp38 could form a channel with average conductance of 2.7 nS. High time resolution BLM measurements displayed ion current blockages of seven antimicrobial agents in a concentration-dependent manner with the translocation on-rate (kon) following the order: norfloxacin >> ertapenem > ceftazidime > cefepime > imipenem > meropenem > penicillin G. The dwell time of a selected antimicrobial agent (ertapenem) decayed exponentially with increasing temperature. The energy barrier for the ertapenem binding to the affinity site inside the BpsOmp38 channel was estimated from the Arrhenius plot to be 12 kT and for the ertapenem release to be 13 kT at +100 mV. The BLM data obtained from this study provide the first insight into antimicrobial agent translocation through the BpsOmp38 channel.

Topology prediction suggested that Tyr-119 may act as a pore-constricting residue that controls the permeability of hydrophilic species through *Bps*Omp38. Antibiotic susceptibility assay showed that the Omp-deficient *E. coli* expressing BpsOmp38Y119A and Y119F mutants were more susceptible to meropenem and ceftazidime, but less susceptible to doripenem compared to the *E. coli* expressing BpsOmp38 wild-type porin. Liposome-swelling assay suggested that the permeability rates of neutral sugars through the *Bps*Omp38 variants increased as the molecular weight of the sugar decreased. However, the permeation of antibiotics through the *Bps*Omp38 porins showed modest correlation between the molecular weight and the diffusion rates were observed as follows: amoxicillin (M_r 365) > norfloxacin (M_r 319) > gentamycin (M_r 478) > meropenem (M_r 384) > ceftazidime (M_r 547). The result suggested that not only the pore diameter, but the interactions between the antibiotic and the residues lining the pore interior also play an important role in the permeation of those antibitoitcs through *Bps*Omp38. In conclusion, the present study demonstrates, for the first time, the ion channel properties of the outer membrane porin BpsOmp38 derived from the highly virulent and drug resistant bacterium *B. pseudomallei*. High-time resolution analysis of different classes of antimicrobial agents provided initial insights into the transport mechanisms of antimicrobial agents through the BpsOmp38 channel. The results obtained from this study may pave the way for further studies based on thoughtfully, genetically-engineered BpsOmp38 and those that exploit joint applications of structural, functional and computational assays to develop highly efficacious drugs against clinical melioidosis.

5. เอกสารอ้างอิง

[1] W. J. Wiersinga, T. van der Poll, N. J. White, N. P. Day, S. J. Peacock (2006) *Melioidosis: insights into the pathogenicity of Burkholderia pseudomallei*. Nature Rev. Microbiol. 4, 272.

[2] A. C. Cheng, B. J. Currie (2005) *Melioidosis: Epidemiology, pathophysiology, and management.* Clin. Microbiol. Rev. 18, 383.

[3] S. Galdiero, M. Galdiero, C. Pedone (2007) *Beta-barrel membrane bacterial proteins: Structure, function, assembly and interaction with lipids*. Curr. Protein Pept. Sci. 8, 63.

[4] H. Nikaido (2003) *Molecular basis of bacterial outer membrane permeability revisited*. Microbiol. Molec. Bio.Rev. 67, 593.

[5] G. E. Schulz (2002) *The structure of bacterial outer membrane proteins*. Biochim. Biophys. Acta, Biomembr. 1565, 308.

[6] J. Siritapetawee, H. Prinz, C. Krittanai, W. Suginta (2004) Expression and refolding of Omp38 from *Burkholderia pseudomallei* and *Burkholderia thailandensis*, and its function as a diffusion pore. Biochem. J. 384, 609.

[7] J. Siritapetawee, H. Prinz, W. Samosornsuk, R. H. Ashley, W. Suginta (2004) *Functional, reconstitution, gene isolation and topology modelling of porins from Burkholderia pseudomallei and Burkholderia thailandensis*. Biochem. J. 377, 579.

[8] K. Zeth, K. Diederichs, W. Welte, H. Engelhardt (2000) Crystal structure of Omp32, the anion-selective porin from *Comamonas acidovorans*, in complex with a periplasmic peptide at 2.1 A resolution. Structure 15,981.

[9] A. W. J. Jenney, G. Lumb, D. A. Fishera, B. J. Currie (2001) *Antibiotic susceptibility of Burkholderia pseudomallei from tropical northern Australia and implications for therapy of melioidosis*. Int. J. Antimicrob. Agents 17, 109.

[10] A. J. H. Simpson, S. M. Opal, J. M. Angus, J. E. Palardy, N. A. Parejo, W. Chaowagui, N. J. White (2000) *Differential antibiotic-induced endotoxin release in severe melioidosis*. J. Infect. Dis. 181, 1014.

[11] R. A. Moore, D. DeShazer, S. Reckseidler, A. Weissman, D. E. Woods (1999) *Efflux-mediated aminoglycoside and macrolide resistance in Burkholderia pseudomallei*. Antimicrob. Agents Chemother. 43, 465.

[12] J. J. LiPuma (2007) *Update on Burkholderia nomenclature and resistance.* Clin. Microbiol. Newslett. 29, 65.

[13] A. Kumar, H. P. Schweizer (2005) *Bacterial resistance to antibiotics: Active efflux and reduced uptake*. Adv. Drug Delivery Rev. 57, 1486.

[14] X. Z. Li, H. Nikaido (2004) *Efflux-mediated erential antibiotic-induced endotoxin release in severe melioidosis*. J. Infect. Dis. 181, 1014-1019.

[15] K. Poole (2002) *Mechanisms of bacterial biocide and antibiotic resistance*. J. Appl. Microbiol. 92, 555.

[16] M. Luckey, H. Nikaido (1980) *Specificity of diffusion channels produced by X phage receptor protein of Escherichia coli*. Proc. Natl. Acad. Sci. USA 77, 167.

[17] C. Danelon, E.M. Nestorovich, M. Winterhalter, M. Ceccarelli, S.M. Bezrukov (2006) *Interaction of Zwitterionic Penicillins with the OmpF Channel Facilitates their Translocation.* Biophys. J. 90, 1617.

[18] A. Schulte, S. Ruamchan S, P. Khunkaewla P, W. Suginta (2009) The outer membrane Protein VhOmp from *Vibrio harveyi*: The pore-forming properties in black lipid membranes. *J. Membr. Biol.* (In press)

[19] A. Prilipov, P.S. Phale, P. Van Gelder, J.P. Rosenbusch, R. Koebnik (1998) Coupling site-directed mutagenesis with high-level expression: large scale production of mutant porins from *E. coli*, FEMS Microbiol. Lett. 163,65.

[20] R.M. Garavito, J.P. Rosenbusch (1986) Isolation and crystallization of bacterial porin, Methods Enzymol. 125 (1986) 309.

[21] J.P. Rosenbusch (1974) Characterization of the major envelope protein from *Escherichia coli*. Regular arrangement on the peptidoglycan and unusual dodecyl sulfate binding, J. Biol. Chem. 249 (1974) 8019.

[22] B. Lugtenberg, L. Van Alphen (1983) Molecular architecture and functioning of the outer membrane of *Escherichia coli* and other gram-negative bacteria, Biochim. Biophys. Acta 737,51.

[23] E.M. Nestorovich, C. Danelon, M. Winterhalter, S.M. Bezrukov (2002) Designed to penetrate: time-resolved interaction of single antibiotic molecules with bacterial pores, Proc. Nat. Acad. Sci. U.S.A. 99,9789.

[24] K.R. Mahendran, E. Hajjar, T. Mach, M. Lovelle, A. Kumar, I. Sousa, E. Spiga, H. Weingart, P. Gameiro, M. Winterhalter, M. Ceccarelli (2010) Molecular basis of enrofloxacin translocation through OmpF, an outer membrane channel of *Escherichia coli*-when binding does not imply translocation, J. Phys. Chem. B. 114,5170.

[25] N. Eswar, B. Webb, M. A. Marti-Renom, M. S. Madhusudhan, D. Eramian, M. Y. Shen, U. Pieper, A. Sali (2007) Comparative protein structure modeling using MODELLER, Curr. Protoc. Protein. Sci. Chapter 2, Unit 2.9

[26] B.Wallner, A. Elofsson (2005) Can correct proteins models be identified? Protein Sci. 12,1073.

[27] M. Luckey M, H. Nikaido (1980) Diffusion of solutes through channels produced by phage

lambda receptor protein of Escherichia coli: inhibition by higher oligosaccharides of maltose series. Biochem. Biophys. Res. Commun. 93,166.

[28] F. Yoshimura, H. Nikaido (1985) Diffusion of beta-lactam antibiotics through the porin channels of *Escherichia coli* K-12. Antimicrob. Agents. Chemother. 27,84.

[29] Q.T. Tran, K.R. Mahendran, E. Hajjar, M. Ceccarelli, A.D. Regli, M. Winterhalter, H. Weingart, J.M. Pages (2010) Implication of porins in ß -lactam resistance of *Providencia stuartii*. J. Biol. Chem. 285,32273.

[30] K. Zeth, K. Diederichs, W. Welte, H. Engelhardt (2000) Crystal structure of Omp32, the anion-selective porin from *Comamonas acidovorans*, in complex with a periplasmic peptide at 2.1 A resolution. Structure. 15,981.

[31] S. Pezeshki, C. Chimerel, A.N. Bessonov, M. Winterhalter, U. Kleinekathöfer (2009) Understanding ion conductance on a molecular level: an all-atom modeling of the bacterial porin OmpF, Biophys. J. 97,1898.

ภาคผนวก

ผลงานวิจัยตีพิมพ์และเผยแพร่

- <u>ผลงานตีพิมพ์จากข้อเสนอโครงการโดยตรง</u>

1. **Suginta W*,** Mahendran KR, Chumjan W, Hajjar E, Schulte A, Winterhalter M and Weingart H. (2011) Molecular analysis of antimicrobial agent translocation through the membrane porin *Bps*Omp38 from an ultraresistant *Burkholderia pseudomallei* strain. **BBA-Biomembr**. 1808, 1552-1559 (IF2011 = 3.99)
2. Aunkhum A and **Suginta W***. Mutation of the pore-restriction residue alters the channel properties of BpsOmp38 from *Burkholederia pseudomallei*. Manuscript in preparation for submission to **BBA-Biomembr (first draft complete, working on final revision and submission)**.

- <u>ผลงานตีพิมพ์ที่เกี่ยวข้อง</u>

3. **Suginta W***, Chumjan W, Mahendran KR, Janning P, Schulte A & Winterhalter A. (2013) Molecular uptake of chitooligosaccharides through chitoporin from the marine bacterium *Vibrio harveyi*. **PLoS One.** 8, e55126. (IF2011 = 4.091)
4. **Suginta W** & Smith MF* (2013) Single-molecule trapping dynamics of sugar-uptake channels in marine bacteria. **Phys Rev Lett.** 110, e238102. (IF2011 = 7.37)

- <u>ผลงานวิจัยอื่นที่ได้รับการสนับสนุนจากทุนวิจัยนี้</u>

5. **Suginta W**, Khunkaewla P & Schulte A* (2013) Electrochemical biosensor applications of the polysaccharides chitin and chitosan. Chem Rev. 113, 5458-5479. (IF2011 = 40.197)

- <u>ผลงานตรงที่นำเสนอในรูปวาจาหรือโปสเตอร์</u>

1. <u>**Suginta W***</u>. Bacterial chitinases and porins. Special seminar, School of Biomolecular and Biomedical Science, Conway Institute of Biomolecular and Biomedical Research, University College Dublin, Ireland, November 23rd, 2009**. *Invited talk***.
2. <u>**Suginta W***</u>, Antibiotic transport through outer membrane protein channel of the melioidosis bacterium *Burkholderia pseudomallei*. Special seminar, School of Science and Engineering, Jacobs University Bremen, February 15th, 2010. ***Invited talk***.
3. <u>**Suginta W***</u>, Mahendran KR, Chumjan W, Hajjarc E, Schulte A, Weingart H, Winterhalter M. Study of Antibiotic Resistance through a Porin Channel of the Melioidosis Bacterium *Burkholderia pseudomallei*. TRF Annual Meeting, October 2012. ***Oral presentation***.
4. <u>Aunkhum A</u> and **Suginta W***. Mutation of the pore-restriction residue alters the permeability of the outer membrane porin BpsOmp38 of *Burkholderia pseudomallei*. The 5th Annual Symposium of the Protein Society of Thailand, Conventional Center,

Chulabhorn Research Institute Bangkok, Thailand, August 5-7th, 2013. ***3rd prize poster presentation award***.

5. **Suginta W***, Mahendran KR, Weingart H, Chumjan W, Hajjar E, Schulte A and Winterhalter M. High-time resolution analysis of antibiotic translocation through BpsOmp porin from the highly drug-resistant bacterium *Burkholderia pseudomallei*. The 5th Annual Symposium of the Protein Society of Thailand, Conventional Center, Chulabhorn Research Institute Bangkok, Thailand, June 23rd-26th, 2010, p77. ***Poster presentation***.
6. **Suginta W***, Mahendran KR, Chumjan W, Weingart H and Winterhalter M. Molecular transport through the outer membrane porin of the Melioidosis bacterium *Burkholderia pseudomallei*. North German Biophysical Meeting, January 2010, Borstel, Germany. ***Poster presentation***.
7. **Suginta W***, Mahendran KR, Chumjan W, Weingart H and Winterhalter M. Molecular transport through the outer membrane porin of the Melioidosis bacterium *Burkholderia pseudomallei*, Alexander von Humboldt Network Meeting, Odenburg, Germany, October 7th-9th, 2009. ***Poster presentation*.**

- **ผลงานที่เกี่ยวข้องที่นำเสนอในรูปวาจาหรือโปสเตอร์**

8. **Suginta W*.** Chitooligosaccharide uptake through chitoporin: An evolutionary adaptation of marine bacteria to thrive under nutrient depleted conditions. 10th Asia-Pacific Chitin-Chitosam Symposiun, Yonako, Japan, October 4-8th, 2013. ***Invited talk*.**
9. **Chumjan W,** Schulte A, Mahendran KR, Winterhalter M and Suginta W*. Chitin Catabolism in the Marine Bacterium *Vibrio harveyi* 650 (Part I): Identification of a Chitooligosaccharide-Specific Porin. The 13th FAOBMB Congress, Bangkok International Trade & Exhibition Center, Bangkok, Thailand, November 25-29th, 2012, p212. ***Outstanding poster presentation award.***
10. Chumjan W, Schulte A, Weingart H, Benz R, Winterhalter M and Suginta W*. Chitoporin (ChiP) from Vibrio harveyi 650: Gene isolation, recombinant expression and molecular translocation of chitin oligosaccharides. The 6th Annual Symposium of the Protein Society of Thailand, Conventional Center, Chulabhorn Research Institute Bangkok, Thailand, Aug30th-Sept2nd, 2011, p75. ***Outstanding poster presentation award.***

***เครื่องหมายแสดงผู้เขียนเป็น corresponding author**

Biochimica et Biophysica Acta 1808 (2011) 1552–1559

Contents lists available at ScienceDirect

Biochimica et Biophysica Acta

journal homepage: www.elsevier.com/locate/bbamem

Molecular analysis of antimicrobial agent translocation through the membrane porin *Bps*Omp38 from an ultraresistant *Burkholderia pseudomallei* strain

Wipa Suginta [a,*], Kozhinjampara R. Mahendran [b], Watcharin Chumjan [a], Eric Hajjar [c,1], Albert Schulte [a], Mathias Winterhalter [b], Helge Weingart [b,*]

[a] Biochemistry-Electrochemistry Research Unit, Schools of Chemistry and Biochemistry, Institute of Science, Suranaree University of Technology, Nakhon Ratchasima 30000, Thailand
[b] School of Engineering and Science, Jacobs University Bremen, D-28759 Bremen, Germany
[c] Instituto Officina dei Materiali/CNR UOS SLACS and Department of Physics, University of Cagliari, I-09042 Monserrato, Italy

ARTICLE INFO

Article history:
Received 10 August 2010
Received in revised form 27 October 2010
Accepted 28 October 2010
Available online 13 November 2010

Keywords:
Black lipid membrane reconstitution
Burkholderia pseudomallei
Melioidosis
Outer membrane protein
Porin

ABSTRACT

Burkholderia pseudomallei (*Bps*) is a Gram-negative bacterium that causes melioidosis, an infectious disease of animals and humans common in northern and north-eastern parts of Thailand. Successful treatment of melioidosis is difficult due to intrinsic resistance of *Bps* to various antibacterial agents. It has been suggested that the antimicrobial resistance of this organism may result from poor permeability of the active compounds through porin channels located in the outer membrane (OM) of the bacterium. In previous work, a 38-kDa protein, named "*Bps*Omp38", was isolated from the OM of *Bps*. A topology prediction and liposome-swelling assay suggested that *Bps*Omp38 comprises a β-barrel structure and acts as a general diffusion porin. The present study employed black lipid membrane (BLM) reconstitution to demonstrate the single-channel conductance of the trimeric *Bps*Omp38 to be 2.7 ± 0.3 nS in 1 M KCl. High-time resolution BLM measurements displayed ion current blockages of seven antimicrobial agents in a concentration-dependent manner with the translocation on-rate (k_{on}) following the order: norfloxacin ≫ ertapenem > ceftazidime > cefepime > imipenem > meropenem > penicillin G. The dwell time of a selected antimicrobial agent (ertapenem) decayed exponentially with increasing temperature. The energy barrier for the ertapenem binding to the affinity site inside the *Bps*Omp38 channel was estimated from the Arrhenius plot to be 12 kT and for the ertapenem release to be 13 kT at + 100 mV. The BLM data obtained from this study provide the first insight into antimicrobial agent translocation through the *Bps*Omp38 channel.

1. Introduction

Burkholderia pseudomallei (*Bps*) is a soil-dwelling Gram-negative bacterium commonly found in Southeast Asia and Northern Australia and a cause of a deadly disease of mammalian species termed melioidosis [1–4]. Patients infected with *Bps* usually develop skin ulcers, visceral abscesses, pneumonia and septicemia that imperatively require immediate antimicrobial treatment to avoid fatal progression of the disease. Very often, antimicrobial treatment is quite a challenge due to the high intrinsic broad spectrum resistance that most *Bps* strains exhibit towards a broad spectrum of antimicrobial agents including but not limited to β-lactam antibiotics, aminoglycosides, macrolides, and cephalosporins [1–4]. Due to the high incidence of drug resistance and very high virulence, *Bps* is regarded a potential bioterrorism and warfare agent [5]. As such, this organism has been listed by the US Centre for Disease Control and Prevention as a category B health hazard [6,7]. Clinical and security concerns associated with *Bps* have justified intensive research in attempt to address the structural and functional organization of this pathogen as a prelude to the design of novel and efficacious anti-*Bps* therapeutic agents. Most of ongoing studies include characterization of biological and pathophysiological aspects of the agent, unraveling the mechanisms of genomic plasticity and evolution, as well as understanding the molecular mechanisms underlying drug resistance. The publication of the sequences of the entire *Bps* genome [8], as well as data from drug susceptibility testing [9–12], and recent reports on *Bps* vaccines [13–15] are important developments in the search for an effective anti-melioidosis treatment.

Current scientific evidence suggests that *Bps* successfully utilizes the strategy of genetic evolution, modified protein expression and/or mutation more than most other bacteria. These features underscore the ability of the pathogen to establish troublesome resistance against many antimicrobial agents. Some of the mechanisms of drug resistance include: alteration of intracellular drug action sites, generation of enzymes for the modification and/or complete degradation of drug molecules within the cytosol, and restriction of intracellular drug accumulation through impaired uptake and/or enhanced drug efflux [16–19].

* Corresponding authors.
E-mail addresses: wipa@sut.ac.th (W. Suginta), h.weingart@jacobs-university.de (H. Weingart).
[1] Present address: Biozentrum University of Basel, SIB Swiss Institute of Bioinformatics, 4056 Basel, Switzerland.

0005-2736/$ – see front matter © 2010 Elsevier B.V. All rights reserved.
doi:10.1016/j.bbamem.2010.10.018

In the present study, we addressed limitation of cellular drug uptake which in a number of other bacteria is associated with reduced molecular transport of the active compounds through bacterial outer membrane protein (Omp) channels. Also known as porins, Omp channels are typical β-barrel protein structures that independently or as oligomeric units are inserted into the outer lipid bilayer of the bacterial cell wall to form pores through which extracellular species can diffuse and gain access to the periplasmic space and cytosol [20–22]. Membrane trafficking via porins has been elegantly measured at molecular level using the black lipid membrane (BLM) technique [23–25]. In BLM experiments, the parameter measured is the voltage-induced charge flow through an artificial lipid bilayer membrane that separates two electrolyte compartments and one that has the study porin artificially inserted. Recordings of the transmembrane current at microsecond time resolution enable visualization of insertions of the porin in their open state as stepwise increases in the signal. Movement of individual drug/other molecules through a stably open unit is detected by means of transient current fluctuations derived from physical channel blockade during the residence time of compounds traveling through the porin. Mechanistically, bacterial cells can counteract the influx of drug molecules through reduction of the total number of porins in their outer membrane, a decrease in the cross-sectional dimension of the protein channels, and/or through modification of the electrostatics and/or hydrophobicity of the pore interior through point mutations of the amino acids lining the protein pores. Quantitative correlation of the entry of specific drug molecules with a firm structural and predictive computational analysis may lead to a better understanding of the molecular basis of antimicrobial agent permeability, facilitating the design of effective drugs that have greater penetrating power [26].

While functional [27–32] and computational [33–35] BLM studies focused on membrane drug permeation have been performed on a number of bacterial porins, no similar research has investigated analogous proteins from clinically important *Bps* strains. In previous work, an Omp with an apparent molecular weight (MW) of 38 kDa, referred to as *Bps*Omp38, was isolated from the *Bps* cell wall [36,37]. Topology prediction and molecular modeling suggested that *Bps*Omp38 has a β-barrel structure, a feature that is common among membrane porins. Subsequently, a liposome-swelling assay on this protein confirmed its channel-forming properties [37]. In the present study, a detailed functional characterization of the *Bps*Omp38 porin by BLM-based single ion-channel analysis is described. Ion current measurements were carried out in the absence and in the presence of seven different antimicrobial agents as additional diffusing species in the membrane-bathing electrolyte. The differences in the ability of the selected drugs to move through open *Bps*Omp38 pores and their kinetic behavior are discussed in the context of molecular drug/porin interactions.

2. Materials and methods

2.1. BpsOmp38 expression and purification

The *E. coli* strain BL21 (DE3) Omp8 was a gift from Ralf Koebnik, Laboratoire Génome et Développement des Plantes, Universit é de Perpignan via Domitia, Montpellier, France. This strain of *E. coli* does not express the major outer membrane proteins LamB, OmpA, OmpC and OmpF [38]; it was experimentally transformed with the recombinant plasmid pET23d.*Bps*Omp38. Purification of the recombinant *Bps*Omp38 followed a modified version of protocols described by Garavito and Rosenbusch [39] and Rosenbusch [40]. In brief, transformed cells were grown at 37 °C in Luria–Bertani (LB) liquid medium containing 100 μg/ml ampicillin. At an OD_{600} reading of 0.5, IPTG (isopropyl β-D-thiogalactoside) was added to a final concentration of 0.4 mM. Cell growth was continued for a further 6 h and then cells were harvested by centrifugation at 2948 × *g* for 10 min. The cell pellet was resuspended in buffer containing 20 mM Tris–HCl, pH 8.0, 2.5 mM $MgCl_2$, 0.1 mM $CaCl_2$, 10 μg/ml DNase I and 10 μg/ml RNase A and then disrupted using a high-pressure homogenizer (EmulsiFlex-C3, Avestin Europe, Mannheim, Germany). The recombinant *Bps*Omp38 was further extracted from the peptidoglycan layer using sodium dodecyl sulfate (SDS)-containing solutions based on a procedure reported by Lugtenberg and Alphen [41]. Briefly, SDS was added to the cell suspension to a final concentration of 2% (v/v) and incubation was carried out for 1 h at 60 °C with gentle shaking. The crude extract was then centrifuged at 39,636 × *g* for 60 min at 4 °C. The pellet, which at this stage included the cell envelopes, was resuspended in 20 mM phosphate buffer, pH 7.4 (PBS), containing 0.125% (v/v) octyl-POE (*n*-octyl-polyoxyethylene; ALEXIS Biochemicals, Lausanne, Switzerland). The suspension was incubated at 37 °C with gentle shaking for 60 min and then centrifuged at 109,564 × *g* at 4 °C for 40 min. The new pellet, now rich in outer membranes, was resuspended in 20 mM phosphate buffer, pH 7.4 containing 3% (v/v) octyl-POE and the suspension incubated at 37 °C with shaking at 250 rpm for 1 h to solubilize the porin. Insoluble material was removed by centrifugation at 109,564 × *g* at 20 °C for 40 min and the porin-rich supernatant concentrated using Amicon Ultra-15 centrifugal filter devices with a nominal MW limit of 30 kDa (Millipore, Schwalbach, Germany). Amicon centrifugal filters were also used to exchange the original preparation buffer with 20 mM PBS, containing 1% (v/v) octyl-POE. Aliquots of the final protein sample were used for absorbance measurement at 280 nm for the determination of protein concentration using NanoDropT 1000 Spectrophotometer (Thermo Fisher Scientific, Wilmington, DE, USA) and for SDS–polyacrylamide gel electrophoresis (SDS–PAGE) for the assessment of sample purity.

2.2. Lipid bilayer measurements and single-channel analysis

The following chemicals were used: NaCl, KCl, MES, *n*-pentane, and hexadecane (Sigma-Aldrich, Hamburg, Germany); ceftazidime, norfloxacin, and penicillin G (Sigma-Aldrich); cefepime, imipenem, meropenem, and ertapenem (Basilea Pharmaceutica Ltd., Basel, Switzerland); and 1,2-diphytanoyl-*sn*-glycero-3-phosphatidylcholine (DPhPC) (Avanti Polar Lipids, Alabaster, AL, USA). Double distilled and deionized water was used to prepare chemical reagents and the freshly made solutions passed through a 0.4-μm filter. The drug stock solutions for translocation experiments were prepared with 1 M KCl in electrolyte buffer (20 mM phosphate buffer, pH 7.0 or in 20 mM HEPES, pH 8.0).

Lipid bilayer measurements and single-channel analysis were performed as described elsewhere [27–32]. Briefly, a cell with a 40–60 μm diameter aperture in a 15-μm-thick Teflon partition provided a two-compartment black lipid membrane (BLM) chamber and two silver–silver chloride electrodes at either side of the dividing wall allowed voltage control of solvent-free planar lipid bilayers that were formed using a solution of DPhPC in pentane. Low levels of the study *Bps*Omp38 channel were introduced to the *cis* or *trans* side of the bilayers by adding the protein stock solution of about 1–2 μg/ml containing 1% (v/v) octyl-POE (ALEXIS, Switzerland). In the trials addressing the temperature dependence of drug translocation, a peltier element (Dagan Corporation, Minneapolis, MN, USA) was used for accurate temperature regulation of the BLM chamber. At an applied transmembrane voltage of +50 mV, spontaneous channel insertion was usually obtained within a few minutes after adding the protein solution. Conductance measurements were performed using an Axopatch 200B amplifier (Molecular Devices, Sunnyvale, CA, USA) in the voltage clamp mode and the internal filter at 10 kHz. Amplitude, probability, and single-channel analyses were performed using pClamp v.10.0 software (Molecular Devices). Control experiments (refer to Supplementary S3, upper left recording) showed no

dependence of the *Bps*Omp38 conductance and open channel noise on the presence of the buffer alone.

Black lipid bilayer measurements with *Bps*Omp38 from an earlier preparation with mass spectrometry (MS) identification (Supplementary S1) established that the single-channel conductance of the targeted reconstituted protein channel is about 2.7 ± 0.3 nS in 1 M KCl. A channel of identical conductance also routinely appeared when freshly formed solvent-free DPhPC bilayer membranes were exposed to the protein prepared by the procedure described in the preceding section. Accordingly, translocation of drug molecules was analyzed in recordings of this particular channel. Another channel that frequently incorporated during the BLM experiments was not used for the translocation studies after its small conductance (0.3 nS in 1 M KCl) and MS data suggested it was a maltoporin.

2.3. Porin homology modeling

The structural model of recombinant *Bps*Omp38 was built based upon the Modeller suite of programs [42]. Initially, several iterations of the PSI-BLAST protein sequence search program in the pdb database were performed to allow detection of remote homologues of the *Bps*Omp38 porin. Only the templates with non-redundant structures were kept and further used for building the homology model. Such templates included the pdb codes 3K1B (OmpF), 2IXX (OmpC), 1E54 (Omp32), 1OSM (Ompk36) and 3A2R (PorB). A multiple-sequence alignment revealed a complete coverage of the homology sequence, although only about 24% sequence identity was observed between the *Bps*Omp38 and the template amino acid residues. Fifty structural models of the *Bps*Omp38 trimers were further generated by the Modeller program, from which the "representative model" was defined as the one that minimized both the overall 'Modeller objective function' and the 'Dope score evaluation function'. Finally, the "final best model" was assessed with the energetic based validation suite ProQ [43] and the geometric based PROCHECK, with the latter showing only 2.8% of Ramachandran disallowed regions and absence of close (or "bad") contacts.

3. Results and discussion

We have previously reported the recombinant expression of the *Bps*Omp38 gene in *E. coli* BL21 Origami (DE3) cells [36,37]. The recombinant *Bps*Omp38 protein, which was in the form of inclusion bodies, was further refolded into trimeric form using 10% (w/v) Zwittergent™ 3-14. In the present study, the *Bps*Omp38 gene, including a 20-amino acid signal peptide fragment, was subcloned into a pET23d(+) vector so it could be incorporated and fully expressed as a fully functional trimeric protein in the cell wall of the mutant *E. coli* BL21 (DE3) Omp8 strain. After extraction by 2% SDS and solubilization in 1% (v/v) octyl-POE, SDS–PAGE analysis demonstrated migration of the extracted porin as a protein band with an apparent MW of 100 kDa (Fig. 1A, lane 2). This was assumed to be the trimeric form of *Bps*Omp38. Upon heat treatment at 100 °C for 10 min, the presumed trimer was denatured and a new band with apparent MW of 35 kDa appeared as expected for the *Bps*Omp38 monomer (Fig. 1A, lane 3).

When *Bps*Omp38 was reconstituted in stable DPhPC lipid bilayers, the study protein (porin) behaved like an ion channel and allowed a specific current flow under controlled voltage application. Single trimeric *Bps*Omp38 units in the bilayer membrane showed a characteristic conductance of 2.7 ± 0.3 nS in 1 M KCl/20 mM HEPES pH 8.0 but the channels were prone to close at high transmembrane potentials (above ± 100 mV). A typical membrane current recording that was obtained for a single trimeric *Bps*Omp38 channel at an elevated transmembrane potential of + 150 mV is shown in Fig 1B. Within the time span of a few seconds, the fully open *Bps*Omp38 channel changed sequentially by a three-step process into the fully closed state. This process appeared as a three-stage decrease in conductance signal and confirmed once again the trimeric channel organization that had already been suggested by the SDS–PAGE gel analysis (Fig. 1A). The biological relevance of the successive closure of the individual units of multimeric bacterial porins is poorly understood, bearing in mind that, *in vivo*, the potential difference across the bacterial outer membrane is usually negligible. On the other hand, parameters such as pH, ion composition of the internal and external

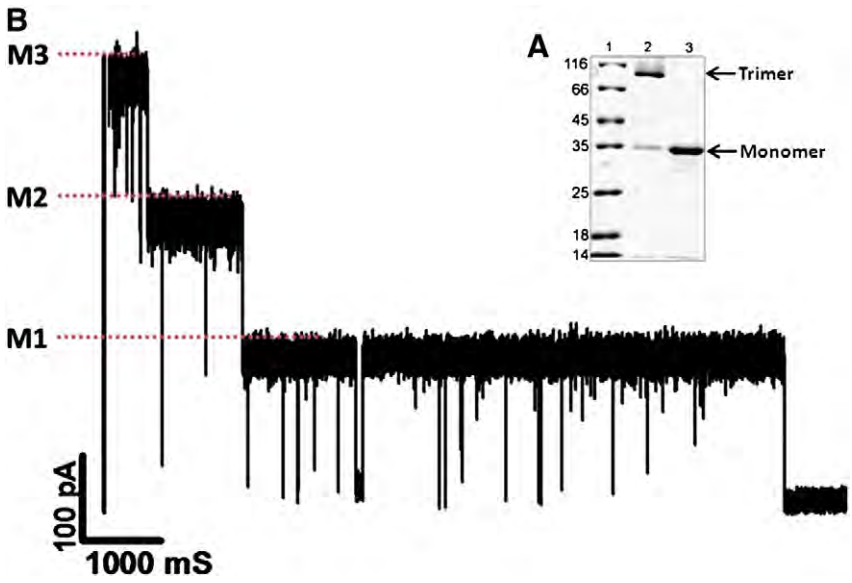

Fig. 1. Trimeric *Bps*Omp38 porin from *Burkholderia pseudomallei*. The recombinant protein was expressed in a mutant *E. coli* BL21 (DE3) Omp8 strain lacking major intrinsic porins, isolated by sodium dodecyl sulfate-extraction and then solubilized by 1% (v/v) octyl-POE in 1 M KCl/20 mM HEPES, pH 8.0. A. Sodium dodecyl sulphate–polyacrylamide gel electrophoresis analysis of recombinant *Bps*Omp38. Track 1: low molecular weight protein markers (PageRuler, Fermentas Inc., USA); Track 2: intact *Bps*Omp38 trimers under non-denaturing conditions; Track 3: *Bps*Omp38 subunit after denaturing condition at 100 °C for 10 min. B. A single-channel recording of the *Bps*Omp38 reconstituted in solvent-free DPhPc membranes. A three-step closure was induced by increasing the applied voltage to + 150 mV.

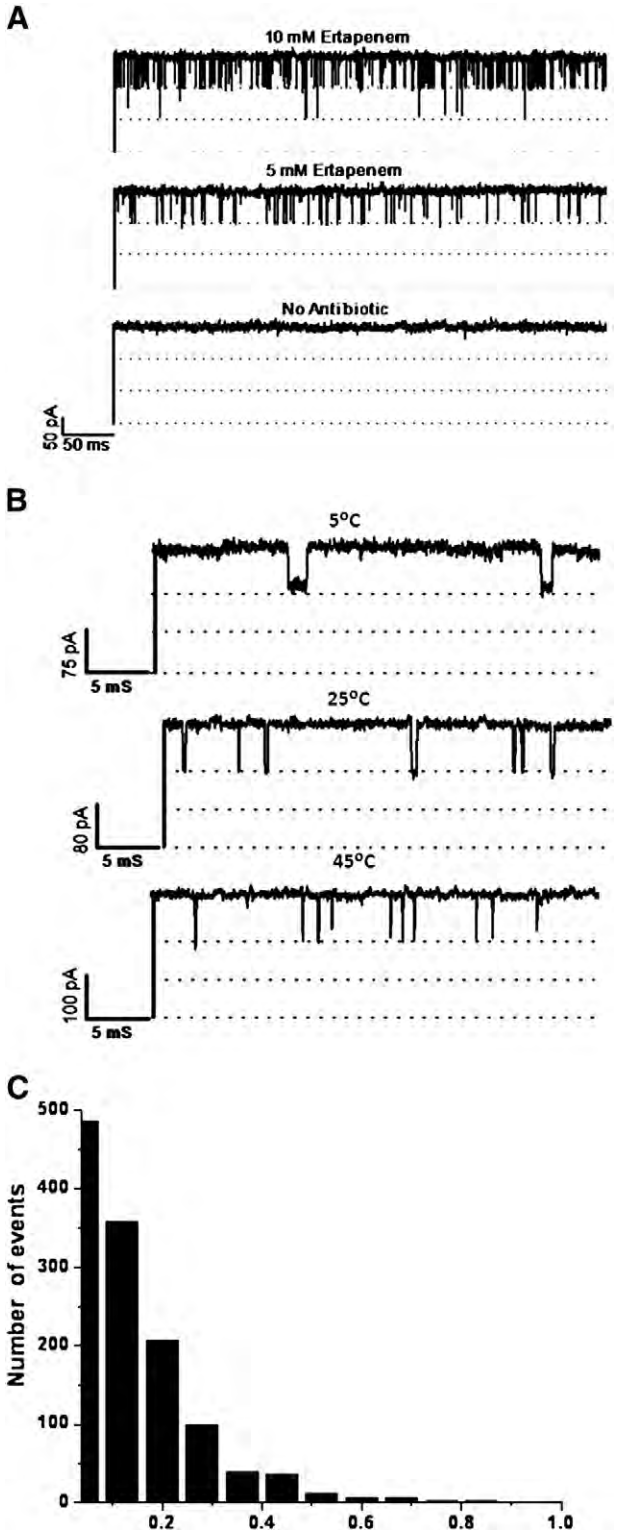

Fig. 2. Kinetic analysis of antimicrobial agent translocation through *Bps*Omp38. A. Effect of ertapenem concentrations. No blockage event was detected when a single trimeric channel was recorded in the absence of antimicrobial agents, whereas complete blockage events were observed as a direct proportion to increased concentrations of ertapenem from 2.5, 5, 7.5, and 10 mM. Here, only 5 and 10 mM concentrations are presented. B. Effect of temperature. An increased number of blockage events were observed upon increases in temperature from 5, 10, 15, 20, 25, 30, 35, 40, and 45 °C. On the other hand, the dwell time of ertapenem translocation decreased exponentially with increasing temperatures. Here, only the BLM recordings at 5, 25 and 45 °C are presented. The single-channel recordings were recorded at +100 mV. Similar ion blockage patterns were also seen with +50 mV (not shown). C. Dwell time histogram. Ertapenem (10 mM) was added on the *cis* side of the lipid membranes. The average dwell time was obtained when the data was fitted using the standard exponential curve fit available in pClampfit v10.0.

Table 1
Kinetic analysis of antibiotic translocation through the *Bps*Omp38 channel.

Antibiotic	k_{on} (s^{-1} M^{-1})	k_{off} (s^{-1})	K (M^{-1})
Penicillin G	n.d.[a]	n.d.	n.d.
Meropenem	25	6700	0.004
Imipenem	150	6700	0.02
Cefepime	1300	5500	0.24
Ceftazidime	4200	7000	0.60
Ertapenem	8200	6900	1.2
Norfloxacin	300,000	10,000	30

[a] n.d. represents non-detectable event.

cell milieu and pressure influence, to a certain extent, the membrane potential and response to variations of these factors may contribute to the physiological significance of channel closing.

To study the translocation of drug molecules through the isolated porin, a potential was applied across the incorporating lipid membranes at which reconstituted *Bps*Omp38 channels predominantly existed in their fully open state. Ion current blockages through the open channels were then analyzed after applying the selected antimicrobial agent to either the *cis* or *trans* side of the bilayer. Drug translocation trials were performed with a set of antimicrobial agents including three β-lactam antibiotics (penicillin G, meropenem, imipenem), two cephalosporins (cefepime, ceftazidime), one fluoroquinolone (norfloxacin) and one carbapenem (ertapenem) (refer to Supplementary S2 for chemical structures). With the exception of penicillin G, all the test antimicrobial agents interacted with the *Bps*Omp38 channel in such a way that spontaneous fast fluctuations of the BLM membrane current were induced. Overall, the number of current deflections in the recording of certain length varied linearly with concentrations that were independent of the type of antibiotic tested. Ertapenem, for example, produced a consistent response as shown in Fig. 2A. In high-time resolution current recordings, the

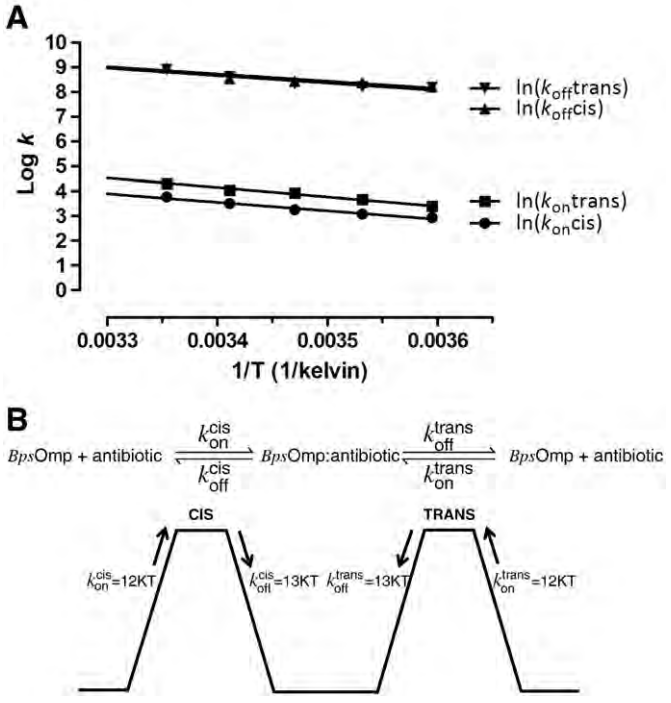

Fig. 3. Arrhenius plots for the ertapenem translocation through *Bps*Omp38 protein pores. A. The logarithmic values of the on-rate and off-rate constants obtained from both *cis* and *trans* sides were plotted as a function of temperature. B. A diagram representing symmetrical values of the energy barriers required for ertapenem binding and releasing from most likely the identical affinity site localized within the *Bps*Omp38 pore.

complete obstruction of individual units of the single trimeric *Bps*Omp38 channel was well resolved. As previously suggested for translocation measurements with other Omps [27–35], the observed current deflections are taken to indicate the brief presence of antibiotic (in this case ertapenem) molecules within the porin channel during the time of their passage, which consequently blocks the ion flux and thus decreases the membrane current. In the absence of ertapenem, the stable open *Bps*Omp38 channel membrane current was typically free of significant fluctuations. At a concentration of 5 mM, ertapenem consistently blocked one monomer of a single trimeric channel for a fraction of a millisecond. Simultaneous blockage of two of the three available monomers at a time became visible at higher concentrations (e.g. 10 mM). A complete and simultaneous blockade of all the three porin subunits was also infrequently observed. For a given concentration of ertapenem, addition of the antibiotic to the *trans* side of the BLM chamber led to about a two-fold

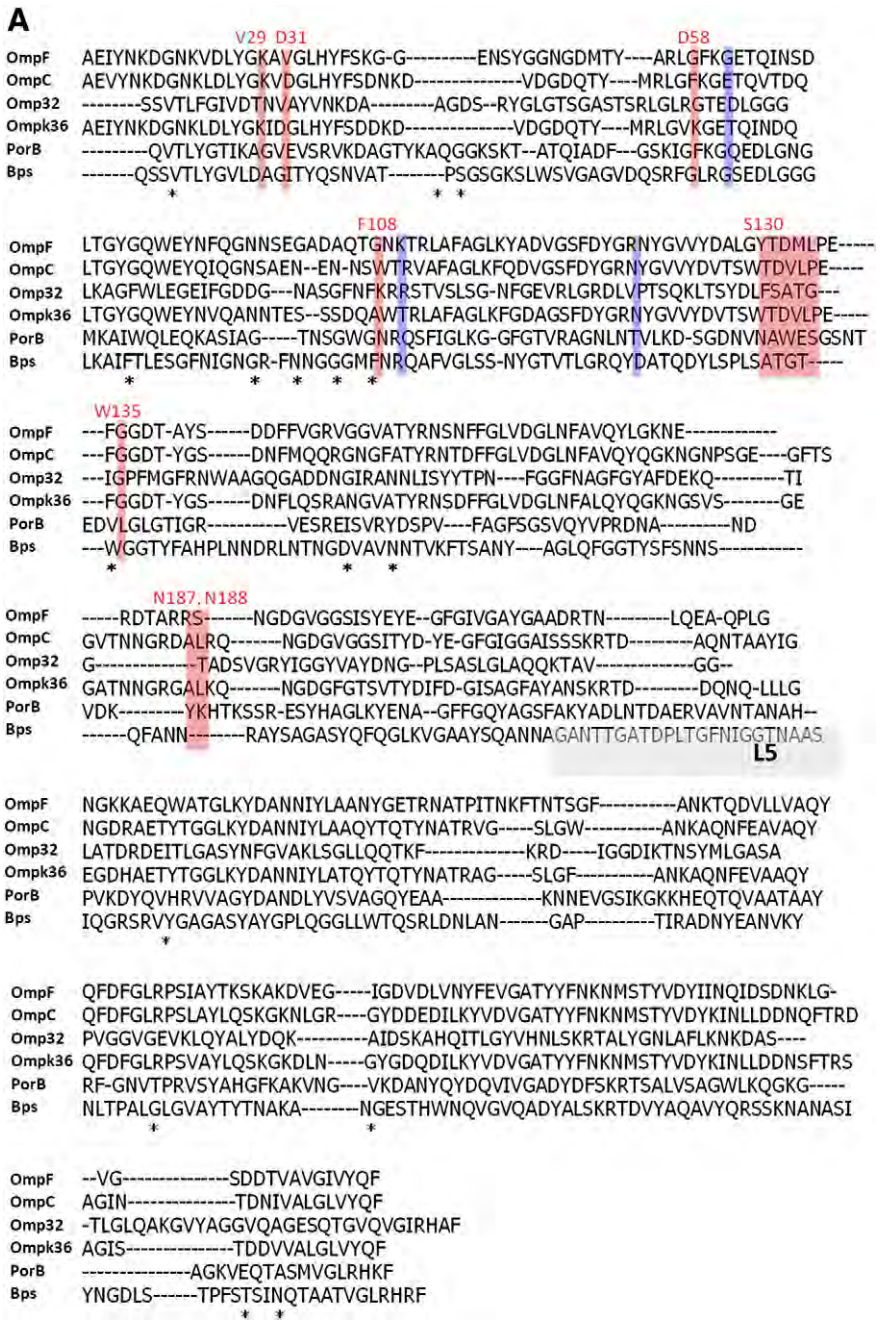

Fig. 4. The modeled structure of *Bps*Omp38 based on multiple templates. A. A multiple alignment of the *Bps*Omp38 sequence lacking the 22-amino-acid-signal peptide with the selected templates was performed by SALIGN from the Modeller suite of programs (see texts). The pdb codes used as the homology templates are: 3K1B (OmpF); 2IXX (OmpC), 1E54 (Omp32); 1OSM (Ompk36); 3A2R (PorB), and the modeled structure of *Bps*Omp38 (*Bps*). Highlights are the conserved residues known to be important for antimicrobial agent translocation of OmpF or OmpC (blue) and the substituted ones (red). Numbering of the *Bps*Omp38 residues follows the complete sequence containing the 20-aa-signal peptide (not included here) (GenBank accession no: AY312416). B. A snapshot of the homology model of *Bps*Omp38 (top view). The lipid bilayer membrane inserted around the porin is illustrated by its molecular surface properties. Differences in the known key residues of OmpF compared to the *Bps*Omp38 (corresponding to the alignment in Fig. 4A) are highlighted with the residues in "sticks" representation and colored green for polar, blue for positively charged, and red for negatively charged. The backbone of the *Bps*Omp38 porin is displayed in cartoons in order to highlight its secondary-structure elements with the loop L3 colored in orange.

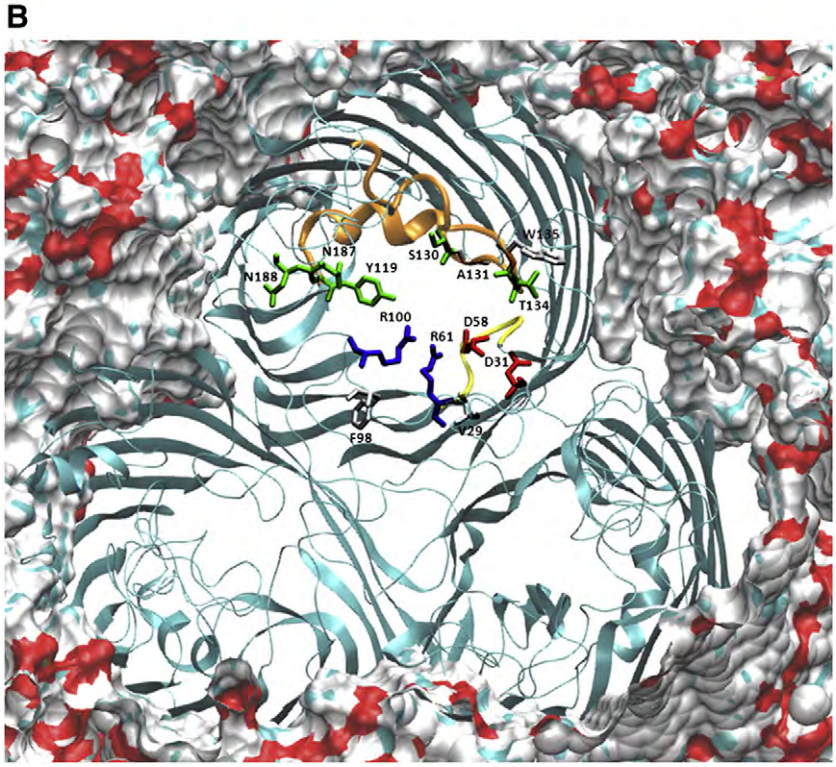

Fig. 4 (*continued*).

higher number of blocking events than when the same amount of the substrate was added to the *cis* side. Black lipid bilayer measurements taken between 5 and 45 °C in the presence and absence of the substrate demonstrated that temperature had a strong impact on the rate of ertapenem translocation through the *Bps*Omp38 channel (Fig. 2B). At non-physiologically low temperature of 5 °C, relatively few membrane current blockages with rather long blocking times of over 1 ms were observed. Increasing the temperature to 45 °C elevated the frequency of current deflections while decreasing the dwell time (τ) of the penetrating molecules. Average τ values for defined conditions in terms of temperature and concentration were obtained through a statistical analysis of raw BLM data and a single-exponential fitting of blockage time histograms as shown in Fig. 2C for ertapenem interaction with *Bps*Omp38 measured at 25 °C. The average τ of ertapenem molecules inside the *Bps*Omp38 channel decreased exponentially with increasing temperature, did not appear to depend on the concentration of the antibiotic, nor was it influenced by the side of the BLM chamber to which the antimicrobial agent was added. Taken together, these observations support the existence of a single affinity site for the ertapenem molecules in the *Bps*Omp38 channel. The rates of channel entry and exit are critical factors in the net flux of an antibiotic through a bacterial Omp pore. The BLM-based observation of the molecular interaction of ertapenem with the *Bps*Omp38 channel at various temperatures and concentrations allowed calculation of: i) the drug binding kinetics and the second-order on-rate constant k_{on} (M^{-1} s^{-1}), ii) the first-order off-rate constant k_{off} (s^{-1}), and iii) the equilibrium binding constant K (the ratio of k_{on}/k_{off}; M^{-1}). Table 1 gives a comprehensive list of the three parameters k_{on}, k_{off} and K for all seven antimicrobial agents whose translocation through the *Bps*Omp38 channel was investigated in the present study (refer to Supplementary S3 for blockage characteristics of the ion flow through *Bps*Omp38 by representatives of each class of the antimicrobial agents). Note that ion blockage by ertapenem applied to the *cis* side of the lipid membrane at a transmembrane potential +100 mV occurred with $k_{on} = 8200\ M^{-1}\ s^{-1}$ and a binding constant of about 1.2 M^{-1}. These values reasonably agree with those for the interaction of ertapenem with the major *Enterobacter aerogenes* Omp36 [30]. Furthermore, the off-rates did not vary significantly for this panel of antimicrobial agents, while a ranking of k_{on} and K saw the three β-lactam antibiotics with rather low values that were clearly at the bottom end, the two cephalosporin drugs at the middle, and carbapenem and fluoroquinolone antibiotics at top positions. Greater values of k_{on} and K indicated that translocation of the newer class of drugs through the *Bps*Omp38 pore took place more rapidly.

Temperature dependence measurements were used to calculate the free energy profile of transporin antibiotic permeation. For ertapenem, the effective energy barriers (E) to reach and cross the internal binding site of a *Bps*Omp38 channel from the *cis* ($E_{on,cis}$) or *trans* ($E_{on,trans}$) side of the bilayer were estimated from the typical Arrhenius plots (Fig. 3A). The analysis of the relevant plots revealed that effective energy barriers $E_{on,cis}$ and $E_{on,trans}$, representing the binding of ertapenem to the affinity site of a *Bps*Omp38 protein pore at +100 mV transmembrane voltage, were estimated to be 12 kT. The Arrhenius plots for the off rates, which allowed calculation of the effective energy barriers $E_{off,cis}$ and $E_{off,trans}$ for the ertapenem release from the affinity site of the *Bps*Omp38 channel at +100 mV, were 13 kT (see Fig. 3B). Estimation of symmetrical values of the energy barriers required for ertapenem binding and release from *cis*-to-*trans* side and from *trans*-to-*cis* side further supports a single affinity site inside the *Bps*Omp38 channel as earlier on suggested.

The homology model of the porin *Bps*Omp38 was built based on five different templates obtained from homologous Gram-negative bacterial porins with non-redundant structures (refer to Materials and methods). Despite an observed low-sequence identity (~24%), the overall fold of the generated *Bps*Omp38 trimers was found to be conserved. The alignment in Fig. 4A shows that the target sequence is completely covered by the different templates and that a few insertions and deletions are all found in the extracellular loops except for the small protrusion of a four-residue loop in the middle of the

second strand of each monomer (see Fig. 4B). This small protrusion was also reported in the previously characterized Omp32 [44].

The *Bps*Omp38 model was compared with the structure of the porin OmpF, for which the structure–function relationship of antibiotic translocation has been extensively studied [34]. Compared with OmpF, however, the amino acid sequences of various regions that participate in pore-forming properties were found to be different. These include the L3 loop that forms the constriction region of the channel, the arginine residues at the mouth of the OmpF channel, and the basic cluster in the anti-L3 side. In the case of the *Bps*Omp38 channel, more acidic residues are observed instead in such regions. Within the known key residues of OmpF that were aligned with *Bps*Omp38, segments with conserved or amino acid substitutions are highlighted as shown in Fig. 4A.

Fig. 4B is a graphic representation of the modeled *Bps*Omp38 trimeric structure, when incorporated into phospholipid bilayer membranes. Highlights indicate an obstructing internal protrusion, as well as the polar to acidic character of certain channel wall residues that point towards the lumen of the pore. It is predictable that the substitutions from OmpF to *Bps*Omp38 of the residues: K16V29, V20D31, K80F108, D113S130, F118W135, R167N187, and R168N188 may have an effect on drug transport through the *Bps*Omp38 porin (see Fig. 4B). However, this hypothesis has to be confirmed by a combined approach, including microbiological assays, site-directed mutations and biophysical measurements, together with molecular dynamic simulations of antibiotic transport as previously described for OmpF [34,35].

In conclusion, the present study demonstrates, for the first time, the ion-channel properties of the outer membrane porin *Bps*Omp38 derived from the highly virulent and drug resistant bacterium *B. pseudomallei*. High-time resolution analysis of different classes of antimicrobial agents provided initial insights into the transport mechanisms of antimicrobial agents through the *Bps*Omp38 channel. We highly recommend further studies that base on thoughtfully genetically engineered *Bps*Omp38 and those that exploit joint applications of structural, functional and computational assays to develop highly efficacious drugs against clinical melioidosis.

Acknowledgments

This research was financially supported by the Alexander von Humboldt Foundation (Germany) through the Alexander von Humboldt Fellowships for Experienced Researchers, the Thailand Research Fund (Grant no: RMU5380055). This was supplemented by Suranaree University of Technology (Grant no: SUT 1-102-52-24-02) to WS and by the EU Grant MRTN-CT-2005-019335 (translocation) to EH.

Appendix A. Supplementary data

Supplementary data to this article can be found online at doi:10.1016/j.bbamem.2010.10.018.

References

[1] W.J. Wiersinga, T. van der Poll, N.J. White, N.P. Day, S.J. Peacock, Melioidosis: insights into the pathogenicity of *Burkholderia pseudomallei*, Nat. Rev. Microbiol. 4 (2006) 272–282.
[2] S.J. Peacock, Melioidosis, Curr. Opin. Infect. Dis. 19 (2006) 421–428.
[3] P. Aldhous, Tropical medicine: melioidosis? Never heard of it..., Nature 434 (2005) 692–693.
[4] A.C. Cheng, B.J. Currie, Melioidosis: epidemiology, pathophysiology, and management, Clin. Microbiol. Rev. 18 (2005) 383–416.
[5] J.B. Woods, Antimicrobials for biological warfare agents, in: L.L. Lindler, F.J. Lebeda, G.W. Korch (Eds.), Biological Weapons Defense: Infectious Diseases and Counter Bioterrorism, Humana Press Inc., Totowa, 2005, pp. 285–315.
[6] Centers for Disease Control and Prevention. Bioterrorism Agents/Diseases, www.bt.cdc.gov/agent/agentlist-category.asp.
[7] National Center for Zoonotic, Vector-Borne, and Enteric Diseases, Melioidosis. www.cdc.gov/nczved/divisions/dfbmd/diseases/melioidosis.
[8] M.T.G. Holden, R.W. Titball, S.J. Peacock, A.M. Cerdeño-Tárraga, T. Atkins, L.C. Crossman, T. Pitt, C. Churcher, K. Mungall, S.D. Bentley, M. Sebaihia, N.R. Thomson, N. Bason, I.R. Beacham, K. Brooks, K.A. Brown, N.F. Brown, G.L. Challis, I. Cherevach, T. Chillingworth, A. Cronin, B. Crossett, P. Davis, D. DeShazer, T. Feltwell, A. Fraser, Z. Hance, H. Hauser, S. Holroyd, K. Jagels, K.E. Keith, M. Maddison, S. Moule, C. Price, M.A. Quail, E. Rabbinowitsch, K. Rutherford, M. Sanders, M. Simmonds, S. Songsivilai, K. Stevens, S. Tumapa, M. Vesaratchavest, S. Whitehead, C. Yeats, B.G. Barrell, P.C.F. Oyston, J. Parkhill, Genomic plasticity of the causative agent of melioidosis, *Burkholderia pseudomallei*, Proc. Natl. Acad. Sci. USA 101 (2004) 14240–14245.
[9] L.A. Trunck, K.L. Probst, W. Wuthiekanun, A. Tuanyok, S.M. Beckstrom-Sternberg, J.S. Beckstrom-Sternberg, S.J. Peacock, P. Keim, S.W. Dow, H.P. Schweizer, Molecular basis of rare aminoglycoside susceptibility and pathogenesis of *Burkholderia pseudomallei* clinical isolates from Thailand, PLoS Negl. Trop. Dis. 3 (2009) e0000519.
[10] S. Kanthawonga, K. Nazmic, S. Wongratanacheewina, J.G.M. Bolscherc, V. Wuthiekanund, S. Taweechaisupapong, In vitro susceptibility of *Burkholderia pseudomallei* to antimicrobial peptides, Int. J. Antimicrob. Agents 34 (2009) 309–314.
[11] R. Karunakaran, S.D. Puthucheary, *Burkholderia pseudomallei*: in vitro susceptibility to some new and old antimicrobials, Scand. J. Infect. Dis. 39 (2007) 858–861.
[12] F.M. Thibault, E. Hernandez, D.R. Vidal, M. Girardet, J.-D. Cavallo, Antibiotic susceptibility of 65 isolates of *Burkholderia pseudomallei* and *Burkholderia mallei* to 35 antimicrobial agents, J. Antimicrob. Chemother. 54 (2004) 1134–1138.
[13] Y. Hara, R. Mohamed, S. Nathan, Immunogenic *Burkholderia pseudomallei* outer membrane proteins as potential candidate vaccine targets, PLoS ONE 4 (2009) e6496.
[14] C. Druar, F. Yu, J.L. Barnes, R.T. Okinaka, N. Chantratita, S. Beg, C.W. Stratilo, A.J. Olive, G. Soltes, M.L. Russell, D. Limmathurotsakul, R.E. Norton, S.X. Ni, W.D. Picking, P.J. Jackson, D.I. Stewart, V. Tsvetnitsky, W.L. Picking, J.W. Cherwonogrodzky, N. Ketheesan, S.J. Peacock, E.J. Wiersma, Evaluating *Burkholderia pseudomallei* Bip proteins as vaccines and Bip antibodies as detection agents, FEMS Immunol. Med. Microbiol. 52 (2008) 78–87.
[15] A. Haque, K. Chu, A. Easton, M.P. Stevens, E.E. Galyov, T. Atkins, R. Titball, G.J. Bancroft, A live experimental vaccine against *Burkholderia pseudomallei* elicits CD4+ T cell-mediated immunity, priming T cells specific for 2 type III secretion system proteins, J. Infect. Dis. 194 (2006) 1241–1248.
[16] J.A. Torres, M.V. Villegas, J.P. Quinn, Current concepts in antibiotic-resistant Gram-negative bacteria, Experts Rev. Anti-Infect. Ther. 5 (2007) 833–843.
[17] A. Kumar, H.P. Schweizer, Bacterial resistance to antibiotics: active efflux and reduced uptake, Adv. Drug Deliv. Rev. 57 (2005) 1486–1513.
[18] K. Poole, Mechanisms of bacterial biocide and antibiotic resistance, J. Appl. Microbiol. 92 (2002) 55S–64S.
[19] B.G. Spratt, Resistance to antibiotics mediated by target alterations, Science 264 (1994) 388–393.
[20] S. Galdiero, M. Galdiero, C. Pedone, Beta-barrel membrane bacterial proteins: structure, function, assembly and interaction with lipids, Curr. Protein Pept. Sci. 8 (2007) 63–82.
[21] H. Nikaido, Molecular basis of bacterial outer membrane permeability revisited, Microbiol. Molec. Biol. Rev. 67 (2003) 593–656.
[22] G.E. Schulz, The structure of bacterial outer membrane proteins, Biochim. Biophys. Acta Biomembr. 1565 (2002) 308–317.
[23] H. Weingart, M. Petrescu, M. Winterhalter, Biophysical characterization of in- and efflux in Gram-negative bacteria, Curr. Drug Targ. 9 (2008) 789–796.
[24] H.T. Tien, A.L. Ottova, The lipid bilayer concept and its experimental realization: from soap bubbles, kitchen sink, to bilayer lipid membranes, J. Membr. Sci. 189 (2001) 83–117.
[25] M. Winterhalter, Black lipid membranes, Curr. Opin. Colloid Interface Sci. 5 (2000) 250–255.
[26] J.-M. Pages, C.E. James, M. Winterhalter, The porin and the permeating antibiotic: a selective diffusion barrier in Gram-negative bacteria, Nat. Rev. Microbiol. 6 (2008) 893–903.
[27] K.R. Mahendran, E. Hajjar, T. Mach, M. Lovelle, A. Kumar, I. Sousa, E. Spiga, H. Weingart, P. Gameiro, M. Winterhalter, M. Ceccarelli, Molecular basis of enrofloxacin translocation through OmpF, an outer membrane channel of *Escherichia coli*—when binding does not imply translocation, J. Phys. Chem. B 114 (2010) 5170–5179.
[28] K.R. Mahendran, M. Kreir, H. Weingart, N. Fertig, M. Winterhalter, Permeation of antibiotics through *Escherichia coli* OmpF and OmpC porins: screening for influx on a single-molecule level, J. Biomol. Screen. 5 (2010) 302–307.
[29] K.R. Mahendran, C. Chimerel, T. Mach, M. Winterhalter, Antibiotic translocation through membrane channels: temperature-dependent ion current fluctuation for catching the fast events, Eur. Biophys. J. 38 (2009) 1141–1145.
[30] C.E. James, K.R. Mahendran, A. Molitor, J.-M. Bolla, A.N. Bessonov, M. Winterhalter, J.-M. Pagès, How β-lactam antibiotics enter bacteria: a dialogue with the porins, PLoS ONE 4 (2009) e5453.
[31] T. Mach, P. Neves, E. Spiga, H. Weingart, M. Winterhalter, P. Ruggerone, M. Ceccarelli, P. Gameiro, Facilitated permeation of antibiotics across membrane channels—interaction of the quinolone moxifloxacin with the OmpF channel, J. Am. Chem. Soc. 130 (2008) 13301–13309.
[32] E.M. Nestorovich, C. Danelon, M. Winterhalter, S.M. Bezrukov, Designed to penetrate: time-resolved interaction of single antibiotic molecules with bacterial pores, Proc. Nat. Acad. Sci. USA 99 (2002) 9789–9794.
[33] M. Ceccarelli, C. Danelon, A. Laio, M. Parrinello, Microscopic mechanism of antibiotic translocation through a porin, Biophys. J. 87 (2004) 58–64.
[34] E. Hajjar, K.R. Mahendran, A. Kumar, A. Bessonov, M. Petrescu, H. Weingart, P. Ruggerone, M. Winterhalter, M. Ceccarelli, Bridging timescales and length scales: from macroscopic flux to the molecular mechanism of antibiotic diffusion through porins, Biophys. J. 98 (2010) 569–575.

[35] S. Pezeshki, C. Chimerel, A.N. Bessonov, M. Winterhalter, U. Kleinekathöfer, Understanding ion conductance on a molecular level: an all-atom modeling of the bacterial porin OmpF, Biophys. J. 97 (2009) 1898–1906.
[36] J. Siritapetawee, H. Prinz, C. Krittanai, W. Suginta, Expression and refolding of Omp38 from *Burkholderia pseudomallei* and *Burkholderia thailandensis*, and its function as a diffusion porin, Biochem. J. 384 (2004) 609–617.
[37] J. Siritapetawee, H. Prinz, W. Samosornsuk, R.H. Ashley, W. Suginta, Functional reconstitution, gene isolation and topology modelling of porins from *Burkholderia pseudomallei* and *Burkholderia thailandensis*, Biochem. J. 377 (2004) 579–587.
[38] A. Prilipov, P.S. Phale, P. Van Gelder, J.P. Rosenbusch, R. Koebnik, Coupling site-directed mutagenesis with high-level expression: large scale production of mutant porins from *E. coli*, FEMS Microbiol. Lett. 163 (1998) 65–72.
[39] R.M. Garavito, J.P. Rosenbusch, Isolation and crystallization of bacterial porin, Methods Enzymol. 125 (1986) 309–328.
[40] J.P. Rosenbusch, Characterization of the major envelope protein from *Escherichia coli*. Regular arrangement on the peptidoglycan and unusual dodecyl sulfate binding, J. Biol. Chem. 249 (1974) 8019–8029.
[41] B. Lugtenberg, L. Van Alphen, Molecular architecture and functioning of the outer membrane of *Escherichia coli* and other gram-negative bacteria, Biochim. Biophys. Acta 737 (1983) 51–115.
[42] N. Eswar, B. Webb, M.A. Marti-Renom, M.S. Madhusudhan, D. Eramian, M.Y. Shen, U. Pieper, A. Sali, Comparative protein structure modeling using MODELLER, Curr. Protoc. Protein Sci. (2007), Chapter 2, Unit 2.9.
[43] B. Wallner, A. Elofsson, Can correct protein models be identified? Protein Sci. 12 (2003) 1073–1086.
[44] K. Zeth, K. Diederichs, W. Welte, H. Engelhardt, Crystal structure of Omp32, the anion-selective porin from *Comamonas acidovorans*, in complex with a periplasmic peptide at 2.1 A resolution, Structure 15 (2000) 981–992.

OPEN ACCESS Freely available online

PLOS ONE

Molecular Uptake of Chitooligosaccharides through Chitoporin from the Marine Bacterium *Vibrio harveyi*

Wipa Suginta[1]*, Watcharin Chumjan[1], Kozhinjampara R. Mahendran[2], Petra Janning[3], Albert Schulte[1], Mathias Winterhalter[2]

1 Biochemistry-Electrochemistry Research Unit, Schools of Chemistry and Biochemistry, Institute of Science, Suranaree University of Technology, Nakhon Ratchasima, Thailand, **2** School of Engineering and Science, Jacobs University Bremen, Bremen, Germany, **3** Department of Chemical Biology, Max-Planck Institute of Molecular Physiology, Dortmund, Germany

Abstract

Background: Chitin is the most abundant biopolymer in marine ecosystems. However, there is no accumulation of chitin in the ocean-floor sediments, since marine bacteria *Vibrios* are mainly responsible for a rapid turnover of chitin biomaterials. The catabolic pathway of chitin by *Vibrios* is a multi-step process that involves chitin attachment and degradation, followed by chitooligosaccharide uptake across the bacterial membranes, and catabolism of the transport products to fructose-6-phosphate, acetate and NH_3.

Principal Findings: This study reports the isolation of the gene corresponding to an outer membrane chitoporin from the genome of *Vibrio harveyi*. This porin, expressed in *E. coli*, (so called *Vh*ChiP) was found to be a SDS-resistant, heat-sensitive trimer. Immunoblotting using anti-ChiP polyclonal antibody confirmed the expression of the recombinant ChiP, as well as endogenous expression of the native protein in the *V. harveyi* cells. The specific function of *Vh*ChiP was investigated using planar lipid membrane reconstitution technique. *Vh*ChiP nicely inserted into artificial membranes and formed stable, trimeric channels with average single conductance of 1.8 ± 0.13 nS. Single channel recordings at microsecond-time resolution resolved translocation of chitooligosaccharides, with the greatest rate being observed for chitohexaose. Liposome swelling assays showed no permeation of other oligosaccharides, including maltose, sucrose, maltopentaose, maltohexaose and raffinose, indicating that *Vh*ChiP is a highly-specific channel for chitooligosaccharides.

Conclusion/Significance: We provide the first evidence that chitoporin from *V. harveyi* is a chitooligosaccharide specific channel. The results obtained from this study help to establish the fundamental role of *Vh*ChiP in the chitin catabolic cascade as the molecular gateway that *Vibrios* employ for chitooligosaccharide uptake for energy production.

Citation: Suginta W, Chumjan W, Mahendran KR, Janning P, Schulte A, et al. (2013) Molecular Uptake of Chitooligosaccharides through Chitoporin from the Marine Bacterium *Vibrio harveyi*. PLoS ONE 8(1): e55126. doi:10.1371/journal.pone.0055126

Editor: Daniel J. Muller, Swiss Federal Institute of Technology Zurich, Switzerland

Received November 14, 2012; **Accepted** December 18, 2012; **Published** January 29, 2013

Funding: This work is financially supported by the Thailand Research Fund (contract no. RMU5380055). WS was a Humboldt fellow under the Alexander von Humboldt Fellowship for Experienced Researchers, The Alexander von Humboldt Foundation, Germany. WC was funded by the Commission of Higher Education, Ministry of University Affairs (MUA), Thailand through a CHE-PHD-SW scholarship (contract no 60/2550). MW acknowledges funding through WI 2278/18-1 of the Deutsche Forschungsgemeinschaft (DFG). The funders had no role in study design, data collection and analysis, decision to publish, or preparation of the manuscript.

Competing Interests: The authors have declared that no competing interests exist.

* E-mail: wipa@sut.ac.th

Introduction

Chitin, a β-1,4-linked homopolymer of *N*-acetylglucosamine (GlcNAc), is the most abundant polysaccharide in marine ecosystems, because it is a major component of the shells of crustaceans and marine zoo-plankton. It has been estimated that multi-million tons of chitin-containing substances are produced annually in the aquatic biosphere [1]. However, there is no substantial accumulation of chitin on the ocean floor. This is because of bioconversion of this mass of biomaterials, primarily by marine bacteria of the family *Vibrionaceae* [2]. These bacteria utilize chitinous materials very efficiently, converting them into organic compounds that then can be used as nitrogen and carbon sources.

The catabolic cascade of chitin utilization by marine *Vibrios* has been demonstrated elegantly in *Vibrio furnissii* [3–8] and *V. cholerae* [9,10]. The cascade incorporates a large number of genes and enzymes, which are orchestrated in a complex signal transduction pathway [9,11]. Roseman and co-workers previously identified chitoporin (ChiP) from *V. furnissii* [12] and suggested that it acts as a chitooligosaccharide-specific channel, based on their findings that expression of native ChiP was significantly induced when the *V. furnissi* cells were grown in the presence of chitooliogsaccharides ($GlcNAc_{2-6}$). A null mutant of *V. furnissii* ChiP also showed an impaired growth in the culture supplemented with chitotriose. Phylogenic analysis of marine bacteria of the *Vibrionacae* family identified a *chiP* gene in 16 out of 19 species [13]. Such results indicate that this protein is well conserved within this family. DNA microarray expression profiles further confirmed that expression of the *chiP* gene in *V. cholerae* responded positively to chitin oligosaccharides and that the genes responsible for chitin degradation are under the stringent control of the *chiS* regulon [6,13].

Although ChiP was identified more than a decade ago, its physiological function as a chitooligosaccharide-specific channel remains unproved. Here, we report cloning and recombinant expression of chitoporin (referred to as *Vh*ChiP) from the marine bacterium *V. harveyi* (formerly *V. carchariae*) type strain 650. The physicochemical properties of *Vh*ChiP were determined using a planar black lipid membrane (BLM) reconstitution technique. High-time resolution single channel current recordings, together with liposome swelling assays, provide strong evidence that *Vh*ChiP is a highly specific channel for the molecular uptake of chitin oligosaccharides.

Methods

Ethics Statement

The anti-rabbit polyclonal antibody production procedure was approved by the Animal Care Commission of Suranaree University of Technology. Two adult (8-week-old) female rabbits were purchased from the Animal Caring Center, Mahidol University, Bangkok, Thailand. The rabbit was housed in a standard animal facility under conditions of controlled temperature (25°C) and photoperiod (a 12:12-hour light/dark schedule), with food and water provided ad libitum.

Bacterial strains and vectors

V. harveyi type strain 650 was a marine isolate from Greek sea bass and was a gift from Professor Brian Austin, Heriot-Watt University, Edinburgh, United Kingdom. *E. coli* strain DH5α was used for routine cloning and plasmid preparations. pGEM®-T easy vector used for subcloning purpose was a product of Promega (Promega Pte Ltd, Singapore Science Park I, Singapore). The pET23d(+) expression vector and *E. coli* mutant strain BL21(DE3) Omp8 Rosetta were gifts from Professor Dr. Roland Benz, Jacobs University Bremen, Germany. The *E. coli* mutant was genetically engineered to have defective genes encoding the major outer membrane porins: OmpA, OmpC, OmpF and LamB [14] and was therefore suitable for production of recombinant porin.

Gene identification, cloning and sequencing

A BlastP search using chitoporin from *V. furnissei* (UniProtKB/TrEMBL entry: Q9KK91 and ref. 12) as protein template identified putative chitoporins from several marine bacteria in family *Vibrionaceae*, including a hypothetical protein VIBHAR_01269 (accession number YP_001444474) from *V. harveyi* type strain ATCC BAA-1116 BB120. Therefore, specific oligonucleotides were designed from the hypothetical gene of the BAA-1116 BB120 strain in order to obtain the gene encoding chitoporin from our laboratory strain (*V. harveyi* type strain 650). Genomic DNA was prepared from this bacterium using PureLink™ Genomic DNA Kits (Invitrogen, Gibthai Company Ltd., Bangkok, Thailand) and used as the DNA template for PCR amplification. The oligonucleotides used for amplification were 5′-ATACCATGGCGTCTTACCTAAAGAAAAG-3′ for the forward primer and 5′-AACCTCGAGTTAGAAGTAGTATTCAACAC-3′ for the reverse primer. The PCR product was of the expected size (1.1 kbp) and was cloned into pET23d(+) expression vector using *Nco* I and *Xho* I cloning sites (sequences underlined) following the protocol supplied by the manufacturer. Nucleotide sequences of sense and anti-sense strands of the PCR fragment were determined by automated sequencing (First BASE Laboratories Sdn Bhd, Selangor Darul Ehsan, Malaysia).

Recombinant expression and protein purification

E. coli BL21 (DE3) Omp8 Rosetta host strain was transformed with the plasmid pET23d(+)/*chiP*. Expression and preparation of the recombinant ChiP followed the protocols described by Garavito and Rosenbusch [15] and Rosenbusch [16]. In brief, transformed cells were grown at 37°C in Luria-Bertani (LB) liquid medium containing 100 $\mu g \cdot mL^{-1}$ ampicillin and 25 $\mu g\ mL^{-1}$ kanamycin. At an OD_{600} reading of 0.5–0.7, IPTG (isopropyl β-D-thiogalactoside) was added to a final concentration of 0.5 mM. Cell growth was continued for a further 6 h and cells were then harvested by centrifugation at 4,500×g at 4°C for 20 min. The cell pellet was resuspended in a buffer containing 20 mM Tris-HCl, pH 8.0, 2.5 mM $MgCl_2$, 0.1 mM $CaCl_2$, 10 $\mu g \cdot mL^{-1}$ DNase I and 10 $\mu g\ mL^{-1}$ RNase A. Cells were lysed on ice by sonication for 10 min (30% duty cycle; amplitude setting 20%) using a Sonopuls Ultrasonic homogenizer with a 6-mm-diameter probe. The recombinant *Vh*ChiP was extracted from the peptidoglycan layer with sodium dodecyl sulphate (SDS) based on the method of Lugtenberg and Alphen [17]. Briefly, SDS was added to the cell suspension to a final concentration of 2% (v/v) and incubation was carried out for 1 h at 60°C with gentle shaking. The crude extract was then centrifuged at 40,000×g for 60 min at 4°C. The pellet, which at this stage included the cell envelopes, was re-suspended in 20 mM phosphate buffer, pH 7.4, containing 0.125% (v/v) octyl-POE (n-octyl polyoxyethylene; ALEXIS Biochemicals, Lausanne, Switzerland), using a Potter-Elvehjem homogenizer. The suspension was incubated at 37°C with gentle shaking for 1 h and then centrifuged at 100 000×g at 4°C for 40 min. The new pellet, now rich in outer membranes, was resuspended in 20 mM phosphate buffer, pH 7.4 containing 5% (v/v) octyl-POE and the suspension incubated at 37°C for 60 min. Insoluble material was removed by centrifugation at 100,000×g at 20°C for 40 min. After exchange of the detergent to 0.2% (v/v) LDAO (lauryldimethylamine oxide; Sigma-Aldrich Pte. Ltd., Singapore) by dialysis, the *Vh*ChiP-rich sample was subjected to ion-exchange chromatography using a Hitrap Q HP prepacked column (5×1 mL) connecting to an ÄKTA Prime plus FPLC system (GE Healthcare Life Sciences, Life Sciences Instruments, ITS (Thailand) Co., Ltd., Bangkok, Thailand). Bound proteins were eluted with a linear gradient of 0–1 M KCl in the phosphate buffer, containing 0.2% (v/v) LDAO. Purity of the eluted proteins was confirmed by SDS-PAGE. Fractions containing only *Vh*ChiP were pooled and the protein concentration was determined using the Pierce BCA protein assay kit (Bio-Active Co., Ltd., Bangkok, Thailand).

Antibody production and immunological analysis

Production of anti-*Vh*ChiP antiserum was carried out using an in-gel method. Outer membrane fraction extracted by 5% (v/v) octyl-POE was applied to eight wells in parallel on an 8% polyacrylamide gel. Following electrophoresis and Coomassie Blue staining, the proteins were resolved into two bands. The upper band, just above 40 kDa, was identified by mass spectrometry as *E. coli* OmpN, while the lower band, slightly below 40 kDa, was chitoporin (*Vh*ChiP). The lower bands were excised from the gels, combined (ca. 80 μg protein) and homogenized in 200 μL PBS, pH 7.4, then emulsified with 500 μL Freund's complete/incomplete adjuvant (Pierce). The emulsified mixture was injected subcutaneously into a female white rabbit to produce *Vh*ChiP antiserum. Antibody titres and cross-reactivities against other membrane proteins, including *E. coli* OmpF, *E. coli* OmpN and *Burkholderia pseudomallei* Omp38 were checked by Western blotting. Signals representing antibody-protein interaction were detected with HRP-conjugated IgG using the enhanced chemiluminescence method (ECL, Amersham, UK). Anti-OmpN serum was prepared

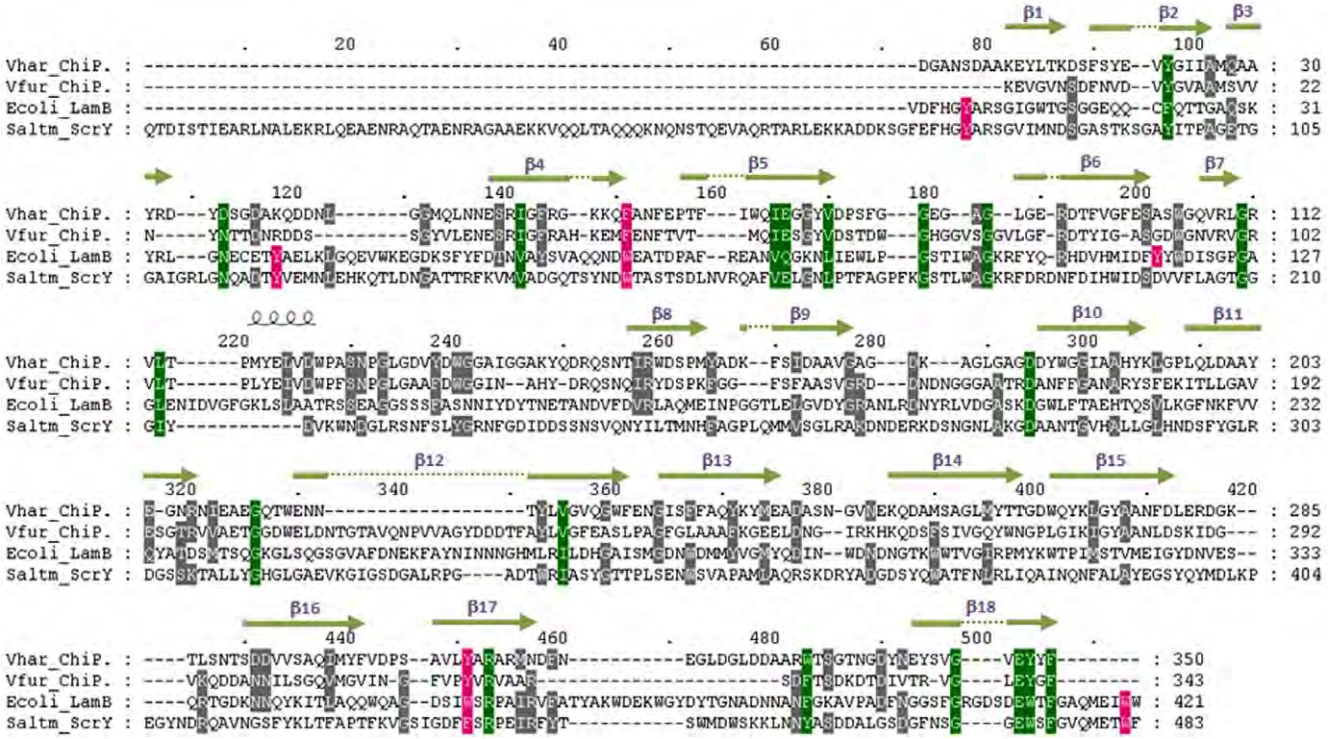

Figure 1. Alignment of the putative *V. harveyi* chitoporin sequence with other sugar-specific porins. Amino acid sequences of *V. furnissii* chitoporin (Q9KK91), *E. coli* LamB or maltoporin (P02943), and *S. typhimurium* ScrY (P22340) were retrieved from the SwissProt/UniProtKB protein databases, aligned using "CLASTALW" algorithm in the DNASTAR package, and displayed in Genedoc. The secondary structure of *Vh*ChiP was constructed by ESPript v. 2.2 according to the structure of *Delftia acidovorans* Omp32 (pdb 2GFR and ref 37). The residues that are aligned with Y6, Y41, Y118, W74, W358, and W420 of *E. coli* LamB are shaded in magenta. Green shading refers to amino residues conserved within the four sequences. β-strands are represented as green lines with an arrow.
doi:10.1371/journal.pone.0055126.g001

using purified *E. coli* OmpN, its titres and cross-reactivities being tested in the same way as the *Vh*ChiP antiserum.

For expression of native *Vh*ChiP, a 5-mL overnight culture of *V. harveyi* 650 grown in marine medium [18] was transferred to a 2-L flask containing 500 mL of marine medium. The cells were grown at 30°C with agitation until OD_{600} reached 0.6, then 1% (wet w/v) colloidal chitin was added to induce chitoporin expression. Aliquots of 1 mL of cell culture were taken at various time points (1, 2, 3, 4, 5, and 6 h). Cell pellets collected after centrifugation were solubilized in 5× SDS-gel loading buffer, and then analyzed by SDS-PAGE, followed by western blotting.

Black lipid bilayer measurements and single channel analysis

Black lipid bilayer (BLM) measurements and single channel analysis were performed as described elsewhere [19–24]. The lipid bilayer cuvette consisted of two chambers with a 25 μm-thick Teflon film sandwiched in between. The latter had a small aperture of 60–100 μm in diameter across which a virtually solvent free planar lipid bilayer was formed. The chambers were filled with electrolyte solution and an electrode (Ag/AgCl electrodes; World Precision Instruments, Sarasota, FL) immersed on either side of the Teflon film. The electrolyte used was 1 M KCl adjusted to pH 7.5, and buffered by 20 mM HEPES. 1,2-Diphytanoyl-sn-glycero-3-phosphatidylcholine (DPhPC; Avanti Polar Lipids, Alabaster, AL) lipid was used for lipid bilayers formation. In order to form the bilayer first the aperture was pre-painted with 1 μL of 1% (v/v) hexadecane in pentane (Sigma Aldrich). One of the electrodes was used as ground (*cis*) whereas the other electrode was connected (*trans*) to the headstage of an Axopatch 200B amplifier (Axon Instruments, Foster City, CA). Trimeric *Vh*ChiP channel (50–100 $ng \cdot mL^{-1}$) was added to the *cis* side of the lipid membrane. At applied transmembrane potentials of ±200 mV, a single channel was frequently inserted within a few minutes. The protein solution in the chamber was gently diluted out by multiple additions of the working electrolyte to prevent multiple insertions. Single channel current measurements were performed with an Axopatch 200B amplifier (Molecular Devices, Sunnywale., CA, U.S.A.) in the voltage clamp mode, with the internal filter set at 10 kHz. Amplitude, probability, and single channel analyses were performed using pClamp v.10.0 software (all from Molecular Devices, Sunnyvale, CA).

To investigate sugar translocation, a chitooligosaccharide was added to either the *cis* or the *trans* side of the chamber to a final concentration of 80 μM. Occlusions of ion flow observed as a result of sugar diffusion through the inserting channel were usually recorded for 2 min. To see the effect of sugar translocation on individual subunit blockages, discrete concentrations of chitohexaose (1, 120, and 400 μM) were tested.

Liposome swelling assay

Trimeric *Vh*ChiP channel was reconstituted into liposomes as described previously [25,26]. *E. coli* total lipid extract was used to form liposomes and 15% dextran (MW 40,000) was entrapped in the liposomes. The size of the formed liposomes was checked using a Nano-ZS ZEN3600 zetasizer. The isotonic solute concentration

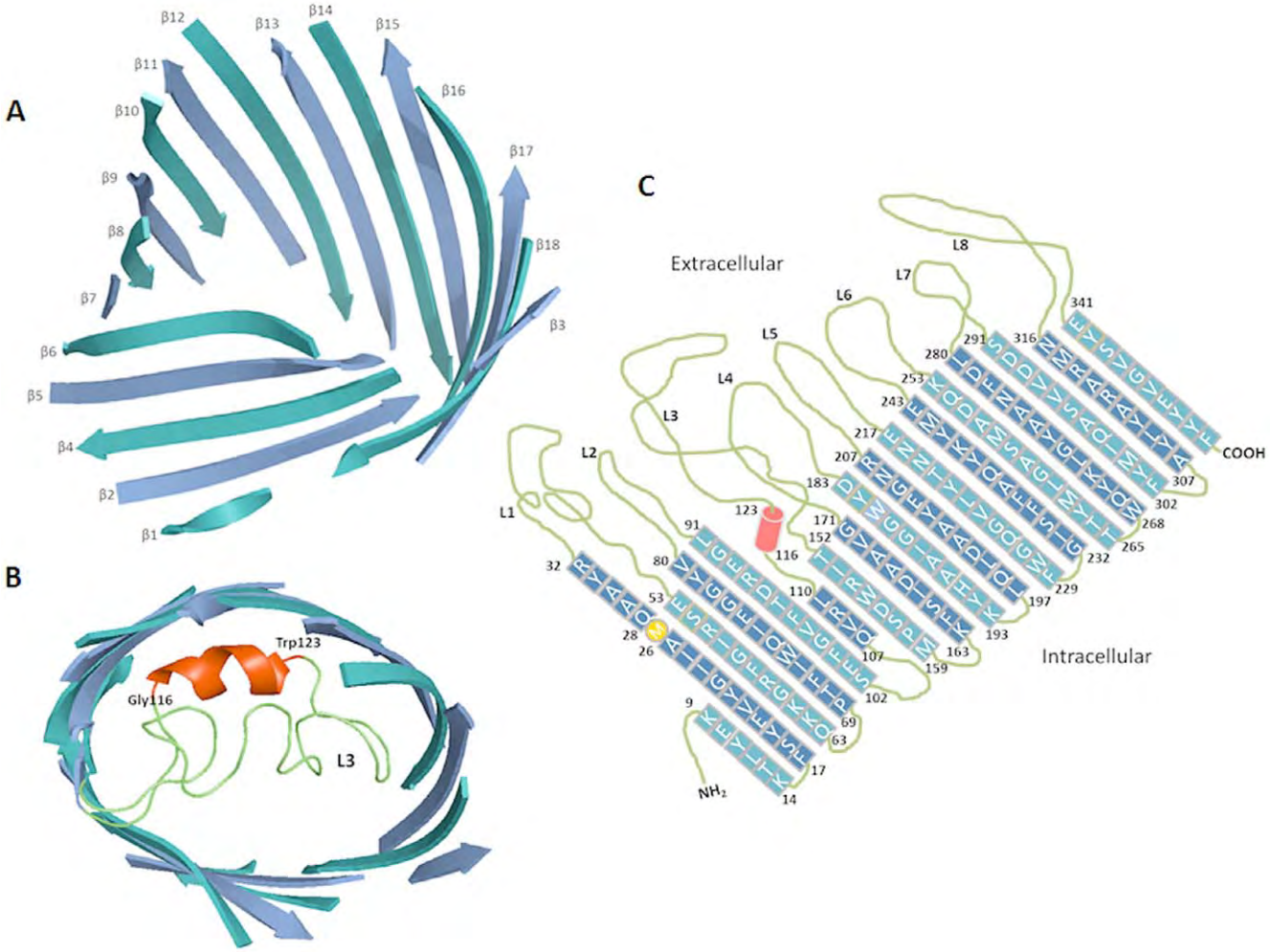

Figure 2. The Swiss-Model 3D-structure of *V. harveyi* chitoporin. A) Side view of a ribbon representation of *Vh*ChiP. The homology structure was constructed by the SWISS-MODEL program using an automated mode (http://swissmodel.expasy.org/). The x-ray structure of *D. acidovorans* Omp32 (pdb 2GFR) was selected as structure template (see texts). B) Top view of the modeled structure, showing L3 as the pore-confining loop with a short helix consisting 8 amino acids (G116-W123) presented in red. C) Transmembrane domains of *Vh*ChiA were depicted based on the homology structure (Fig. 2A–B) and the structure-based alignment (Fig. 1).
doi:10.1371/journal.pone.0055126.g002

was determined with different concentrations of raffinose solution (prepared in 20 mM HEPES buffer, pH 7.5) added into the protoliposome suspension. The value obtained for isotonic concentration of raffinose was used as an approximation to facilitate the adjustment of isotonic concentrations for different solutes. Twenty microliters of liposome or proteoliposome solution was diluted into 500 µL of the isotonic test solution in a 1-mL cuvette and mixed manually. The initial swelling rate upon addition of the isotonic sugar solutions (maltose, sucrose, maltopentaose, maltohexaose, and chitohexaose) was monitored using a UV-Vis spectrophotometer with the wavelength set at 500 nm. The absorbance change over the first 60 sec was used to estimate the swelling rate (s^{-1}) following the equation: $\Phi = (1/A_i)dA/dt$, in which Φ is the swelling rate, A_i the initial absorbance, and dA/dt the rate of absorbance absorbance change during the first 60 s. The swelling rate of each sugar was normalized by setting the rate of arabinose (MW 150.14 Da) to 100%. Values presented are averages obtained from four to six determinations. Protein-free liposomes and proteoliposomes without sugars were used as negative controls.

Results

Gene isolation, cloning, sequence analysis and transmembrane topology

The availability of the complete genome sequence of *V. harveyi* type strain ATCC BAA-1116 BB120 in the GenBank® database enabled us to identify an open reading frame that encodes a hypothetical chitoporin (ChiP). To isolate the gene encoding ChiP from the genome of the closely related species *V. harveyi* type strain 650, specific oligonucleotide primers were designed, based on the identified *chiP* gene from the BAA-1116 BB120 strain. The full-length *chiP* cDNA was amplified by the PCR technique. The nucleotide sequence of the identified gene comprises 1,125 bps, which was translated to a putative polypeptide of 375 amino acids, including the 25-aa signal sequence. The theoretical mass of the full-length *Vh*ChiP was 41,089.10 Da, with a predicted *p*I of 4.09. BLAST searching of the translated *Vh*ChiP sequence gave high-score hits with putative chitoporin of several species in the family *Vibrionaceae* in the SwissProt/UniProtKB database.

*Vh*ChiP shows low sequence identity (<20%) with other functionally characterized outer membrane porins, such as *E. coli*

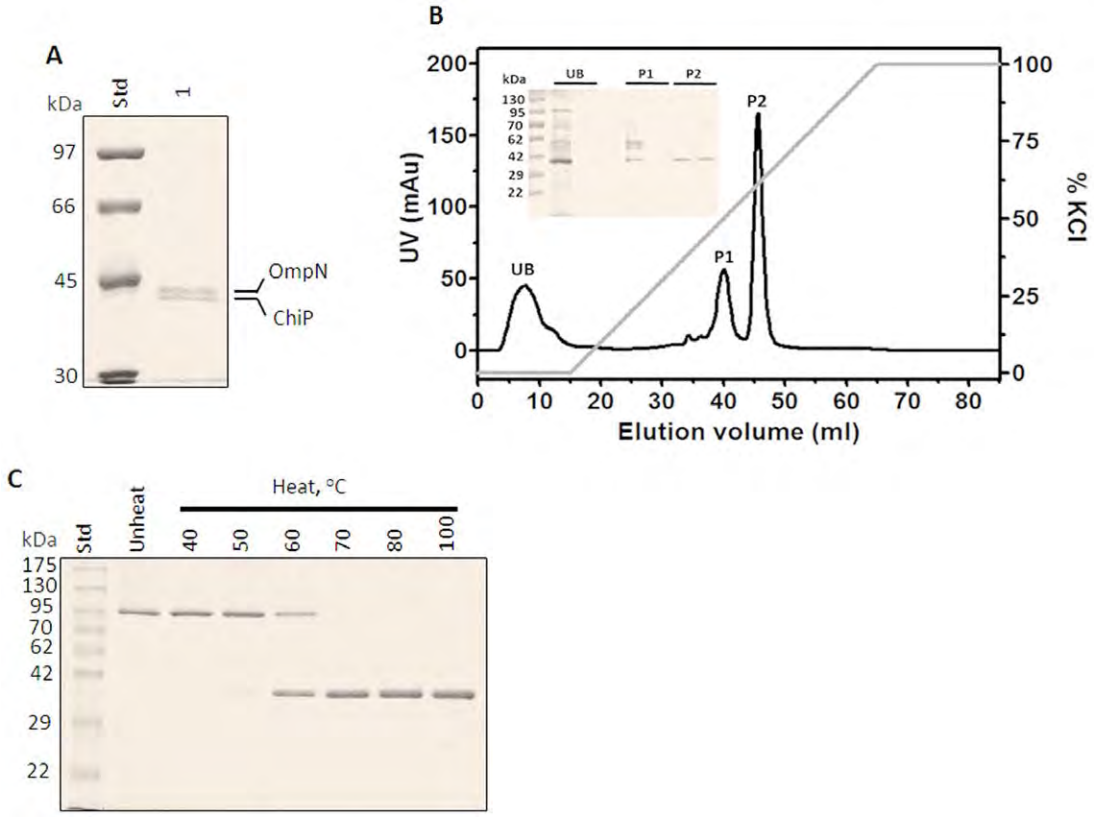

Figure 3. SDS-PAGE analysis of *V. harveyi* chitoporin. A) SDS-PAGE of outer membrane proteins extracted with 2% (w/v) SDS, followed by 5% (v/v) octyl-POE. *E. coli* OmpN and *Vh*ChiP bands were identified by mass spectrometry. B) Chromatographic profile of *Vh*ChiP purification with a Hitrap Q HP prepacked column (5×1 mL) connecting to an ÄKTA Prime plus FPLC system. The column was eluted with a linear gradient of 0–1 M KCl. SDS-PAGE analysis of unbound (UB) and bound fractions P1 and P2 is shown in an inset. C) Heat stability of *Vh*ChiP. The purified ChiP was subjected to different temperatures (40–100°C) and then run on a 10% polyacrylamide gel.
doi:10.1371/journal.pone.0055126.g003

OmpF (P02931), *E. coli* OmpC (P06996), *E. coli* OmpA (P0A910), *E. coli* OmpN (P47747), *Pseudomonas fluorescens* OprD (Q3LAG8), and *Neisseria gonorrhoeae* PorB (Q5XKX0). Fig. 1A presents amino acid sequence alignment of *Vh*ChiP with chitoporin from *V. furnissii* (accession number 09KK91) [12], *E. coli* LamB or maltoporin (maltose-specifc porin) (P02943) [27], and *Salmonella typhimurium* ScrY (sucrose-specific porin) (P22340 [28]. The sequence identity of *Vh*ChiP with *V. furnissii* chitoporin is 40%, while it shows remarkably low identity with other sugar-specific porin: LamB (15.3%), and ScrY (12.9%). It is also only 15.7% identical to a carbohydrate-selective porin *Pseudomonas aeruginosa* OprB [29,30]. In LamB, six aromatic residues (Y6, Y41, W74, F229, W358 and W420) located in the pore lumen form a polar track, which aids ion and sugar transport [31–34]. Y118, on the other hand, controls the central constriction of the LamB channel [35,36].

Sequence alignment (Fig. 1) shows that the residues Y6, Y41, W74, W358 and W420 of LamB are well aligned with Y78, Y118, W151, F435 and W482, respectively, of ScrY. In marked contrast, *Vh*ChiP displays substantial sequence dissimilarities with both LamB and ScrY. Only two residues in LamB (W74 and W358) are aligned with F64 and Y310 of *Vh*ChiP. Furthermore, Y118 of LamB shows no match with any aromatic residue of *Vh*ChiP, which indicates that the functionality of pore constriction by Y118, as found in LamB, is governed by a different residue located elsewhere in the *Vh*ChiP sequence.

Submission of the putative sequence of *Vh*ChiP through the Swiss-Model database generated a structural model of *Vh*ChiP (Fig. 2) using *Delftia acidovorans* Omp32 as template (pdb 2GFR) [37]. Compared with all porins with known 3D-structures, *Vh*ChiP is closest to Omp32 with sequence identity of 20.5%. Fig. 1 shows the secondary structural features of *Vh*ChiP, which are similar to those of most Gram negative bacterial porins, with 18 β-strands forming a barrel structure (Fig. 2A). These predicted 18 anti-parallel β-strands make up only 16 putative membrane-spanning domains, as strand β2 is connected with β3 and forms the first transmembrane domain, whereas strand β1 with β18 are part of the last domain (Figs. 1 and 2A). The predicted transmembrane topology (Fig. 2C) indicates considerable irregularity of the extracellular loops (L1–L8), while the eight periplasmic turns are short and of similar length. The longest extracellular loop (L3), comprising 41 amino acids (G111→N151), lies between strands β7 and β8. A typical right-handed α-helix is found at the early part of L3 at positions P116 to W123 (Fig. 2B). This loop, known as a pore-confined loop, is responsible for the size-selectivity of sugar-specific porins (LamB and ScrY) [28,31] and general diffusion porins [38,39].

Recombinant expression, purification and mass identification

After the correct nucleotide sequence was confirmed, the full-length *chiP* DNA obtained from PCR amplification was cloned into pET23D(+) expression vector, which was ready to be

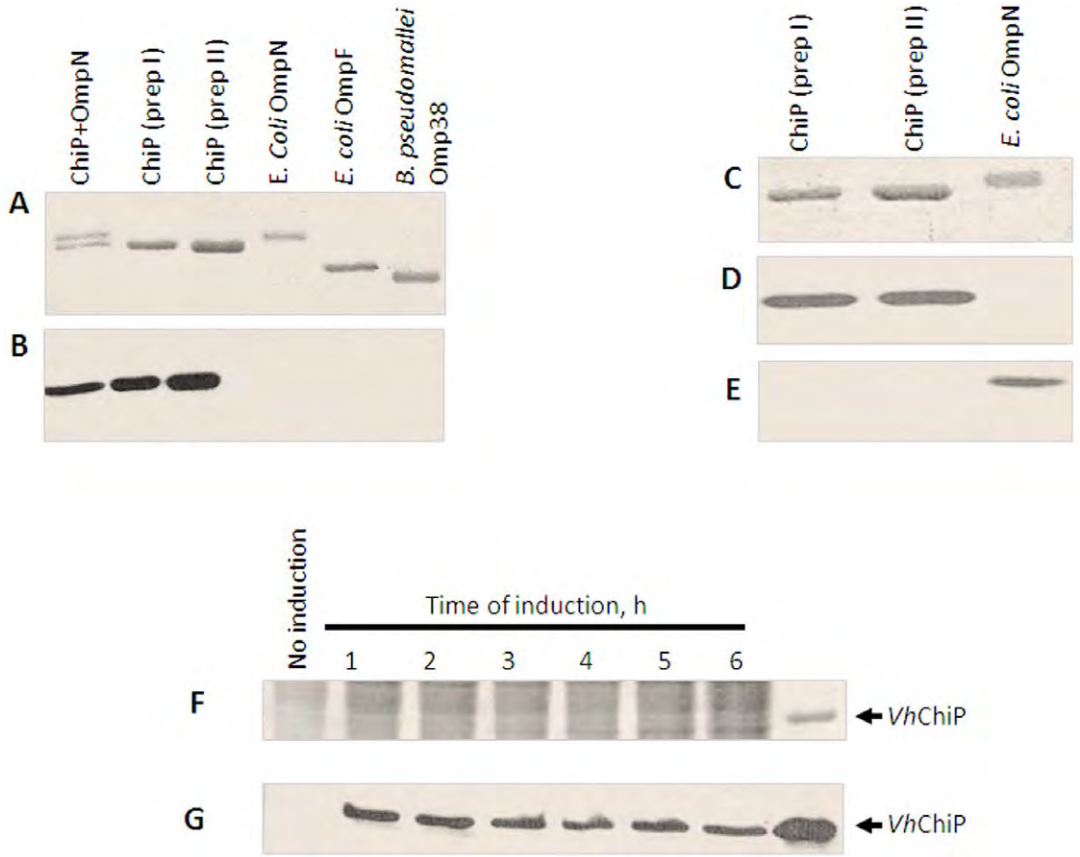

Figure 4. Immunoblot analysis of *V. harveyi* chitoporin. A–B: Cross-reactivity of *VhChiP* antiserum with other outer membrane porins. A. Coomassie blue-stained SDS-polyacrylamide gel, and B. The corresponding immunoblot detected with anti *Vh*ChiP antibody C–D: Cross-reactivity of *Vh*ChiP and *E. coli* OmpN with anti *Vh*ChiP and anti OmpN antibodies. C. Coomassie blue-stained SDS-polyacrylamide gel, D. and E. The corresponding immunoblots showing cross-reactivity with anti *Vh*ChiP antiserum, and anti OmpN antiserum, respectively. F–G: Endogenous expression of chitoporin in *V. harveyi* F. Coomassie blue-stained SDS-polyacrylamide gel, and G. Immunoblot of cell lysate of *V. harveyi* cultured in the presence of 1% (w/v) colloidal chitin at various times of 1–6 h.
doi:10.1371/journal.pone.0055126.g004

expressed in *E. coli* BL21(DE3) Omp8 Rosetta strain. The recombinant protein was expressed with the 25-amino acid *N*-terminal signal sequence attached, to aid protein targeting to the bacterial cell envelope. After proteolytic removal of the signal sequence, the mature *Vh*ChiP contains 350 amino acid residues and has a predicted MW of 38,508.97 Da. After cell-wall extraction by SDS, following 0.125% (v/v), and then 5% (v/v) octyl-POE, the solubilized fraction contained enriched *Vh*ChiP and a contaminant, which was later identified as *E. coli* OmpN. SDS-PAGE analysis (Fig. 3A) revealed two major protein bands. The upper band migrated close to 40 kDa and the lower band migrated to slightly lower than 40 kDa. Identification of tryptic peptides by high resolution ESI MS gave a primary hit with gi | 3273514 porin OmpN from *E. coli* for the higher MW band, while the lower protein band was identified as gi|28897534 putative chitoporin from *V. parahaemolyticus* RIMD 2210633, as well as gi|153834464 outer membrane protein from *V. harveyi* HY01, and gi|156973567 hypothetical protein from *V. harveyi* ATCC BAA-1116. Given that no functionally-identified chitoporin of the *V. harveyi* species is available in the NCBInr database, we assume that the identified peptides of the lower MW protein were derived from chitoporin (see Fig. S1: nine tryptic peptides are unambiguously identified within the internal segments of the putative *Vh*ChiP sequence).

After several attempts to remove OmpN contamination, we discovered that OmpN was solubilized in 5% octyl-POE, but not in 3%. Therefore, later batches of *Vh*ChiP were prepared in 3% octyl-POE so that OmpN remained in the precipitate. To obtain highly purified *Vh*ChiP for functional characterization, the detergent-extracted *Vh*ChiP was further purified by ion exchange chromatography using a HiTrap DEAE FF column. Fig. 3B shows a chromatographic profile from *Vh*ChiP purification. After removal of the unbound fraction ('UB'), the bound proteins were then eluted in two peaks ('P1' and 'P2') when a linear gradient of 0–1 M KCl was applied. SDS-PAGE analysis shows that *Vh*ChiP was in the second peak (P2) and the protein was purified to homogeneity (Fig. 3B, inset) by ion-exchange chromatography. The pooled sample from peak P2 was heat-treated at different temperatures for 10 min, and then analyzed by SDS-PAGE. Fig. 3C shows migration of the purified *Vh*ChiP to above 95 kDa, corresponding to the trimeric form, when unheated (lane 1). The trimer remained intact when the temperature was raised to 40°C, but began to dissociate at 50°C. At 60°C, more than half of the *Vh*ChiP trimers were dissociated to monomers and at 70°C or above, no trimers remained. These results indicate that *Vh*ChiP is a heat-sensitive, SDS-stable trimer; each subunit has apparent MW of approximately 39 kDa, consistent with the predicted MW of the translated polypeptide lacking the signal sequence.

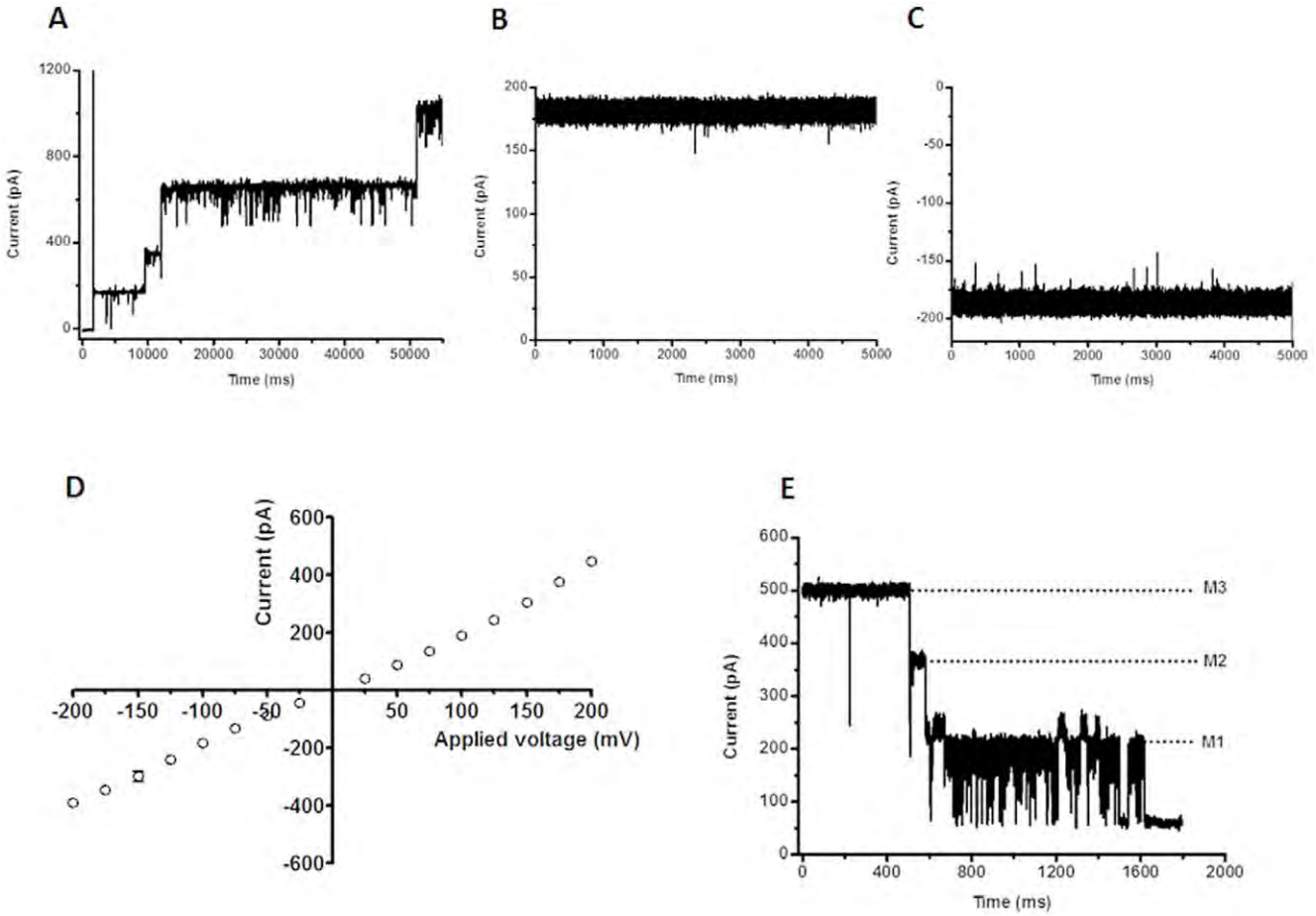

Figure 5. Single channel recordings of chitoporin in artificial lipid membranes. Trimeric *Vh*ChiP was expressed in *E. coli* BL21 (DE3) Omp8 Rosetta mutant, lacking major intrinsic porins. The protein was isolated by SDS-extraction, and then solubilized with 3% (v/v) octyl-POE. The protein was further purified by ion exchange chromatography as described in the text. The BLM measurements were carried out in the electrolyte containing 1 M KCl in 20 mM HEPES, pH 7.5. The protein was added on the *cis* side of the chamber. A. Multiple insertions of *Vh*ChiP were induced at an applied potential of +100 mV. B. Typical ion current trace of a single channel at fully-open state of *Vh*ChiP at applied voltage of +100 mV; and C. at −100 mV. The ion currents were normally recorded for a period of 120 s. D. Analysis of current-voltage (I–V) relationship. The average current values were obtained by stepwise ramping of the potential, preformed in triplicate. E. Three-step closure, induced by increasing the applied voltage to +200 mV.
doi:10.1371/journal.pone.0055126.g005

Immunoblotting and endogenous expression of VhChiP

To ensure that the recombinant protein obtained was chitoporin and not contaminating OmpN, which was co-expressed by the *E. coli* host strain Omp8 Rosetta, polyclonal antibodies against OmpN and *Vh*ChiP were raised independently. Fig. 4A shows a Coomassie Blue stained gel of different porins, corresponding to the immunoblot with anti-*Vh*ChiP antiserum (Fig. 4B). It is clear that the antibody recognized only the *Vh*ChiP band (Fig. 4A lower band and lanes 2 and 3), but not *E. coli* OmpN (lane 1, upper band and lane 4), *E. coli* OmpF (lane 5) and *B. peudomallei* Omp38 (lane 6). The results suggest no cross reactivity of anti-*Vh*ChiP antibody with other porins. Fig. 4C–E further confirmed that there was no cross-reactivity of the anti-*Vh*ChiP serum with OmpN and anti-*E. coli* OmpN serum with *Vh*ChiP. Anti-*Vh*ChiP serum recognized only *Vh*ChiP (Fig. 4D, lanes 1 and 2), and correspondingly, anti-OmpN serum reacted only with OmpN (Fig. 4E, lane 3).

To determine whether expression of native chitoporin in *V. harveyi* type strain 650 was controlled by the chitin-induced operon, expression profiles of *Vh*ChiP were evaluated after the bacterial cells were grown in the presence of chitin. Fig. 4F shows a Coomassie stained gel of the cell lysates prepared at different times of induction, while Fig. 4G shows the corresponding immunoblot with anti-*Vh*ChiP antibody. It is seen that the antibody reacted with the protein bands in the position of purified *Vh*ChiP when the cells were exposed to 1% (w/v) colloidal chitin for 1 h or more. No positive signal was detected in the lysate prepared from the cells grown in the absence of chitin. We also observed chitoporin expression in the *V. harveyi* cells after induction with crystalline α-chitin, but the signals were not as strong as when colloidal chitin was used (data not shown).

Single channel properties of VhChiP and chitin oligosaccharide translocation

The pore-forming properties of *Vh*ChiP were investigated at the molecular level using a planar lipid bilayer (BLM) set-up for ion current recordings. The signals for functional analysis were acquired on application of a small potential across two Ag/AgCl wires, one either side of an artificial bilayer of diphytanoylphosphatidylcholine (DPhPC) in 1 M KCl (pH 7.5), and the parallel measurement of the electrostatically driven ion (current) flow through the normally non-conducting lipid membrane, on the

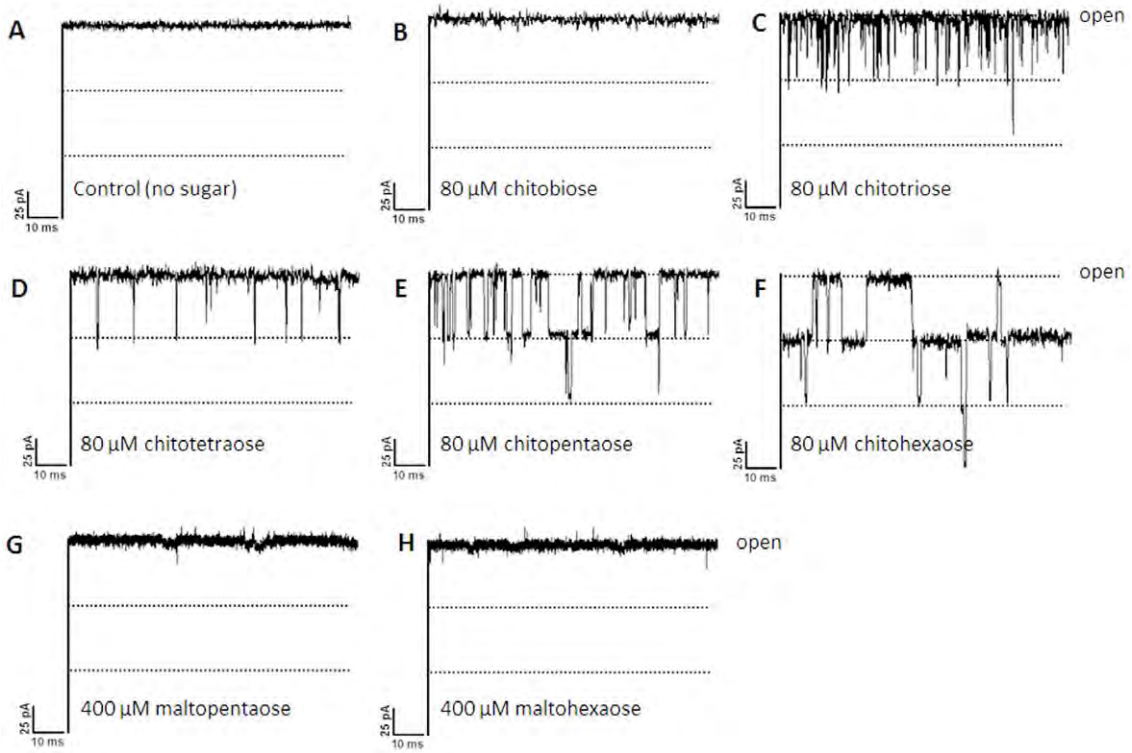

Figure 6. Effect of chitooligosaccharides on chitoporin ion currents. A single channel of *Vh*ChiP was inserted in the artificial membrane in A. a fully open state. Then, chitooligosaccharide: chitobiose, -triose, -tetraose, -pentaose, and -hexaose were added on the *cis* side of the chamber to a final concentration of 80 μM. Control recordings were made with maltopentaose and maltohexaose at a concentration of 400 μM. Ion current fluctuations were monitored for 120 s at applied voltages of ±100 mV. Here, only ion traces for +100 mV are presented.
doi:10.1371/journal.pone.0055126.g006

inclusion of single pore-forming units. Reconstitution of trimeric *Vh*ChiP into a previously formed lipid bilayer membrane was reproducibly obtained through the addition of a small amount of the purified protein to the bulk phase of the membrane-bathing KCl solution on one or other side of the bilayer. Membrane insertions of *Vh*ChiP were visible in the continuous current recordings as well-defined, step-like increases of about +/−180 pA per protein entity at +/−100 mV transmembrane potential (Fig. 5A). At higher concentrations of *Vh*ChiP ($\mu g \cdot mL^{-1}$) added in the measuring buffer, multiple insertions of *Vh*ChiP were frequently seen and the resultant current traces displayed numerous fluctuations due to transient channel closures. However, the addition of much lower concentrations of added protein (<1 $ng \cdot mL^{-1}$) resulted in the incorporation of a single protein molecule in more constantly open state and this was the favored situation for inspecting the *Vh*ChiP single channel conductance and chitin oligosaccharide translocation. Figure 5B and 5C are characteristic examples of membrane current recordings (5 s out of 120 s measuring time) from individual *Vh*ChiP trimers inserted in a DPhPC bilayer in 1 M KCl under applied transmembrane potentials of +100 and −100 mV, respectively. The traces indicate that the inserted *Vh*ChiP channel is fully open, with a stable ionic current over the time of recording. Occasionally transient current deflections occur as one of the three subunits apparently closes and opens rapidly in a stochastic manner. In multiple measurements, single reconstituted trimeric *Vh*ChiP channels showed an average conductance of 1.8±0.13 nS (n = 50) in 1 M KCl (pH 7.5). As with many other bacterial porins, currents through DPhPC-incorporated *Vh*ChiP pores followed Ohm's Law, being directly proportional to the applied voltage over the range ±200 mV (Fig. 5D). Finally, *Vh*ChiP channels showed the typical voltage gating properties of bacterial porins and closed in a characteristic three-step fashion upon abrupt application of higher voltages (Fig. 5E). The threshold potential (critical voltage) inducing the trimeric closure of the channels was found to be ±150 mV, while at less than or equal to 100 mV the channels were not affected by gating perturbations and so were suitable for studies on chitin oligosaccharide translocation.

Chitoporin has been proposed to facilitate the movement of chitin degradation products from the extracellular into the periplasmic space of marine *Vibrios* [12,13] before they are further transported to the cytoplasm and used as an energy source. To test this function we performed experiments to investigate the effects of chitooligosaccharides of various sizes (see Fig. S2 for the chemical structure of chitobi-, tri-, tetra-, penta-, and hexaose) on fully-open pores of *Vh*ChiP in artificial phospholipid bilayer membranes. Fig. 6 shows current recordings from single *Vh*ChiP channels with all the tested chitooligosaccharides (Fig. 6A–F) as well as those acquired in comparative trials with the structurally related maltopentaose and maltohexaose (Fig. 6G and H). With no chitosugars in the measuring buffer (Fig. 6A), the ion current through a fully open *Vh*ChiP trimer was stable and the standard value of ~180 pA was measured with a transmembrane potential of +100 mV. The response of the system to the addition of the set of chitosugars was diverse. For instance, no transient decreases were observed when the reconstituted *Vh*ChiP was exposed to chitobiose (Fig. 6B). The current traces obtained had, however, slightly greater noise levels than controls without added solute. In marked contrast, the presence of higher MW chitosugars ($GlcNAc_{4,5,6}$) in the solution on the *cis* side of the membrane

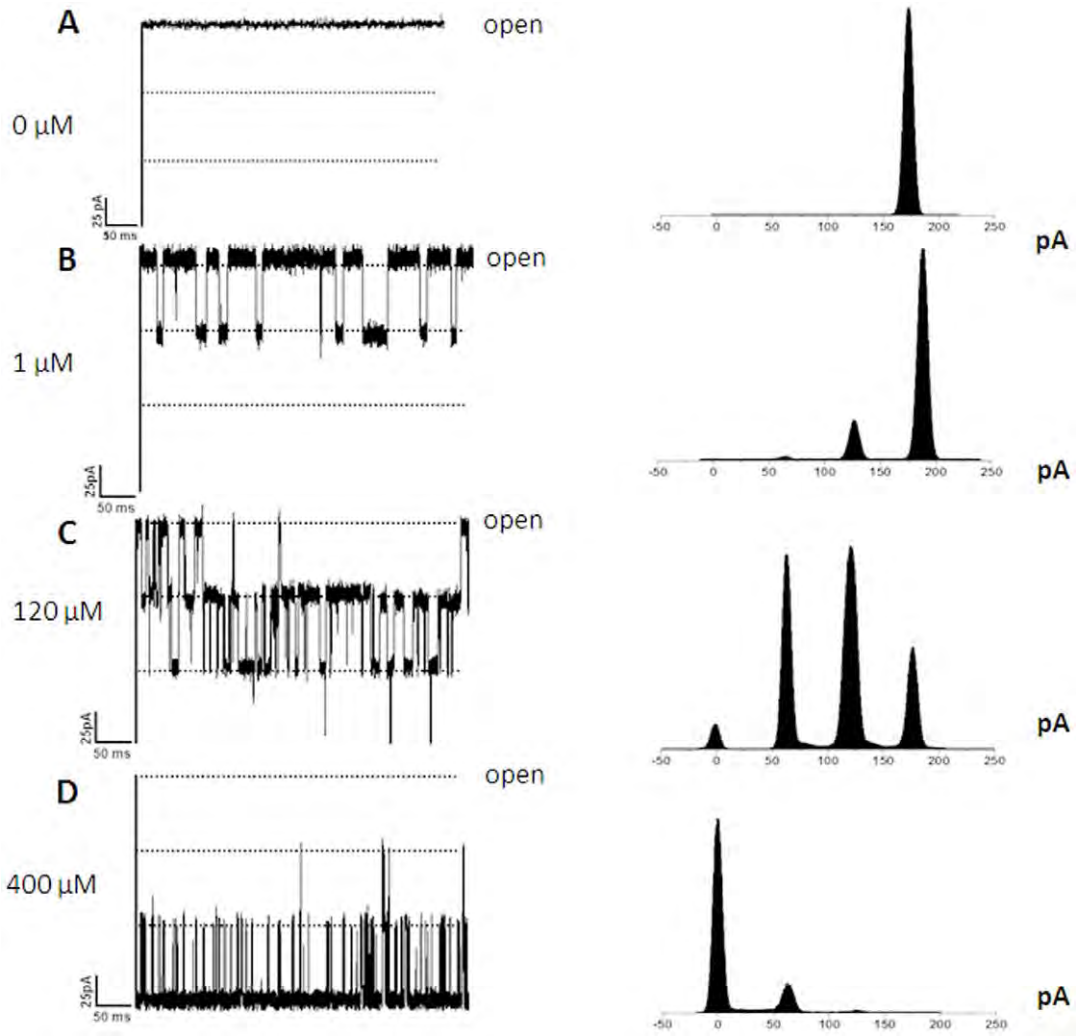

Figure 7. Effects of chitohexaose diffusion on subunit closure. The fully open *Vh*ChiP channel was exposed to different concentrations of chitohexaose (A–D). Right panel: the original traces displaying ion current blockade. Left panel: the corresponding frequency/current histograms, reflecting discrete changes in the subunit conductance upon sugar diffusion through the channel.
doi:10.1371/journal.pone.0055126.g007

produced clear short-lived downward current deflections (Fig. 6C to F). These correspond to the time-resolved blockade of the trimeric pores of *Vh*ChiP by individual chitooligosaccharide molecules that physically obstruct the channels in course of contact. Occlusion of ion flow during sugar diffusion apparently occurred as a reversible process by which each of the brief current decreases was caused by a single sugar molecule entering the *Vh*ChiP channel and leaving it very shortly later. Characteristic current traces for 80 µM chitotriose and chitotetraose showed that no more than one of the three subunits of a *Vh*ChiP trimer was blocked by such chitosugars, the other two remaining unaffected during that period (Fig. 6C and D). The frequency of the single subunit blockades was considerably higher for the triose than for the tetraose. At the same concentration, diffusion of chitopentaose also caused two-subunit blockage (Fig. 6E) and with chitohexaose, even blockage of all three channel subunits could be observed (Fig. 6F). Chitooligosaccharides were also added into the solution on the *trans* side of the bilayer membrane. As with sugar supplementation on the *cis* side, distinct channel blockades were observed in the corresponding membrane current recordings; however, for the same solute concentration the blocking effect was slightly less pronounced. The magnitude of the sugar-induced current depressions is the same for all compounds, corresponding to the quantized blockade of individual subunits; however, the shorter the oligosaccharide, the shorter the time of current blockage. Importantly, the exposure of single *Vh*ChiP channels to maltopentaose and maltohexaose did not cause the transient drops of ion flow that were observed with the chitosugars, even when five times higher concentrations (400 µM) of the maltosugars were used (Fig. 6G and H, respectively).

BLM trials with different chitosugars identified chitohexaose to be most potent in terms of pore obstruction (Fig. 6). Chitohexaose was thus chosen for evaluating the concentration dependence of chitosugar-induced *Vh*ChiP blockade. Membrane current recordings were taken for the same single channel, while the chitohexamer concentration was progressively increased from 0 µM to 1, 120 and 400 µM, respectively. Fig. 7 shows the original membrane current measurements (A–D, left panel) together with a statistical analysis of the raw data as current magnitude histograms (A–D, right panel). Clearly, the open probability of the channel decreases with increased concentrations of the sugar. On addition of 1.0 µM chitohexaose to the *cis* side of the chamber, the protein

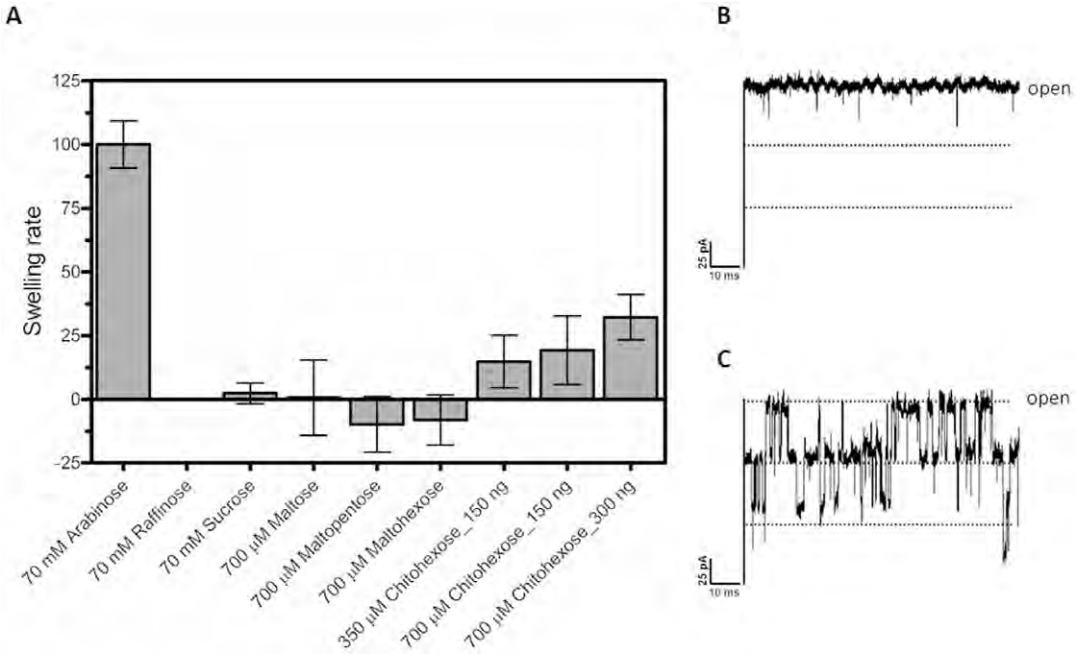

Figure 8. Liposome swelling assays. Multilamellar liposomes, prepared as described in the text, were reconstituted with purified *Vh*ChiP (150 or 300 ng). The isotonic concentration was defined as the concentration of raffinose added into the proteoliposome suspension that did not cause change in absorbance at 500 nm for a period of 60 s. Permeation of different types of sugars through *Vh*ChiP reconstituted liposomes were then tested. A) The swelling rates were normalized, with the rate of swelling in arabinose set to100%. Values presented are averages of 4–6 independent experiments. B) BLM measurement of *Vh*ChiP ion current with the isotonic concentration of raffinose (70 mM) added. C) BLM measurement of *Vh*ChiP in the presence of 70 mM raffinose and 200 μM chitohexaose.
doi:10.1371/journal.pone.0055126.g008

channel instantaneously transformed from being constantly fully open (Fig. 7A) to a state in which one subunit of *Vh*ChiP was temporarily occluded (Fig. 7B). This is shown by a decrease of the channel conduction by one-third of the full conductance. As its concentration was raised to 120 μM (Fig. 7C), the sugar began to occupy two subunits, decreasing the conductance by two-thirds. At this concentration, occupation of the third subunit was periodically observed, with the channel conductance reduced to zero. At 400 μM chitohexaose (Fig. 7D), two of the three subunits were constantly blocked, and the effect of increased chitohexaose concentration on the third subunit was apparent. The probability of complete closure of the trimeric channel was approx. 0.8, indicating that the *Vh*ChiP channel was nearly saturated by chitohexaose at this concentration.

The most likely explanation for the short-term inhibition by chitooligosaccharides of ion conduction by *Vh*ChiP is that these molecules permeate the membrane through *Vh*ChiP. Bulk entry of chitooligosaccharides into proteoliposomes containing *Vh*ChiP was therefore investigated by liposome swelling measurements.

Assay of sugar permeation by liposome swelling

High resolution ion conductance measurements were complemented by proeoliposome swelling assays, which determined the permeation of sugar molecules through *Vh*ChiP channels reconstituted into liposomes. Diffusion rates of sugars through *Vh*ChiP channels determined by these assays indicate influx of solutes into the proteoliposomes. The liposome swelling can be visualized by recording changes in the scattering signal of the liposome solution, using a spectrophotometer. Under isotonic conditions, the scattering signal remains constant throughout the measuring time, indicating neither swelling nor shrinking of the proteoliposomes. In the case of a solute permeation into the proteoliposomes, the total solute concentration inside the vesicles rises, driving the influx of water through the channels and swelling is detected as a decrease in absorbance. It is important to note that the rates of swell provide relative numbers to assess how the translocation varies from one sugar to the other. Here, we used raffinose, a branched sugar (MW 504.42) that is unable to diffuse through the porins and arabinose, a small sugar (MW 150.13) that always permeates through the channel, for comparison. Fig. 8A is an illustration of the swelling of liposomes exposed to chitohexaose, which was the sugar found to be the most potent channel blocker in membrane current measurements. The swelling rates in raffinose, sucrose, maltose, maltopentaose and maltohexaose are included for comparison. When normalized to the swelling rate of arabinose (set to 100%), only chitohexaose at low concentrations (350 and 700 μM) was found to permeate through *Vh*ChiP, and increases of internal osmolality occurred in a concentration-dependent manner. Fig. 8B is *Vh*ChiP single-channel current measurements in the presence of raffinose. The raffinose alone did not cause channel blockage at up to 70 mM, while further addition of a much lower concentration of the chitohexaose (200 μM) to the same bilayer, after the negative results with the raffinose were obtained, immediately produced current deflections (Fig. 8C). Observable swelling of the proteoliposomes apparently reflects permeation of chitohexaose through the embedding *Vh*ChiP pores in the lipid vesicles, but was not significant with other sugars.

Discussion

The chitin catabolic cascade of *Vibrios* is a complex system that involves a cluster of genes in the chitin-induced $GlcNAc_2$ operon, which is stringently controlled by a two-component chitin sensor/

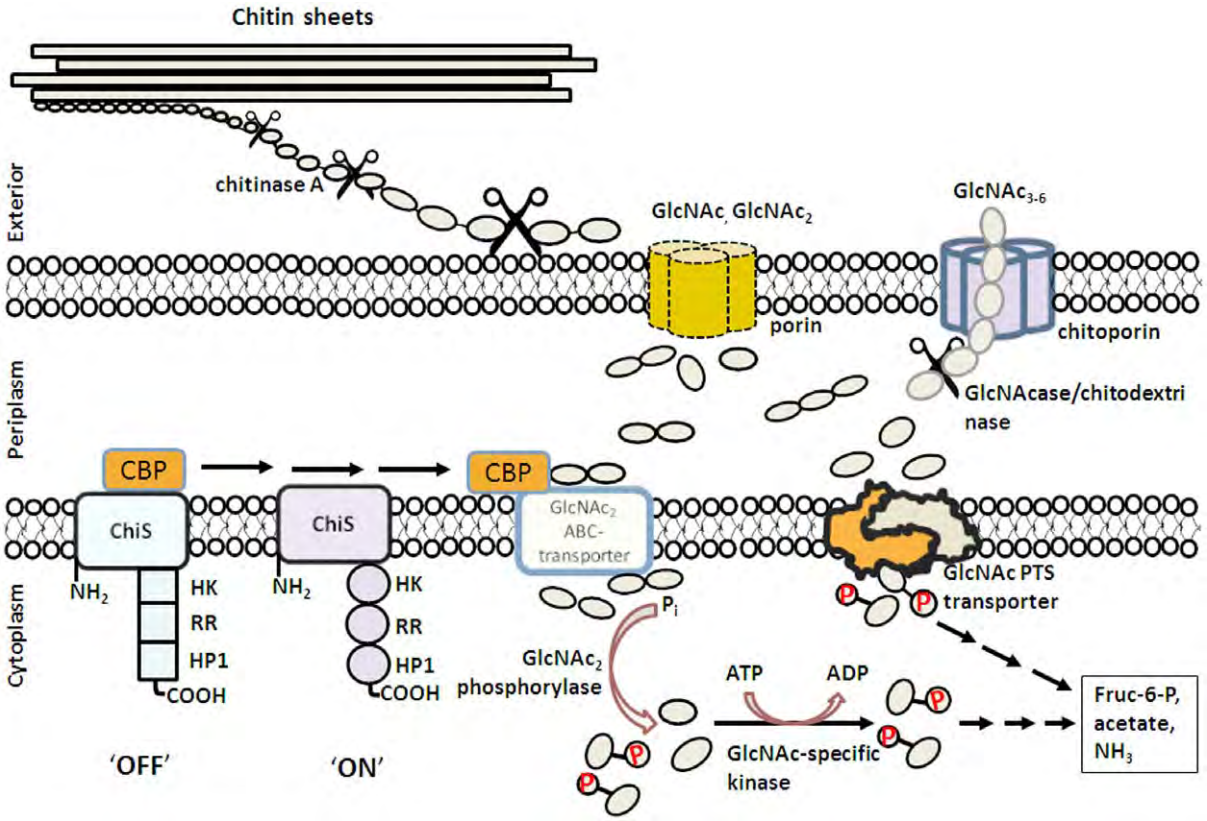

Figure 9. Model of the chitin degradation cascade of the marine bacterium *Vibrio harveyi.* The model was reconstructed from the chitinolytic cascade proposed by Li and Roseman [6]. After chitin degradation by chitinase, the chitin fragments are transported through the outer membrane by diffusion through porin or chitoporin, depending on their sizes. Further enzymatic degradation takes place in the periplasm, producing GlcNAc and $GlcNAc_2$. Binding of $GlcNAc_2$ to CBD activates the ChiS sensor, producing transcription of the genes under control of the $GlcNAc_2$ catabolic operon. GlcNAc is translocated to the cytoplasm by the GlcNAc PTS system, while $GlcNAc_2$ is transported through the inner membrane by the $GlcNAc_2$ ABC permease. Both products are phosphorylated, and finally converted to Fructose-6-P, acetate and NH_3.
doi:10.1371/journal.pone.0055126.g009

histidine kinase (also referred to as ChiS sensor) [6,13]. Fig. 9 summarizes the multiple-step process in the chitin degradation pathway, which involves: i) Chitin binding. Traces of chitooligosaccharides in the surrounding microenvironment are suggested to act as a chemoattractant that triggers adhesion the bacteria to the surface of chitin-containing particles [3,40]. ii) Chitin degradation. Secretion of chitinases leads to partial degradation of chitin to chitoligosaccharides on the extracellular side of the bacterial cell wall. Endochitinases (mainly chitinase A) were shown to mostly be responsible for chitin degradation [5,41]. iii) Molecular uptake of chitooligosaccharides. Chitin degradation products presumably permeate the outer membrane of the bacteria through a substrate-specific porin (referred to as "chitoporin or ChiP" [6,9]. iv) Further breakdown of chitooligosaccharides. In the periplasm, *β-N*-acetylglucosaminidase [42] and chitodextrinase [43] degrade the translocated chitin fragments to GlcNAc and $GlcNAc_2$. $GlcNAc_2$ generated in the periplasm is crucial as it binds to the chitin binding protein (CBP) that is usually attached to ChiS at the outer part of the inner membrane. Dissociation of CBP upon binding to $GlcNAc_2$ successively activates the ChiS sensor, which in turn up-regulates expression of the genes that comprise the *chiS* regulon [6,13]. v) Active transport of GlcNAc and $GlcNAc_2$ into cytoplasm. $GlcNAc_2$ is transported through the inner membrane by the $GlcNAc_2$ ABC-type permease [44], whereas GlcNAc is transported by the phosphoenolpyruvate transferase system (PTS) [45,46]. vi) Generation of metabolic intermediates. Upon arrival in the cytoplasm, individual dimers are phosphorylated by the cytoplasmic $GlcNAc_2$ phosphorylase as follows: $GlcNAc_2 + P_i = GlcNAc\text{-}6\text{-}P + GlcNAc$ [7]. GlcNAc from the ABC transport system is phosphorylated by a specific GlcNAc kinase [47]. Alternatively, PTS converts GlcNAc to GlcNAc-6-P, concurrently with translocation. As a result, the final forms of intracellular intermediates are fructose-6-P, acetate and NH_3, which can readily be metabolized as carbon and nitrogen sources for the cells.

Although the chitin degradation pathway of *Vibrios* has been generally accepted [3–7], some key issues remain to be clarified concerning the functionality of the proteins involved in the pathway, of which chitoporin is an example. Chitoporin was first identified in *V. furnissii* in 2000 [12]. However, its distinctive function as a chitooligosaccharide-specific channel has not been demonstrated hitherto. To understand the specificity of oligosaccharide transport through the outer membrane, it is necessary to establish the physiological role of this protein. In this study, *V. harveyi* was selected as the source organism for two reasons. First, the mechanisms underlying chitin degradation by chitinase A and *N*-acetylglucosaminidases from *V. harveyi* have been studied in detail by our group [48–52]. Second, *V. harveyi* is a fast- growing bioluminescent bacterium through its adaptive ability to grow under anaerobic and respiratory conditions. Therefore, *V. harveyi* contributes significantly to a rapid turnover of chitin in marine ecosystems. It sometimes causes a fascinating phenomenon called

'milky seas', in which, during the night, a uniform blue glow is emitted from the seawater. Some glows cover nearly 6,000 square miles of deep oceans. *Ipso facto*, the chitin utilization machinery of *V. harveyi* is expected to work efficiently.

*Vh*ChiP was successfully cloned and the recombinant gene expressed in the *E. coli* system, as verified by mass-spectrometry (Fig. S1) and immunoblotting (Fig. 4A–E). Detection of endogenous expression of chitoporin when the *V. harveyi* cells were grown on chitin-containing medium suggests that the *chiP* gene is regulated by the same control system (the *chiS* regulon, refs 6,13) as the *chi A* gene. We demonstrated previously that in *V. harveyi* expression of the *Chi A* gene was strongly induced by chitin [41].

Single channel recordings revealed that *Vh*ChiP would insert readily into the artificial membranes and behaved as a pore-forming component with a characteristic trimeric closure when high external membrane potentials were applied (Fig. 5). Its structural homology with other porins (Fig. 2) strongly suggests that *Vh*ChiP has 16 β-stranded transmembrane domains, 8 extracellular loops and 8 periplasmic turns, as is observed for most bacterial porins [38–39,53].

BLM current measurements with high time-resolution were used to demonstrate the interaction of chitooligosaccharides with *Vh*ChiP. These are interpreted as indicating oligosaccharide translocation, confirming the specific function of *Vh*ChiP as a chitooligosaccharide-specific porin. The channel was found to interact with the chitosugars to various extents, depending on the sizes and the types of the sugars (Fig. 6). The observation of no fluctuation of ion current on the addition of chitobiose can be explained by the fact that this disaccharide could not permeate through the *Vh*ChiP channel; it may require a general diffusion porin as already described earlier (see Fig. 9). Alternatively, it may permeate so fast that the residence time is too small to lead to well-resolved blocking events. In contrast, the *Vh*ChiP channel was much more sensitive to higher-MW chitosugars ($GlcNAc_{3–6}$). The channel blocking behavior (Figs. 6 and 7) is comparable to the blockage of maltoporin by maltooligosaccharides [19] and also reflects a common characteristic of substrate-specific channels, in which higher-MW oligosaccharides are preferred substrates [32,54].

BLM measurements revealed no response of *Vh*ChiP to maltopentaose and maltohexaose even at a concentration five-fold greater than that of the chitosugars (Fig. 6). The results of liposome swelling assays additionally confirmed insignificant permeation of other sugars, including raffinose, maltose and sucrose (Fig. 9). These data indicate the high selectivity of the ChiP porin towards chitooligosaccharides. The low sequence identity of between *Vh*ChiP and other sugar-specific porins (less than 20%) (Fig. 1) also demonstrates no detailed structural similarity. *Vh*ChiP appears to be exceptionally specific for chitohexaose, as ion current fluctuation, representing the blockage of individual subunits, was detected at sugar concentrations as low as 125 nM (not shown). The sugar-channel interaction was even stronger at higher concentrations, almost fully blocking all three subunits. Taken together, the results suggest that *Vh*ChiP is a chitooligosaccharide-specific porin. Detailed characterization of channel specificity and binding kinetics towards different chitooligosaccharides has been the subject of our ongoing investigations.

In summary, we employed biochemical assays, together with high-time resolution single channel recordings to address, for the first time, the pore-forming property of chitoporin from the representative *V. harveyi*. The isolated ChiP was found to be highly specific for chitooligosaccharides. The data obtained from this study, therefore, establish the fundamental role of chitoporin in the chitin degradation pathway as the molecular gateway that the marine *Vibrios* employ to efficiently uptake chitooligosaccharides into the cellular interior in order to utilize them as a sole source of energy.

Accession number

The nucleotide sequence of *V. harveyi* chitoporin has been deposited in the EMBL Nucleotide Sequence Database under accession number HF558985.

Supporting Information

Figure S1 Identification of *V. harveyi* chitoporin by mass spectrometry. Tryptic peptides were prepared from the outer membrane fraction extracted with 2% (w/v) SDS, followed by 5% (v/v) octyl-POE by in-gel digestion method. The peptides were resolved by nano-LC/MS. The resultant monoisotopic masses were subjected to Mascot search using the NCBINr database for protein identification. Sequences underlined (P1–P9) are identical to nine internal peptides in the translated sequence of *V. harveyi* chitoporin identified in this study.
(TIF)

Figure S2 Chemical structure of chitin oligosaccharides and maltooligosaccharides.
(TIF)

Author Contributions

Conceived and designed the experiments: WS. Performed the experiments: WS WC PJ. Analyzed the data: WS KRM AS MW. Contributed reagents/materials/analysis tools: WS MW. Wrote the paper: WS KRM AS MW.

References

1. Jeuniaux C, Voss-Foucart MF (1991) Chitin biomass and production in the marine environment. Biochem Syst Ecol 19:347–356.
2. Zobell CE, Rittenberg SC (1938) The occurrence and characteristics of chitinoclastic bacteria in the sea. J Bacteriol 35:275–287.
3. Yu C, Lee AM, Bassler BL, Roseman S (1991) Chitin utilization by marine bacteria. A physiological function for bacterial adhesion to immobilized carbohydrates. J Biol Chem 266:24260–24267.
4. Bassler BL, Gibbons PJ, Yu C, Roseman S (1991) Chitin utilization by marine bacteria. Chemotaxis to chitin oligosaccharides by *Vibrio furnissii*. J Biol Chem 266:24268–24275.
5. Keyhani NO, Roseman S (1999) Physiological aspects of chitin catabolism in marine bacteria. Biochim Biophys Acta 1473:108–122.
6. Li X, Roseman S (2004) The chitinolytic cascade in *Vibrios* is regulated by chitin oligosaccharides and a two-component chitin catabolic sensor/kinase. Proc Natl Acad Sci USA 101:627–631.
7. Park JK, Keyhani NO, Roseman S (2000) Chitin catabolism in the marine bacterium *Vibrio furnissii*. Identification, molecular cloning, and characterization of A N, N′-diacetylchitobiose phosphorylase. J Biol Chem 275:33077–33083.
8. Bassler BL, Yu C, Lee CYC, Roseman S (1991) Chitin utilization by marine bacteria. Degradation and catabolism of chitin oligosaccharides by *Vibrio furnissii*. J Biol Chem 266:24276–24286.
9. Hunt DE, Gevers D, Vahora NM, Polz MF (2008) Conservation of the chitin utilization pathway in the *Vibrionaceae*. Appl Environ Microbiol 74:44–51.
10. Pruzzo C, Vezzulli L, Colwell RR (2008) Global impact of *Vibrio cholerae* interactions with chitin. Environ Microbiol 10:1400–1410.
11. Jung BO, Roseman S, Park JK (2008) The central concept for chitin catabolic cascade in marine bacterium, *Vibrios*. Macromol Res 16:1–15.
12. Keyhani NO, Li XB, Roseman S (2000) Chitin catabolism in the marine bacterium *Vibrio furnissii*. Identification and molecular cloning of a chitoporin. J Biol Chem 275:33068–33076.
13. Meibom KL, Li XB, Nielsen AT, Wu CY, Roseman S, et al. (2004) The *Vibrio cholerae* chitin utilization program. Proc Natl Acad Sci USA 101:2524–2529.
14. Prilipov A, Phale PS, Van Gelder P, Rosenbusch JP, Koebnik R (1998) Coupling site-directed mutagenesis with high-level expression: large scale production of mutant porins from *E. coli*. FEMS Microbiol Lett 163:65–72.
15. Garavito RM, Rosenbusch JP (1986) Isolation and crystallization of bacterial porin. Methods Enzymol 125:309–328.

16. Rosenbusch JP (1974) Characterization of the major envelope protein from *Escherichia coli*. Regular arrangement on the peptidoglycan and unusual dodecyl sulfate binding. J Biol Chem 249:8019–8029.
17. Lugtenberg B, Van Alphen L (1983) Molecular architecture and functioning of the outer membrane of *Escherichia coli* and other gram-negative bacteria. Biochim Biophys Acta 737:51–115.
18. Dando RT, Young EPS (1990) in The NCIMB catalogue of strains: Growth media., p. 172, Aberdeen University Press, Aberdeen
19. Bezrukov SM, Kullman L, Winterhalter M (2000) Probing sugar translocation through maltoporin at the single channel level. FEBS Lett 476:224–228.
20. Schwarz G, Danelon C, Winterhalter M (2003) On translocation through a membrane channel via an internal binding site: kinetics and voltage dependence. Biophys J 84:2990–2998.
21. Danelon C, Brando T, Winterhalter M (2003) Probing the orientation of reconstituted maltoporin channels at the single-protein level. J Biol Chem 278:35542–35551.
22. Kullman L, Winterhalter M, Bezrukov SM (2002) Transport of maltodextrins through maltoporin: a single-channel study. Biophys J 82:803–812.
23. Mahendran KR, Chimerel C, Mach T, Winterhalter M (2009) Antibiotic translocation through membrane channels: temperature-dependent ion current fluctuation for catching the fast events. Eur Biophys J 38:1141–1145.
24. Van Gelder P, Dumas F, Winterhalter M (2000) Understanding the function of bacterial outer membrane channels by reconstitution into black lipid membranes. Biophys Chem 85:153–167.
25. Luckey M, Nikaido H (1980) Diffusion of solutes through channels produced by phage lambda receptor protein of *Escherichia coli*: inhibition by higher oligosaccharides of maltose series. Biochem Biophys Res Commun 93:166–171.
26. Yoshimura F, Nikaido H (1985) Diffusion of beta-lactam antibiotics through the porin channels of *Escherichia coli* K-12. Antimicrob Agents Chemother 27:84–92.
27. Clément JM, Hofnung M (1981) Gene sequence of the lambda receptor, an outer membrane protein of *E. coli* K12. Cell 27:507–514.
28. Forst D, Welte W, Wacker T, Diederichs K (1998) Structure of the sucrose-specific porin ScrY from *Salmonella typhimurium* and its complex with sucrose. Nat Struct Biol 5:37–46.
29. Wylie JL, Worobec EA (1994) Cloning and nucleotide sequence of the *Pseudomonas aeruginosa* glucose-selective OprB porin gene and distribution of OprB within the family *Pseudomonadaceae*. Eur J Biochem 220:505–512.
30. Trias J, Rosenberg EY, Nikaido H (1988) Specificity of the glucose channel formed by protein D1 of *Pseudomonas aeruginosa*. Biochim Biophys Acta 938:493–496.
31. Schirmer T, Keller TA, Wang YF, Rosenbusch JP (1995) Structural basis for sugar translocation through maltoporin channels at 3.1 A resolution. Science 267:512–514.
32. Dumas F, Koebnik R, Winterhalter M, Van Gelder P (2000) Sugar transport through maltoporin of *Escherichia coli*. Role of polar tracks. J Biol Chem 275:19747–19751.
33. Dutzler R, Schirmer T, Karplus M, Fischer S (2002) Translocation mechanism of long sugar chains across the maltoporin membrane channel. Structure 10:1273–1284.
34. Denker K, Orlik F, Schiffler B, Benz R (2005) Site-directed mutagenesis of the greasy slide aromatic residues within the LamB (maltoporin) channel of *Escherichia coli*: effect on ion and maltopentaose transport. J Mol Biol 352:534–550.
35. Orlik F, Andersen C, Benz R (2002) Site-directed mutagenesis of tyrosine 118 within the central constriction site of the LamB (maltoporin) channel of *Escherichia coli*. II. Effect on maltose and maltooligosaccharide binding kinetics. Biophys J 83:309–321.
36. Orlik F, Andersen C, Benz R (2002) Site-directed mutagenesis of tyrosine 118 within the central constriction site of the LamB (Maltoporin) channel of *Escherichia coli*. I. Effect on ion transport. Biophys J 82:2466–24675.
37. Zeth K, Diederichs K, Welte W, Engelhardt H (2000) Crystal structure of Omp32, the anion-selective porin from *Comamonas acidovorans*, in complex with a periplasmic peptide at 2.1 A resolution. Structure 8:981–992.
38. Koebnik R, Locher KP, Van Gelder P (2000) Structure and function of bacterial outer membrane proteins: barrels in a nutshell. Mol Microbiol 37:239–253.
39. Nikaido H (1992) Porins and specific channels of bacterial outer membranes. Mol Microbiol 6:435–442.
40. Bassler BL, Gibbons PJ, Yu C, Roseman S (1991) Chitin utilization by marine bacteria. Chemotaxis to chitin oligosaccharides by *Vibrio furnissii*. J Biol Chem 266:24268–24275.
41. Suginta W, Robertson PA, Austin B, Fry SC, Fothergill-Gilmore LA (2000) Chitinases from *Vibrio*: activity screening and purification of chiA from *Vibrio carchariae*. J Appl Microbiol 89:76–84.
42. Keyhani NO, Roseman S (1996) The chitin catabolic cascade in the marine bacterium *Vibrio furnissii*. Molecular cloning, isolation, and characterization of a periplasmic beta-N-acetylglucosaminidase. J Biol Chem. 271:33425–33432.
43. Keyhani NO, Roseman S (1996) The chitin catabolic cascade in the marine bacterium *Vibrio furnissii*. Molecular cloning, isolation, and characterization of a periplasmic chitodextrinase. J Biol Chem 271:33414–33424.
44. Bouma CL, Roseman S (1996) Sugar transport by the marine chitinolytic bacterium *Vibrio furnissii*. Molecular cloning and analysis of the glucose and N-acetylglucosamine permeases. J Biol Chem 271:33457–33467.
45. Bouma CL, Roseman S (1996) Sugar transport by the marine chitinolytic bacterium *Vibrio furnissii*. Molecular cloning and analysis of the mannose/glucose permease. J Biol Chem 271:33468–33475.
46. Keyhani NO, Wang LX, Lee YC, Roseman S (1996) The chitin catabolic cascade in the marine bacterium *Vibrio furnissii*. Characterization of an N,N′-diacetyl-chitobiose transport system. J Biol Chem 271:33409–33413.
47. Park JK, Wang LX, Roseman S (2002) Isolation of a glucosamine-specific kinase, a unique enzyme of *Vibrio cholerae*. J Biol Chem 277:15573–15578.
48. Suginta W, Vongsuwan A, Songsiriritthigul C, Prinz H, Estibeiro P, et al. (2004) An endochitinase A from *Vibrio carchariae*: cloning, expression, mass and sequence analyses, and chitin hydrolysis. Arch Biochem Biophys 424:171–180.
49. Suginta W, Vongsuwan A, Songsiriritthigul C, Svasti J, Prinz H (2005) Enzymatic properties of wild-type and active site mutants of chitinase A from *Vibrio carchariae*, as revealed by HPLC-MS. FEBS J 272:3376–3386.
50. Suginta W, Songsiriritthigul C, Kobdaj A, Opassiri R, Svasti J (2007) Mutations of Trp275 and Trp397 altered the binding selectivity of *Vibrio carchariae* chitinase A. Biochim Biophys Acta 1770:1151–1160.
51. Songsiriritthigul C, Pantoom S, Aguda AH, Robinson RC, Suginta W. (2008) Crystal structures of *Vibrio harveyi* chitinase A complexed with chitooligosaccharides: implications for the catalytic mechanism. J Struct Biol 162:491–499.
52. Suginta W, Chuenark D, Mizuhara M, Fukamizo T (2010) Novel β-N-acetylglucosaminidases from *Vibrio harveyi* 650: cloning, expression, enzymatic properties, and subsite identification. BMC Biochem 11:40.
53. Schirmer T (1998) General and specific porins from bacterial outer membranes. J Struct Biol 121:101–109.
54. Hilty C, Winterhalter M (2001) Facilitated substrate transport through membrane proteins. Phys Rev Lett 86:5624–5627.

Single-Molecule Trapping Dynamics of Sugar-Uptake Channels in Marine Bacteria

Wipa Suginta

Biochemistry-Electrochemistry Research Unit, Schools of Chemistry and Biochemistry, Institute of Science, Suranaree University of Technology, Nakhon Ratchasima 30000, Thailand

M. F. Smith*

School of Physics, Institute of Science, Suranaree University of Technology, Nakhon Ratchasima 30000, Thailand and Thailand Center of Excellence in Physics (ThEP), Commission of Higher Education, Ministry of Education, Bangkok 10400, Thailand

(Received 25 March 2013; published 4 June 2013)

Stochastic fluctuations of ion current through one chitoporin (ChiP) channel within a bilayer lipid membrane in sugar solution are analyzed. These reflect single-molecule dynamics, which indicate that ChiP has multiple binding sites for sugar and exploits interactions between bound molecules to direct sugar passage. Since ChiP is used by marine bacteria, this is likely an adaptive strategy to enhance sugar translocation from rough water.

DOI: 10.1103/PhysRevLett.110.238102 PACS numbers: 87.16.dp, 87.14.ep, 87.15.hj, 87.15.Vv

Some gram-negative bacteria uptake sugar from ambient fluid through a protein channel, which is an assembly of nanotubes, in their cell membrane [1]. Molecules of a specific sugar that diffuse into the channel can become trapped, remaining bound in a nanotube for many milliseconds before escaping into the cell. A bound molecule obstructs a nanotube so measurements of ionic current through a channel in sugar solution exhibit stepwise changes that track single-molecule dynamics on the millisecond time scale [2–4]. By studying the current profile of channels used by different bacteria, adaptive channel designs can be studied quantitatively.

The bioluminescent bacterium *V. harveyi* is responsible for the disease luminous Vibriosis, a leading cause of death in fish and prawn farms [5,6]. Having a high growth rate and able to survive extreme conditions, the bacteria effect rapid turnover of chitin in marine ecosystems. The bacterium degrades chitin into smaller sugar molecules and selectively uptakes chitohexaose through a channel called chitoporin (or ChiP) [7–14]. ChiP is a trimer, composed of three identical nanotubes (monomers) and thus, similar to other channels, like maltoporin from *E. coli* [1,15–18]. But ChiP operates in more demanding rough-water conditions and, accordingly, translocates sugar across a lipid bilayer more rapidly by orders of magnitude [19] than comparable channels [20–23].

In this Letter, we present data of ion current fluctuations $I(t)$ through a bilayer lipid membrane immersed in chitohexaose solution and perforated with one trimeric ChiP. $I(t)$ fluctuates among discrete bands such that $I(t) \approx I_n = I_0(3 - n)/3$ when n monomers are blocked by sugar. By analyzing the stochastic integer n, we find that (i) each ChiP monomer functions independently, (ii) a monomer has multiple binding sites (or traps) that can be occupied simultaneously, and (iii) there is evidence that molecules bound in the same monomer attract each other.

The results indicate a multiple-trap design that could explain how ChiP uptakes sugar so effectively. Studies on maltoporin were interpreted using single trap models [24]. While one trap is sufficient for uptaking sugar from a congenial environment, multiple traps can stream sugar across the membrane more rapidly. Using the intuitive population-decay approach developed below, multiple-molecule trapping by ChiP is evident from data. This offers advantages over power-spectral analysis, widely used to interpret similar $I(t)$ data, in which such essential properties are identified using fits to model calculations.

We now present details [25]. Two chambers, separated by a 25 μm thick Teflon film barrier with a 30 μm radius aperture, are filled with 1M of KCl. Ag/AgCl electrodes are immersed on respective sides of the barrier. After adding the lipid DPhPC, a bilayer is formed over the aperture [26]. A 100 mV bias produces no current, so the bilayer is impenetrable to K^+ and Cl^- ions. A few minutes after 50–100 ng/mL of *Vh*ChiP is added to the cis side of the membrane, a step increase of $I(t)$ is seen, indicating that the first channel has opened in the bilayer. Here, the cis side of the membrane is defined as the side at higher electrical potential than the opposite, trans side. Studies of maltoporin indicate that the natural mouth of the channel points towards the chamber to which the precursor (*Vh*ChiP) is added, so we regard the cis side as being analogous to the cell exterior [27,28]. After the first ChiP insertion, the protein solution was gently diluted by sequential additions of electrolyte to prevent further insertions.

The current through the open trimer averaged $I_0 \approx$ 186 pA with a 100 mV bias. $I(t) - I_0$ can be fit by a Gaussian with standard deviation $\sigma_0 \approx 8$ pA. With chitohexaose added to the cis side, $I(t)$ fluctuated between bands I_n, see Fig. 1. Band transitions in Fig. 1 indicate that a molecule can enter or leave a monomer in roughly $t_{\min} =$ 0.1 ms. When a molecule enters an unoccupied monomer,

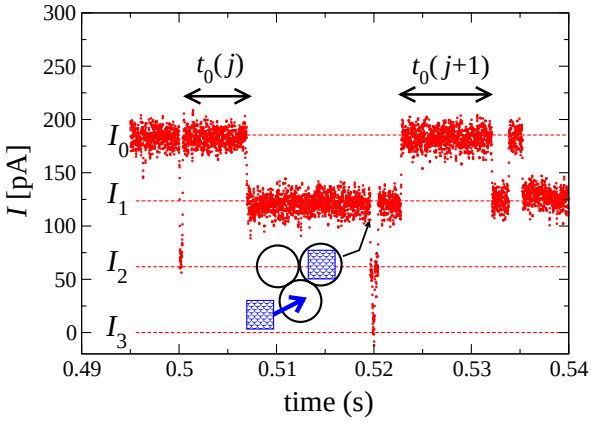

FIG. 1 (color online). Dynamical trapping of single sugar molecules by a ChiP protein channel. The ion current $I(t)$ measured through a single ChiP, which perforates an otherwise intact lipid bilayer, with a sugar concentration of 5 μM on one side of the membrane is measured versus time. The ChiP consists of three identical tubes (or monomers) and the ion current fluctuates such that $I(t) \approx I_n = I_0(3-n)/n$ with $n = 0$, 1, 2, 3 when n monomers are blocked by sugar molecules. $I(t)$ remains in a band for a time $t_n[j]$, where j counts each occurrence, then makes a transition associated with either trapping or detrapping of a single molecule. An $I_1 \rightarrow I_2$ trapping event is illustrated by the cartoon: with one monomer already blocked, a second monomer traps a sugar molecule, resulting in a current decrease.

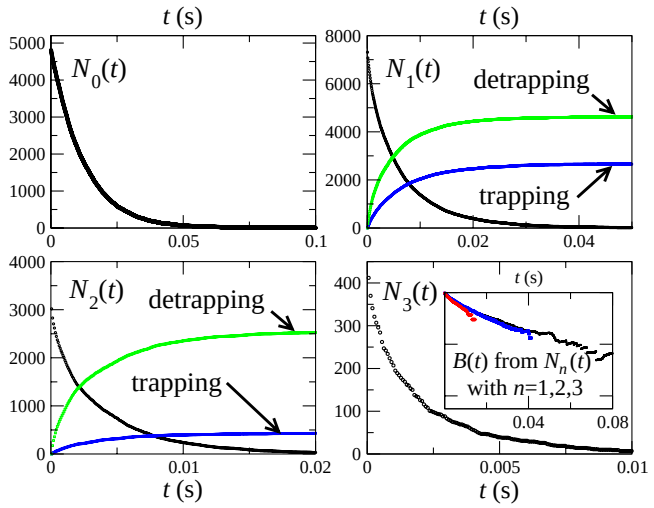

FIG. 2 (color online). Plots of $N_n(t)/N_n(0)$, which is the probability that n monomers of the ChiP trimer remain continuously blocked by sugar molecules bound within them for longer than t. $N_n(t)$ is obtained from $I(t)$ data, like that in Fig. 1, by counting the number of different j for which $t_n[j] > t$. For $n = 0$ ($n = 3$) all segments end when an open (blocked) monomer becomes blocked (open), which we call trapping (detrapping). For $n = 1$, 2, both processes occur. The inset in the lower right shows the $B(t)$ (the logarithm of the probability for a single monomer to remain blocked for time t) as determined from the $n = 1$, 2, and 3 distributions. The fact that they agree means that different monomers in the trimer act independently.

n increases by one. The fact that n can then remain constant for a time $t_n[j] \gg t_{\min}$ means that molecules can be chemically bound (i.e., "trapped") in a monomer [29]. Thermal fluctuations provide the rare, sudden events in which a molecule escapes (i.e., "detraps"). If the escape empties the monomer then n decreases by one.

We record times $t_n[j]$, over which the current remains continuously in band n, where j counts each occurrence. Small values $t_n[j] < t_{\min} = 0.1$ ms are ignored (if $I(t)$ fluctuates away from n but returns within $t_{\min}$ then it is treated as if it never left n). Fluctuations on a time scale less than $t_{\min}$, which could result from a molecule diffusing into a monomer without becoming bound (as well as outlying points of Gaussians straying between bands), are not studied. Correlations between $t_n[j]$ (for the same n but different j) are assessed using the function, $\chi_n(s) \equiv \sum_j (t_n[j] - \bar{t}_n)(t_n[j+s] - \bar{t}_n)/\bar{t}_n^2$ where s is an integer and $\bar{t}_n$ is the average of $t_n[j]$ over all j.

The measured quantity $N_n(t)$ is the number of j for which $t_n[j] > t$. $N_n(t)/N_n(0)$ is interpreted as the probability for n monomers to remain continuously blocked for a time longer than t. Sample distributions $N_n(t)$ are shown in Fig. 2. Almost all $t_n[j]$ ended with a transition in which n changes by $\Delta n = \pm 1$. Events with $|\Delta n| > 1$ were too rare to treat statistically. For an open trimer, $\chi_0(1)/\chi_0(0) \approx 0.01$ for a sample size $N_0(0) \approx 4800$. While for a trimer with one blocked monomer, the value $\chi_1(1)/\chi_1(0) \approx 0.06$ for $N_1(0) \approx 7500$. These weak correlations indicate that $t_n[j]$ and $t_n[j' \neq j]$ are approximately independent.

To determine if trapping in different monomers is correlated, we compare $N_n(t)$ for the trimer to that expected for three independent monomers. We define the probability for a monomer, initially unblocked, to remain continuously unblocked for more than t as $\exp(U[t])$ and the probability for a monomer, initially blocked, to remain continuously blocked for more than t as $\exp(B[t])$. For identical, independent monomers

$$\ln N_n(t) - \ln N_n(0) = (3-n)U(t) + nB(t). \quad (1)$$

Equation (1) relates four measured $N_n(t)$ to two unknowns $U(t)$ and $B(t)$, and can be checked for consistency. Using Eq. (1), we obtained $U(t)$ from $N_0(t)$ and then used $n = 1$, 2, 3 to obtain three estimates of $B(t)$. These estimates, shown together in Fig. 2, agree. This rules out significant correlation between monomers. Each monomer acts independently.

Henceforth, we study a single monomer, characterized by $U(t)$ and $B(t)$. $U(t)$ describes trapping by an open monomer and $B(t)$ describes detrapping from an occupied monomer. Note that the $I(t)$ measurement cannot determine how many molecules occupy a monomer (the first molecule blocks the current so the arrival or departure of

additional molecules has no effect). If a monomer becomes occupied at $t = 0$ then $\exp[B(t)]$ is the probability for it to remain occupied, by at least one molecule, beyond time t.

In Fig. 3, $U(t)$ and $B(t)$ are shown for a range of sugar concentrations $[c]$ on the cis side. $U(t)$ is approximately

$$U(t) \approx -k_{\mathrm{on}}[c]t, \tag{2}$$

where the empirical parameter $k_{\mathrm{on}}[c]$ can be understood as the rate at which sugar molecules are trapped by an open monomer. With a factor of $[c]$ removed, k_{on} is the trapping rate per molar of sugar in solution.

In the upper right panel, $k_{\mathrm{on}}[c]$ is plotted versus $[c]$ and appears linear. The nonzero $[c] = 0$ intercept may result from channel gating: nanotubes exhibit voltage-dependent contractions even in the absence of sugar [17]. Allowing for a nonzero intercept, a linear fit gives $k_{\mathrm{on}} = 4.0\ \mathrm{s}^{-1}\ \mu\mathrm{M}^{-1}$. This is much smaller than the diffusion-limited capture rate per molar $k_{\mathrm{app}} = 4DaN_A$ where a is the nanotube diameter, D is the diffusion coefficient of sugar and N_A is Avogadro's number [30,31]. Using $a \approx 0.5$ nm, we have $k_{\mathrm{app}} \approx 200k_{\mathrm{on}}$, so only $1/200$ of the molecules that diffuse to the mouth of the monomer become stably bound within it.

Turning to detrapping, $B(t)$ drops rapidly for $t < 0.01$ s by an amount that depends on $[c]$. For $t > 0.01$ s, it is described by

$$B(t) \approx -a - k_{\mathrm{off}}t \quad (\text{for } t > 0.01\ \mathrm{s}), \tag{3}$$

where the empirical parameters a and k_{off} are independent of t. From Fig. 3, k_{off} is independent of $[c]$ with a value of roughly $50\ \mathrm{s}^{-1}$. The extrapolated intercept a decreases with $[c]$.

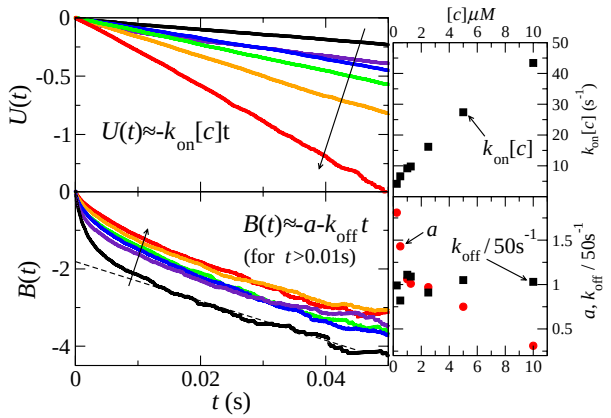

FIG. 3 (color online). Evidence for multiple-molecule trapping by a monomer. Left panels: Horizontal axis is time t and vertical axis is logarithm of the probability that a monomer remains unblocked (upper panel) or blocked (lower panel) for longer than t, denoted by $U(t)$ or $B(t)$. Curves are for different sugar concentrations $[c]$, along arrows: $[c] = 0.25$, 0.5, 1.0, 2.5, 5, and 10 μM. For $t > 0.01$, linear fits to $B(t)$ (the dashed line) can be made, but the low-t nonlinear behavior indicates multiple trapping states. Upper right: slope $k_{\mathrm{on}}[c]$ of linear fit to $U(t)$, versus $[c]$. Lower right: Slope k_{off} and extrapolated $t = 0$ intercept a, from linear fit to $B(t)$ for $t > 0.01$ s, versus $[c]$.

Consider the t and $[c]$ dependence of $B(t)$. At small t, the steep slope describes fast detrapping. Fast detrapping plays an important role at low $[c]$, causing a large drop of $B(t)$, but has less effect at high $[c]$. On a longer t scale, the slow detrapping rate $k_{\mathrm{off}} \approx 50\ \mathrm{s}^{-1}$ sets in. Slow detrapping is most important at high $[c]$ (the fraction of occupied monomers that empty via the slow process is $\exp(-a)$, which increases with $[c]$). The natural interpretation of this behavior is that there are at least two binding states, with different detrapping rates, that can be simultaneously occupied. Fast detrapping affects singly occupied monomers, and slow detrapping affects multiply occupied monomers. As $[c]$ increases, multiple occupation becomes more likely and slow detrapping dominates.

A simple model provides more detail [25]. We use a model monomer with two traps, 1 and 2, that act in series, with 1 nearer the cis end. The monomer can be blocked in three ways (a molecule in trap $\alpha = 1$, 2 or in both, which we denote by $\alpha = 3$). At $t = 0$, the monomer has a probability $p_\alpha(t = 0) = \delta^1_\alpha$ to be in state α. Then $d\mathbf{p}/dt = \mathbf{M} \cdot \mathbf{p}$, where $\mathbf{M}$ is a matrix and $\mathbf{p}$ a vector with components p_α, determines the probability at later t. We have

$$B(t) = \ln\Big(\sum_j \Lambda_j \exp[\mu_j t]\Big), \tag{4}$$

where μ_j are eigenvalues of $\mathbf{M}$, rows of $\mathbf{m}$ are eigenvectors of $\mathbf{M}$, and $\Lambda_j = \Sigma_{\alpha,\beta} p_\alpha(0) m^{-1}_{\alpha,j} m_{j,\beta}$.

A molecule detraps from $\alpha = 1$, 2 at a rate k_α and hops from 1 to 2 at a rate x_+ (or x_- in reverse). These processes are included in a matrix $\mathbf{M}_0$. A smaller term $\mathbf{M}_1$ couples to $\alpha = 3$ with $\mathbf{M} = \mathbf{M}_0 + \mathbf{M}_1$. $\mathbf{M}_1$ includes $\tilde{k}_{\mathrm{on}}[c]$, the trapping rate of a monomer with a molecule in trap 2, and $\tilde{k}_\alpha$, the rate at which a doubly occupied monomer empties trap α. Both molecules detrap at once at a rate $\tilde{k}_{12}$ with $\tilde{k} = \tilde{k}_1 + \tilde{k}_2 + \tilde{k}_{12}$.

To first order in $\mathbf{M}_1$ and at large t, Eq. (4) gives Eq. (3) with

$$k_{\mathrm{off}} = \tilde{k}, \qquad a = -\ln\Big(\frac{\tilde{k}_{\mathrm{on}}[c]x_+}{k_1k_2 + k_2x_+ + k_1x_-}\Big). \tag{5}$$

The large-t slope is constant and equal to the total detrapping rate of a doubly occupied monomer. In Fig. 4, calculations of $B(t)$ are shown. All curves use the same parameters, except for $\tilde{k}_{\mathrm{on}}[c]$, which increases along the arrow: $\tilde{k}_{\mathrm{on}}[c] = 3$, 6, 9, 12, and $15k_1$, respectively. We used: $k_1 = x_- = (1/2)k_2 = (1/20)x_+ = 40\ \mathrm{s}^{-1}$, also $\tilde{k}_1 = \tilde{k}_2 = 0$ and $\tilde{k}_{12} = 51\ \mathrm{s}^{-1}$. There are too many parameters to take quantitative fits seriously but the model captures all aspects of the qualitative behavior of $B(t)$.

We can use transition state theory [32] to estimate the molecular current q. Figure 4 shows the free energy for a monomer with single (ST) and double traps (DT). The

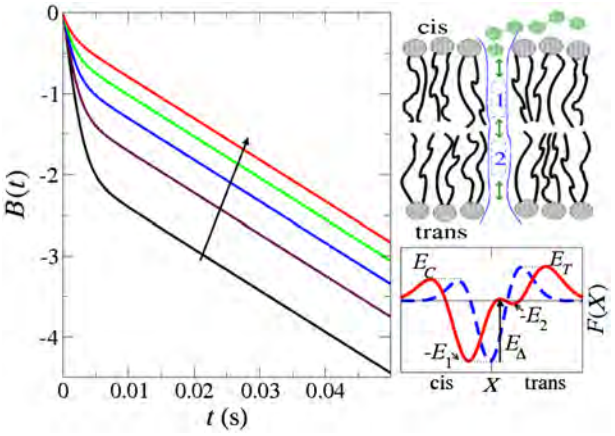

FIG. 4 (color online). Model calculation of $B(t)$ based on a monomer with two traps. Left panel: Calculated $B(t)$ with parameters given in text. The only parameter that varies across curves is the trapping rate of an occupied monomer, which increases along arrow to model increasing concentration. Upper right: Schematic of two-trap model. Lower right: Effective free energy F versus reaction coordinate X for models with one (dashed) or two (solid) traps. The energy barriers, E_C on outside (cis), E_T on inside (trans) and trap level $-E_1$ are common to both models. The two-trap model has another level at $-E_2$, protected by barrier E_Δ.

barriers on the cis and trans ends are E_C and E_T. There is a trap level at $-E_1$ for ST, with frequency ω_1, and levels at $-E_1$ and $-E_2$ for DT, with frequencies ω_1 and ω_2. Molecules hopping from 1 to 2 see a barrier E_Δ. The molecular currents (net rate of molecules passing from cis to trans) are q_{ST} and q_{DT} for ST and DT. Assuming sugar cannot escape the cell interior and ignoring interactions between molecules, we obtain $q_{\mathrm{ST}} = k_{\mathrm{on}}[c]/(1+a)$ and $q_{\mathrm{DT}} = k_{\mathrm{on}}[c]/(1+Za)$ where $a = \mathrm{e}^{\beta[E_T-E_C]} + (k_{\mathrm{on}}[c]/\omega_1)\mathrm{e}^{\beta[E_1+E_T]}$, with $\beta = 1/(k_BT)$ and $Z = (1+\eta)/(1+\theta q_{\mathrm{DT}}/[\eta\omega_1])$ with $\ln\eta = \beta(E_\Delta - E_1 - E_T)$ and $\theta = 1-(\omega_1/\omega_2)\mathrm{e}^{\beta[E_2-E_1]}$. At low $[c]$ ST is more effective, but at high $[c]$, DT can be advantageous [33].

Since *V. harveyi* degrades chitin locally, ChiP may see bursts of high-$[c]$ diffusion current during which a multiple-trap design is preferable. A greater benefit of multiple traps could be realized if molecules in the monomer attractively interact (which was not included in the q_{DT} calculation). From the fit of the model to $B(t)$, the $[c]$ dependence was explained if the first molecule enhances the trapping rate of a second and if both molecules detrap together, which implies attraction. (Note that the longer dwell time of a molecule in a doubly occupied monomer was not simply explained by one molecule blocking the escape of another.) An empty monomer captures a small fraction of incident molecules, but if one bound molecule helps draw others, then the bacterium can well utilize a brief window to uptake sugar in rough water.

In conclusion, we studied ChiP, the nanotubes used by marine bacteria to uptake sugar. By interpreting ion current fluctuations in terms of the trapping or detrapping of sugar molecules, we found that ChiP utilizes multiple traps within a nanotube and exploits correlations between trapped molecules—a novel strategy that enables bacteria to achieve high sugar translocation rates in extreme environments.

M. F. S. was supported by Suranaree University of Technology and the Higher Education Research Promotion and National Research University Project of Thailand, Office of the Higher Education Commission. W. S. was supported by the Thailand Research Fund (Grant No. RMU5380055) and Alexander von Humboldt Foundation, Germany. $I(t)$ measurements were done in the lab of M. Winterhalter at Jacobs University Bremen.

*mfsmith@g.sut.ac.th

[1] T. Schirmer, T. A. Keller, Y. F. Wang, and J. P. Rosenbusch, Science **267**, 512 (1995).
[2] M. Winterhalter, Curr. Opin. Colloid Interface Sci. **5**, 250 (2000).
[3] E. Berkane, F. Orlik, A. Charbit, C. Danelon, D. Fournier, R. Benz, and M. Winterhalter, J. Nanobiotechnol. **3**, 3 (2005).
[4] L. Kullman, P. A. Gurnev, M. Winterhalter, and S. M. Bezrukov, Phys. Rev. Lett. **96**, 038101 (2006).
[5] B. Austin and X.-H. Zhang, Lett. Appl. Microbiol. **43**, 119 (2006).
[6] C. E. Zobell and S. C. Rittenberg, J. Bacteriol. **35**, 275 (1938).
[7] N. O. Keyhani, X. B. Li, and S. Roseman, J. Biol. Chem. **275**, 33 068 (2000).
[8] N. O. Keyhani and S. Roseman, Biochim. Biophys. Acta, Gen. Subj. **1473**, 108 (1999).
[9] X. Li and S. Roseman, Proc. Natl. Acad. Sci. U.S.A. **101**, 627 (2004).
[10] B. L. Bassler, C. Yu, C. Y. C. Lee, and S. Roseman, J. Biol. Chem. **266**, 24 276 (1991).
[11] D. E. Hunt, D. Gevers, N. M. Vahora, and M. F. Polz, Appl. Environ. Microbiol. **74**, 44 (2007).
[12] C. Pruzzo, L. Vezzulli, and R. R. Colwell, Environ. Microbiol. **10**, 1400 (2008).
[13] K. K. Meibom, X. B. Li, A. T. Nielsen, C. Y. Wu, S. Roseman, and G. K. Schoolnik, Proc. Natl. Acad. Sci. U.S.A. **101**, 2524 (2004).
[14] W. Suginta, W. Chumjan, K. R. Mahendran, P. Janning, A. Schulte, and M. Winterhalter, PLoS ONE **8**, e55126 (2013).
[15] R. Dutzler, Y.-F. Wang, P. J. Rizkallah, J. P. Rosenbusch, and T. Schirmer, Structure **4**, 127 (1996).
[16] Y.-F. Wang, R. Dutzler, P. J. RIzkallah, J. P. Rosenbusch, and T. Schirmer, J. Mol. Biol. **272**, 56 (1997).
[17] C. Hilty and M. Winterhalter, Phys. Rev. Lett. **86**, 5624 (2001).
[18] S. M. Bezrukov, L. Kullman, and M. Winterhalter, FEBS Lett. **476**, 224 (2000).
[19] W. Suginta, W. Chumjan, K. R. Mahendran, A. Schulte, and M. Winterhalter, J. Biol. Chem. **288**, 11038 (2013).

[20] C. Andersen, M. Jordy, and R. Benz, J. Gen. Physiol. **105**, 385 (1995).
[21] C. Andersen, R. Cseh, K. Schüelein, and R. Benz, J. Membr. Biol. **164**, 263 (1998).
[22] E. G. Saravolac, N. F. Taylor, R. Benz, and R. R. Hancock, J. Bacteriol. **173**, 4970 (1991).
[23] F. Orlik, C. Andersen, C. Danelon, M. Winterhalter, M. Pajatsch, A. Bock, and R. Benz, Biophys. J. **85**, 876 (2003).
[24] G. Scwharz, C. Danelon, and M. Winterhalter, Biophys. J. **84**, 2990 (2003).
[25] See Supplemental Material at http://link.aps.org/supplemental/10.1103/PhysRevLett.110.238102 for additional information about experimental and analytical procedure.
[26] M. Montal and P. Mueller, Proc. Natl. Acad. Sci. U.S.A. **69**, 3561 (1972).
[27] C. Danelon, T. Brando, and M. Winterhalter, J. Biol. Chem. **278**, 35 542 (2003).
[28] C. Anderson, B. Schiffler, A. Charbitt, and R. Benz, J. Biol. Chem. **277**, 41318 (2002).
[29] J. J. Kasianowicz, J. Robertson, E. Chan, J. Reiner, and V. M. Stanford, Annu. Rev. Anal. Chem. **1**, 737 (2008).
[30] H. C. Berg and E. M. Purcell, Biophys. J. **20**, 193 (1977).
[31] P. C. Bressloff and J. M. Newby, Rev. Mod. Phys. **85**, 135 (2013).
[32] P. Hanggi, P. Talkner, and M. Borkovec, Rev. Mod. Phys. **62**, 251 (1990).
[33] At low $[c]$, $q_{\mathrm{DT}}/q_{\mathrm{ST}} \approx (1+a)/(1+aZ) < 1$. At large $[c]$ q_{ST} saturates at $q_{\mathrm{ST}}^{\max} = \omega_1 e^{\beta[-E_1 - E_T]}$ and q_{DT} at $q_{\mathrm{DT}}^{\max} = \omega_1 e^{\beta[-E_1 - E_T]}(1+\eta-\theta e^{-\beta E_\Delta})^{-1}$, so $q_{\mathrm{DT}}^{\max} > q_{\mathrm{ST}}^{\max}$ if $e^{-\beta E_\Delta}\theta > \eta$.

CHEMICAL REVIEWS

Review

pubs.acs.org/CR

Electrochemical Biosensor Applications of Polysaccharides Chitin and Chitosan

Wipa Suginta, Panida Khunkaewla, and Albert Schulte*

Biochemistry and Electrochemistry Research Unit, Schools of Chemistry and Biochemistry, Institute of Science, Suranaree University of Technology, Nakhon Ratchasima 30000, Thailand

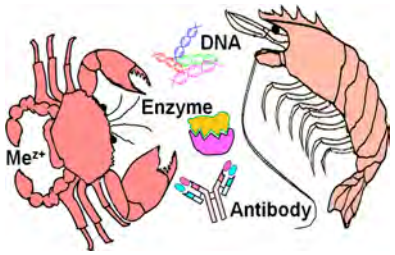

CONTENTS

1. INTRODUCTION

Because of their remarkable structural and functional properties biopolymers chitin and chitosan (Figure 1) have received much attention in fundamental science, applied research, and industrial biotechnology.[1−10] Chitin is a long-chain polymer of *N*-acetyl glucosamine and the structural material of, for instance, fungal cell walls, insect and crustacean exoskeletons, mollusk radulas, and cephalopod beaks. Natural marine chitin or chitin residues are the exclusive nutrient source for many marine bacteria, which use them efficiently as metabolic fuels. Microbial chitin utilization involves enzymatic breakdown of the biopolymer into short-chain chito-oligomers by secreted chitinases[11−15] and subsequent efficient internalization of the resultant chitosugars through specialized bacterial outer membrane proteins ("chitoporins").[16−18] Man-made chitin waste from seafood processing, on the other hand, is a common starting material for production of commercial purified chitin by processes involving harsh chemical treatment. Though not yet developed on an industrial scale, biowaste from the silk, mushroom, and honey-harvesting industries has been proposed as an alternative source for chitin production, and this idea has already delivered promising results in the laboratory.[19−23] Chitosan is the synthetic product of controlled chitin deacetylation and, by varying the chain length of the precursor material or the degree of chemical depolymerization and the extent of deacetylation, is available with a broad range of chemical and physical attributes.

The two materials and their derivatives have practical applications in the form of films, gels, suspensions, microscopic threads, fibers, and spheres in many fields: biotechnology,[24−28] human[29−42] and veterinary[43,44] medicine, pharmacy,[24,45−51] agriculture,[52−55] food engineering,[56−61] environmental technology,[29,62−67] and textile[68,69] and paper[70] industries. An indication of the widespread exploitation and constantly growing importance of chitinous resources is the total of over 10 000 scientific articles and 240 reviews published between January 1, 2005 and July 28, 2012 that have chitin or chitosan in their title. A number of books also include these two particular biomaterials as a key topic.

In addition to the applications already mentioned, chitin and especially chitosan have found widespread use as advanced biofabrication materials. In 2005 Payne's group described the potential of native or chemically modified chitosan in the surface adaptation of cell/protein-integrating biological systems and functional components of diagnostic devices and sensors.[71] About the same time Krajewska discussed the advantages of chitinous polymers for enzyme surface immobilization in preparation of medical sensing devices.[27] The large number of published studies on analytical applications of all sorts that followed these two key reviews and which are reviewed in this review helped raise awareness of the importance and competitiveness of the two materials, and chitosan is now accepted as an important material in the field of advanced sensor technology.

Biosensors incorporate functional proteins, nucleic acids, cell organelles, or even whole living cells, which are fixed ("immobilized") on a physicochemical transducer surface that is able to translate specific interactions of the immobilized bioentity with its corresponding binding partner (analyte) into measurable, concentration-dependent electrical signals.[72,73] The

Received: August 9, 2012

   dx.doi.org/10.1021/cr300325r | *Chem. Rev.* XXXX, XXX, XXX−XXX

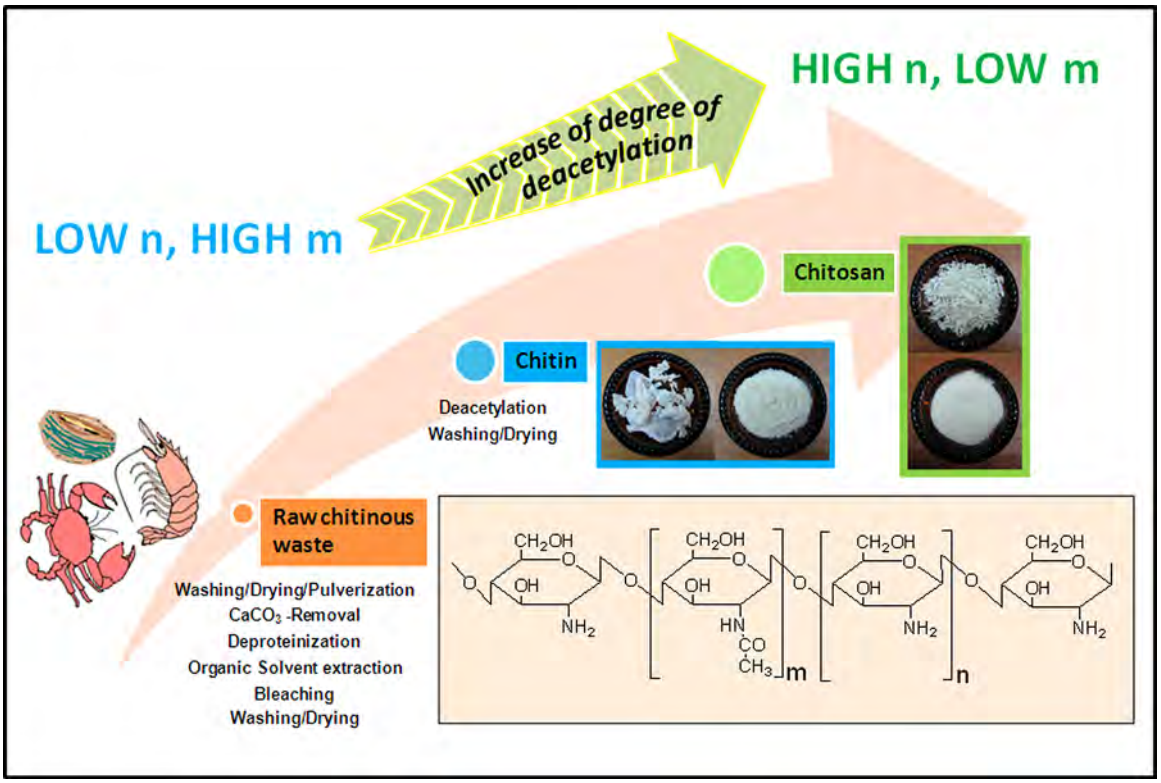

Figure 1. Preparation and chemical structures of chitin and chitosan. For chitin m, the number of acetamido groups, is larger than n, the number of free amino groups, while for chitosan $n > m$. Degrees of deacetylation and acetylation are $(n/(n + m)) \times 100$ and $(m/(n + m)) \times 100$, respectively.

quality of gentle but firm immobilization of the analyte-selective biological component is a determining factor of biosensor performance, and chitin or chitosan films have proved to be useful transducer surface modifiers, compatible with advanced sensor properties, at least under certain circumstances. The properties that make chitin and chitosan valuable for analytical sensor R&D are summarized in Figure 2. The primary advantage of the two chitosugar-based natural polymer materials is their combination of ready availability as highly developed industrial products in a variety of grades with remarkable biocompatibility and pronounced film-forming capability.

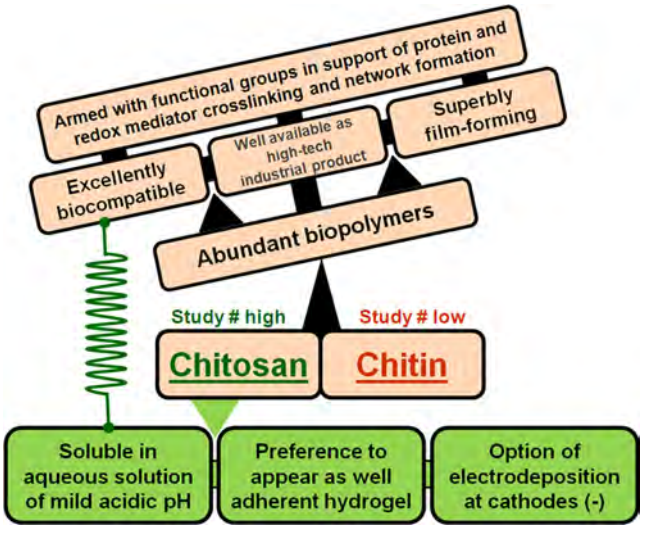

Figure 2. Advantages of chitin and chitosan for biosensor applications. Chitosan, with its higher solubility and its hydrogel-forming[74] characteristics, is by far the more widely used material in this field; balance between the number of published studies with the two materials is thus firmly on the side of chitosan.

Another valuable feature of chitin/chitosan is a chemical structure that includes many intrinsic oxygen- and nitrogen-based functional groups that can serve as the starting points for covalent modification and/or chitosugar chain cross-linking. In addition to these common benefits chitosan has some other important advantages over chitin, namely, its solubility in mildly acidic aqueous solution, an ability to form tough hydrogel-like deposits, and the possibility of being electrodeposited on electrode surfaces as a thin (hydrogel) film in a potential-controlled manner, which is invaluable in miniaturized applications such as micro- and nanobiosensor fabrication. With these additional benefits, chitosan is, unsurprisingly, more widely employed than chitin in the field of sensor technology.

Despite its topicality, the subject chitin/chitosan in biosensors has not yet been specifically reviewed. The aim of this review is thus to overview existing options for electrochemical (EC) biosensors that work with chitin/chitosan-based electrode modifications and offer guidelines for related research and development activities. Basic principles of electrochemical biosensing are considered first to introduce inexperienced but interested readers to the topic of biosensors; then relevant aspects of chitin/chitosan chemistry, biochemistry, and structure are described and discussed with respect to feasible sensor configurations. Finally, we include descriptions of specific applications and give examples of enzyme-based, antibody-based, and single-stranded DNA-based biosensors involving chitin/chitosan as part of the detector architecture.

dx.doi.org/10.1021/cr300325r | Chem. Rev. XXXX, XXX, XXX–XXX

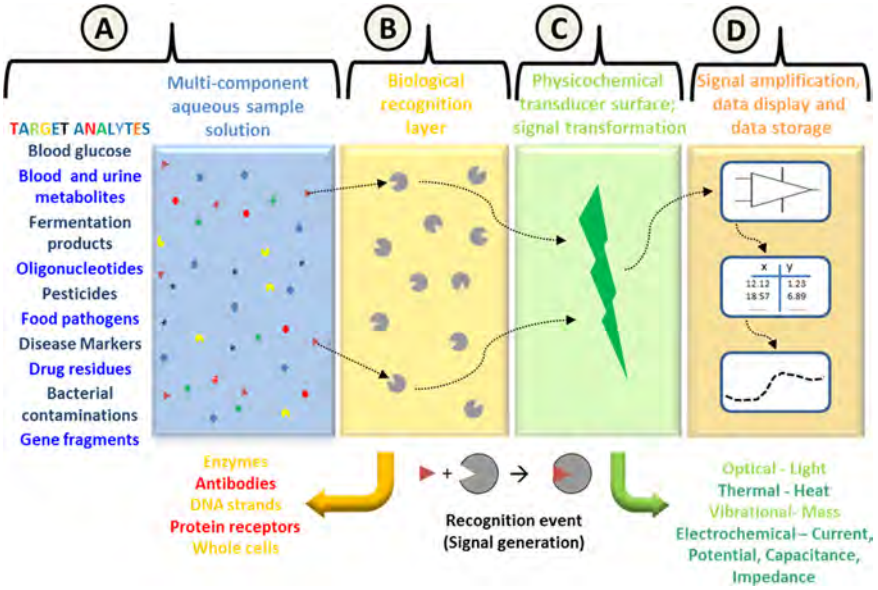

Figure 3. General scheme of a typical biosensor architecture, showing potential analyte species in sample solution (A), immobilization layer for biological recognition elements (B), physicochemical platform (transducer) that generates measurable electrical signal upon interaction of the biological recognition element with the corresponding substrate (C), and electronic module for signal amplification, display, and storage (D).

2. PRINCIPLES OF ELECTROCHEMICAL BIOSENSORS

Enzymes, receptors, antibodies, and single-stranded (ss) DNA are molecular biological recognition elements (BREs) that display high specificity and high affinity for their substrates or binding partners. Figure 3 is a representation of the architecture of biosensors, showing how these tools make use of BREs for analyte detection in a broad range of applications.

An absolute requisite for a well-functioning biosensor is the firm, durable, and nondestructive fixation ("immobilization") of the BRE of choice onto the transducing platform, which can be an optical (spectroscopic) sensing device, the top of a quartz crystal microbalance, the tip of a thermocouple, or the liquid/solid interface of an electrochemical sensor, e.g., the disk face of a gold (Au), carbon (C), or platinum (Pt) electrode or the surface of an ion-selective electrochemical sensor. Immobilization of the BRE locates the molecular recognition event close to or even directly upon the physicochemical detector surface, and concentration-dependent signaling of the process is then possible through conversion of associated light, mass, heat, or impedance/potential/redox changes into a measurable and storable electrical property.

This review focuses on electrochemical biosensing in which signals are generated and transduced by amperometry (current, I, measured over time, t, at fixed working electrode potential, E), voltammetry (I measured as a function of E), potentiometry (equilibrium working electrode potential measured as a function of t at $I = 0$), and potential step and alternating current impedance measurements. The wide range of sensing opportunities that an electrochemical signal transduction offers for analyte detection is exemplified by glucose quantification with glucose oxidase (GOD) enzyme biosensors.[75−80] GOD catalyzes oxidation of α-D-glucose to D-glucono-δ-lactone with concomitant reduction of its flavin adenine dinucleotide (FAD) prosthetic group (reaction 1). Reoxidation of the reduced FAD by dissolved oxygen, the natural electron acceptor, regenerates the enzyme's original state (reaction 2), forming hydrogen peroxide as an electroactive byproduct. In aqueous media the primary product D-glucono-δ-lactone is eventually hydrolyzed to gluconic acid (reaction 3).

$$\beta\text{-D-glucose} + \text{GOD/FAD} \rightarrow \text{D-glucono-}\delta\text{-lactone} + \text{GOD/FADH}_2 \quad (1)$$

$$\text{GOD/FADH}_2 + \text{O}_2 \rightarrow \text{GOD/FAD} + \text{H}_2\text{O}_2 \quad (2)$$

$$\text{D-glucono-}\delta\text{-lactone} \xrightarrow{\text{H}_2\text{O}} \text{D-gluconic acid} \quad (3)$$

Fixation of GOD onto a detector spatially limits the enzyme activity to a zone close to the surface, and the related changes in $[O_2]$, $[H_2O_2]$, and pH occur thus within the entrapping polymer matrix. With traditional electrochemical glucose biosensors the local chemical changes occurring at the sensor/sample solution interface are turned into a quantifiable signal by immobilizing GOD on an electrode that measures oxygen (e.g., a Pt or C disk electrode held at sufficiently negative potential for diffusion-limited oxygen reduction), hydrogen peroxide (e.g., a Pt or C disk electrode held at sufficient positive potential for diffusion-limited peroxide oxidation), or pH (e.g., a glass electrode). In more highly developed versions of amperometric EC glucose biosensors the natural electron acceptor, oxygen, is replaced by dissolved artificial electron acceptors, preferably with an oxidation potential favorably below that of H_2O_2. This pioneering adaptation allows glucose quantification independent of the aeration state of the measuring solution, making analysis possible in the presence of redox contaminants that would interfere at the peroxide oxidation potential. The most advanced glucose sensor designs currently available make use of sophisticated redox polymers/hydrogels as a tailored immobilizing matrix in which interaction between randomly distributed redox relays in the polymer chains establish a nondiffusive flow of electrons ("hopping") between GOD and the electrode in the presence of analyte; otherwise, biosensors may be designed to promote direct electron transfer between oriented GOD molecules and the sensor surface. Establishment of enzyme biosensors that use molecular biocatalysts other than

dx.doi.org/10.1021/cr300325r | Chem. Rev. XXXX, XXX, XXX–XXX

GOD offers similar challenges: proper BRE immobilization, identification of an electrochemically detectable product, and eventually adaptation of amperometric, voltammetric, or potentiometric detection schemes for analyte (substrate) quantification. Examples of successful applications include enzyme biosensors using other oxidases (e.g., galactose, lactate, glutamate, cholesterol, choline, monoamine, and alcohol oxidases), dehydrogenases (e.g., fructose, glucose, glutamate, lactate, cellobiose, formaldehyde, and alcohol dehydrogenases), uricase, penicillinase, and urease to name just a few. A description of all these variants is beyond the scope of this review; however, detailed Supporting Information on the construction and performance of modern enzyme-based biosensors is available in recent review articles[81−85] and books or book chapters.[86−89]

Single-stranded deoxyribonucleic acid (DNA) fragments and antibodies, in contrast to enzymes, do not catalyze chemical reactions and so do not change the concentrations of possibly electroactive substances, such as substrates and cofactors, but instead interact with their substrates simply through high-affinity binding. Design of EC detectors in DNA and immunosensors must take this major distinction into account. One commonly used option is to track changes in relevant electric features of the modified sensor surface. It is, for instance, possible to exploit electrochemical impedance spectroscopy, alternating current voltammetry, or potential step measurements of impedance properties such as the sensor's double-layer capacitance and charge transfer resistance for hybridization recognition and antigen quantification, respectively. Alternatively, synthetic inorganic, organic, or organometallic molecular reporters with a reversible redox activity or enzymes that produce electrochemically detectable species upon exposure to substrate may be used to detect conjugate formation. Several types of redox indicator-supported analysis have been reported: signaling molecules may be diffusible components of the measuring buffer or redox labels covalently bound to the probe or target DNA strands in DNA sensors or to the antibody or antigen in immunosensing. Some recent review articles cover electrochemical detection of DNA hybridization[90−98] and antibody/antigen conjugation.[99−108]

The choice of the BRE and selection of the electroanalytical detection scheme are early steps in EC bio- and immunosensor design; however, the strategy for fixation of the BRE onto the detector must also be decided, and its quality is a main determinant for later sensor performance. Options for BRE immobilization include (A) simple retention of the functional molecular entities behind a thin semipermeable membrane, (B) covalent BRE bonding to reactive functional groups that either are intrinsic to the sensor surface itself or have been introduced through predeposited thin-film coatings, (C) adsorption, (D) covalent cross-linking of the BRE to form a network, and (E) placement of the BRE within a polymer or hydrogel layer.

A variety of synthetic (e.g., polyacrylamides, polyacrylates, and polyvinyl alcohols) and natural (e.g., cellulose, agarose, and collagen) polymers have proved suitable for biosensor assembly: whichever polymer is used, it is essential that the immobilization process does not adversely affect the biomolecules' molecular accessibility and function. With this stipulation in mind chitin and to a considerably greater extent chitosan, a good hydrogel-former, gained favor as immobilizing materials for biosensors as they were well documented in other applications because of their biocompatibility and chemically adaptability through reactions of intrinsic functional groups. The following section is a description of the derivation of usable purified chitin and chitosan from their natural sources and also summarizes their chemical and functional properties that are relevant to biosensor construction and performance.

3. RELEVANT CHEMICAL AND FUNCTIONAL PROPERTIES OF CHITIN AND CHITOSAN

Citations 1−74 broadly link the chemical and physical properties of chitin and chitosan with their potential applications and are suggested as complementary sources of information on uses of these compounds. Chitin and chitosan are both aminoglucopyrans: extended linear chains of (β1 −4)-linked *N*-acetylglucosamine and glucosamine residues, randomly distributed. The chemical difference between purified natural chitin and synthetic chitosan is the degree of acetylation of the 2-amino groups (Figure 1). In chitin more than 50% of these residues are acetylated, while in chitosan they are predominantly deacetylated. More specifically, levels of N-acetylation may be >90% in biologically derived chitin and, if controlled during production, low in special technical chitosan variants.

Well-developed industrial chemical processes are used for production of purified chitin and then chitosan, either from crustacean shell waste from marine food production or from the waste material of the silk, mushroom, and honey-harvesting industries. Acidic carbonate removal, mild alkaline deproteinization, and decoloring and bleaching with organic solvents and hypochlorite makes pure crystalline chitin out of, for instance, finely ground shrimp, crab, and lobster residues, silkworm cuticles, or bee exoskeletons. If desired, the chitin can be converted into chitosan through N-deacetylation by hot and strong alkali. The particle size of the starting material and intensity of later chemical treatments (temperature, duration, and solution concentrations) affect the degree of polymerization and acetylation and the crystallinity and purity of the final products. Enzymatic degradation of chitin with purified deacetylases offers a gentler pathway to chitosan with a controlled ratio of acetylated to deacetylated amino groups;[109−111] however, this process has not yet reached a level of development suitable for generation of larger industrial-scale quantities of chitosan.

Natural chitin has an average molecular weight in the MDa range; however, this is not maintained in industrial purified chitin because of random breakdown of carbohydrate chains during the chemical fabrication procedure, and a few hundreds of kDa are more likely. Commercial chitin comes as whitish powder, flakes, beads, or nanoscale whiskers,[112] typically with 75−95% acetylation. It does not dissolve in simple aqueous media, but dilute solutions can be made in, for instance, alcohol saturated with $CaCl_2$ or *N*,*N*-dimethylacetamide containing LiCl. Like chitin, chitosan is marketed in the physical forms of white powders, flakes, and small beads but with high (>∼500 kDa), medium (∼50−500 kDa), and low (<∼50 kDa) molecular weights and a range of degrees of deacetylation. The plentiful amino functionalities throughout the chitosan polymer can be protonated, so under acidic conditions chitosan is able to dissolve reasonably well in water as an induced polycation, the water solubility depending on the degree of deacetylation. The solubility of chitosan depends on the pH and ionic strength of the aqueous medium and is influenced by the proportion and distribution of acetylated and deacetylated residues along the backbone. The availability of aqueous chitosan solutions under near-physiological conditions con-

dx.doi.org/10.1021/cr300325r | *Chem. Rev.* XXXX, XXX, XXX−XXX

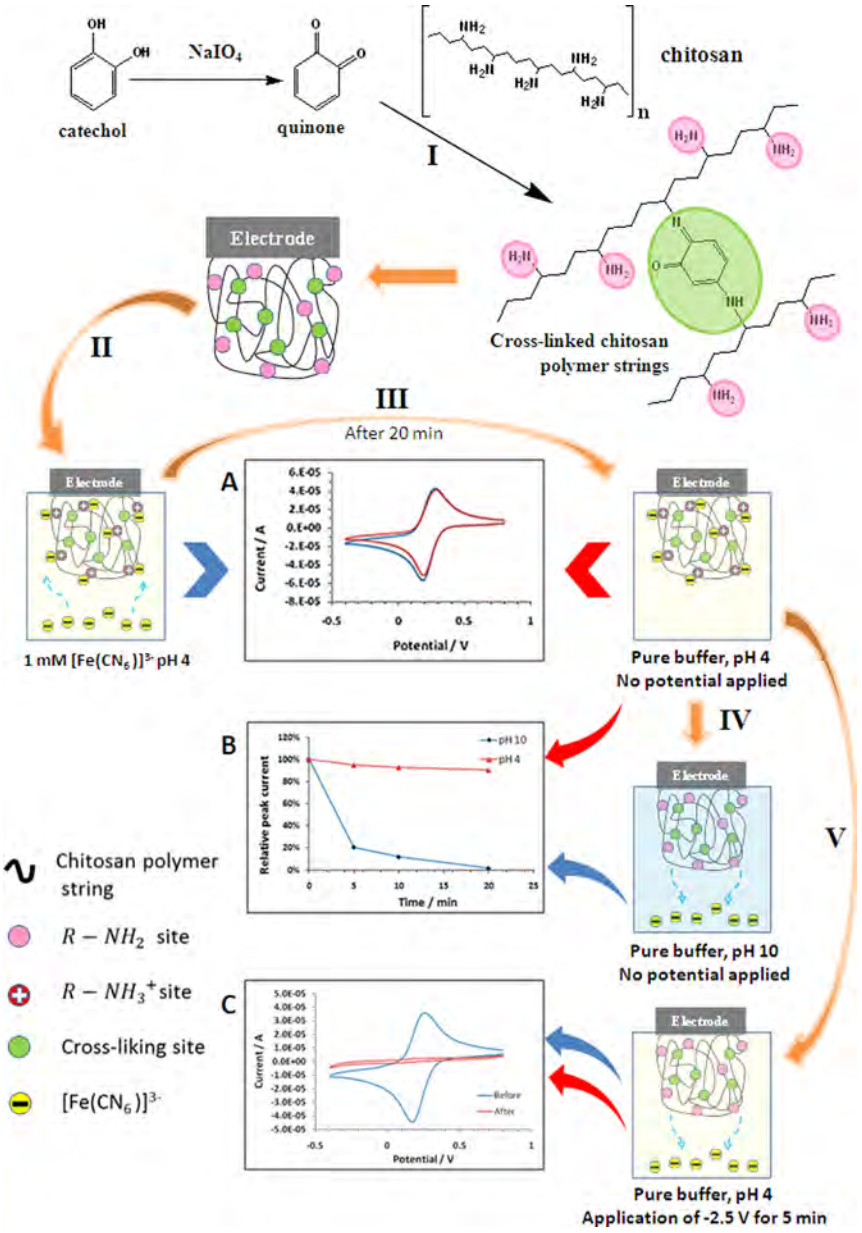

Figure 4. Catechol-induced cross-linking of chitosan polymer strings and pH-responsive release of electrostatically entrapped ferricyanide from a catechol-linked chitosan electrode coating. (I) Principle of the cross-linking procedure. (II) Immersion of modified electrode in 1.0 mM $[Fe(CN_6)]^{3-}$ solution at pH 4; cyclic voltammogram (CV) measured 20 min after immersion; anodic and cathodic current peaks (A, blue) represent the reversible electron transfer reaction of the iron species at the working electrode. (III) Removal of the chitosan-modified working electrode, water rinsing, and subsequent immersion in a buffer solution, still pH 4 but free of $[Fe(CN_6)]^{3-}$; though no dissolved $[Fe(CN_6)]^{3-}$ is present, the CV displays the typical voltammetric ferricyanide redox wave (A, red) with the cathodic peak current remaining stable over time (B, red). Apparently a steady load of ferricyanide in the chitosan matrix exists at pH 4 through charge attraction between $[Fe(CN_6)]^{3-}$ and chitosan's ammonium groups. (IV) $[Fe(CN_6)]^{3-}$-loaded electrode now measured in alkaline buffer solutions, pH 10. Cathodic peak current decays rapidly to zero after 20 min (B, blue). (V) Immersion of a ferricyanide-loaded chitosan-modified electrode into a mediator buffer of pH 4. CVs were recorded before (C, blue) and after (C, red) 5 min application of a cathodic potential of −2.5 V vs reference electrode. Initially observed ferricyanide redox peak disappeared after this treatment, because potential-induced OH^- generation and consequent deprotonation of amino groups in the chitinous electrode coating caused loss of ferricyanide anions into the bulk solution. Scan rate for all cyclic voltammograms was 50 mV s^{-1}.[142]

trasts with the parent material, chitin; for this reason organic solvents can be avoided in the preparation of casting or spinning solutions, which makes exploitation of chitosan more biocompatible and thus widens the range of its applications. Nonetheless, well-adherent thin films of both materials can be simply prepared using their dilute solutions in casting, spinning, or dip-coating procedures, resulting in structures of density and porosity that are adjustable by the number of casting/dipping/spinning repetitions and by the specific composition of the casting/dipping/spinning solutions. It is also noteworthy that dissolution of chitosan salts in NH_4HCO_3 solutions with pH as high as 9.6 is possible and can be used to prepare solutions of chitosan as carbamate ammonium salts for spray-drying applications.[113]

Chitin and chitosan possess good biocompatibility, have potential to form uniform films and hydrogels, and contain

dx.doi.org/10.1021/cr300325r | Chem. Rev. XXXX, XXX, XXX–XXX

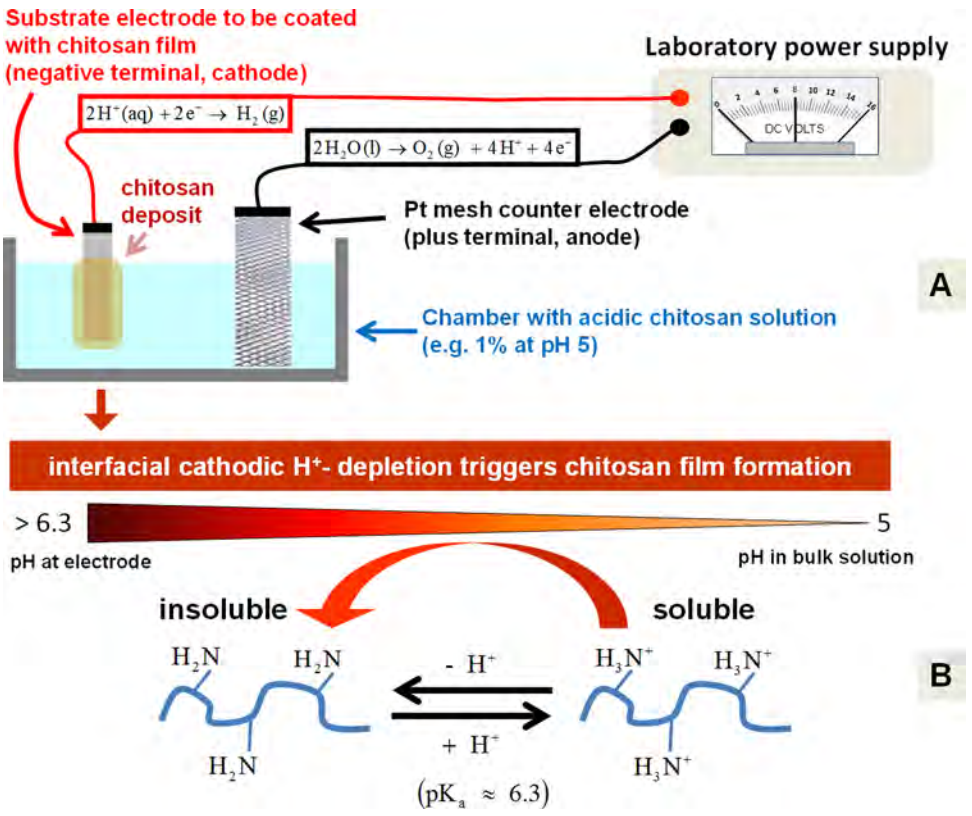

Figure 5. (A) Instrumental setup for electrodeposition of thin chitosan films on substrate electrodes, and (B) mechanism of chitosan precipitation onto cathode surfaces.

multiple oxygen- and nitrogen-based functional groups that can be chemically modified. For in vitro EC work the biocompatibility of the immobilization matrix and its functional constituents determines the integrity and lifetime of the entrapped macromolecules that enable analyte recognition and quantification. A stable and reproducible long-term response is achieved only when the matrix-induced degradation of the immobilized BRE occurs at a negligible rate. The situation is more complex when EC biosensors are used for in vivo measurements, e.g., for metabolite diagnostics in hospitals or in medical or pharmaceutical research with laboratory animals. In these cases the sensing tip of implantable versions of a biosensor is placed in the tissue surrounding the target sites in the bodies of patients or animal models. The compatibility of the immobilizing layer with the BRE is still crucial for durable sensor performance, but in addition, the sensor's composition and tip design should not trigger a local inflammatory host response, as there is a risk of sensor fouling by cellular release of absorbable proteins and lipids or immunoprotective fibrous tip encapsulation. For in vivo applications the aim must therefore be to construct the biosensor from materials that are as nontoxic as possible for both the BRE and the tissue under study. As expected for biological polymers, the tissue compatibility and low immunogenicity of chitin and chitosan have been confirmed in many clinical trials. Laboratory and pilot studies have also indicated their value in mild and curative wound coating,[114−116] as supportive scaffolds for tissue and bone regeneration and engineering,[117−122] and in drug[123−128] and vaccine[129−131] delivery systems, suggesting the possibility of using these biomaterials for improved biosensor design, as explored in this review.

As shown in Figure 1, the structures of chitin and chitosan contain abundant −OH, $-NHCOCH_3$, and $-NH_2$ functional groups throughout the polymer strands. These well-distributed reactive entities permit derivatization of the biopolymers if chemical tailoring would benefit sensor performance or is required for realizing a particular sensing scheme. Chitin and chitosan derivatives that have been synthesized for various applications by covalent modification of the backbone include sugar-modified, phosphorylated, quaternized, cyclodextrin-linked, thiolated, sulfated, azidated, ferrocene-branched, and crown ether-bound versions.[29,34,132−140] An important advantage of chitosan is that modification of its primary amino groups with chosen electron-donating or -withdrawing functional groups alters the charge on the biomaterial, allowing fine tuning of the electrostatic interaction of chitosan immobilization matrices with negatively charged biomolecules and/or electrochemical redox mediators. Introduction of bulky substitutents, on the other hand, is another option for regulating the level of conjugate formation with oppositely charged binding partners by controlled steric hindrance. These strategies were exploited in a recent study that reported addition of $-CH_3$, −Cl, −OH, cyclohexane, benzene, or phthalate entities to the $-NH_2$ groups in chitosan, resulting in clear differences in the efficiency of chitosan variants in binding single-stranded DNA.[141] A more recent study utilized *o*-quinones as bifunctional modifiers of the amino groups of chitosan and produced promising hydrogels of the material.[142] The in situ, metaperiodate-induced oxidation of a dissolved precursor, catechol, generated the reactive quinone that then produced covalent cross-linking of individual chitosan strings by Michael addition and Schiff's base formation (Figure 4).

dx.doi.org/10.1021/cr300325r | *Chem. Rev.* XXXX, XXX, XXX−XXX

When applied to predeposited chitosan electrode coatings this procedure produced adherent hydrogels that in low-pH solutions could entrap the redox probe $[Fe(CN_6)]^{3-/4-}$ by electrostatic interaction with residual amino groups (Figure 4A). The redox probe was, however, readily released when the protonated groups within the catechol-cross-linked chitosan electrode layers were neutralized by exposure to high-pH bulk solutions or application of potentials negative enough to produce cathodic water splitting and hence generation of OH^-. The pH- or voltage-driven switch between capture and release of $[Fe(CN_6)]^{3-/4-}$ was demonstrated by cyclic voltammetry in mediator-containing and mediator-free supporting electrolytes of low and high pH and thus under loading and discharge conditions, respectively (Figure 4B and 4C). Successful establishment of stimulus-responsive chitosan through quinone-based cross-linking is a promising example of the power of material design and an important step toward accomplishment of smart chemically modified systems for sensor and other biomedical devices.

The chitin/chitosan modifications so far cited in this section are representative successful cases and should provide examples for future developments. The accessibility of the entire complement of hydroxyl and acetylamido (for chitin) or amino (for chitosan) groups suggests, moreover, the feasibility of future biosensor advancement through appropriate modification of these functional groups. Before or after formation of chitin or chitosan films on an electrochemical detector surface, endogenous or introduced reactive groups may be used for cross-linking individual strands of the immobilizing polymer, for example, with glutaraldehyde, for linking other functional components in the layer or for extra modification of the chemical sensor after immobilization. Another interesting option is to exploit the free electron pairs on the nitrogen and oxygen atoms and, in the case of chitosan, the charges on protonated C2 amino groups, for internal complex formation, metal ligation, and ionic binding. Metal fixation by chitosan-based composite materials has actually been developed into an efficient procedure for removal of heavy metal[143−147] and dye[148,149] contaminants of industrial wastewater.

In addition to the wide range of adaptations of properties that can be achieved through synthetic chemistry, the feasibility of electrochemical deposition as a thin electrode covering from diluted aqueous solutions is another major asset of chitosan for advanced biosensor fabrication. Thin film chitosan electrodeposition was first reported by Wu et al.[150] In contrast to the common electrodeposition of, for instance, metal coatings from their hydrated ions in solution, chitosan "electrodeposition" does not involve direct or indirect redox conversion of the film-forming material itself. Instead, deposition of chitosan on an electrode is brought about by cathodic hydrogen evolution from water electrolysis, which consumes protons and generates hydroxide ions at the interface between the negatively polarized electrode and the electrolyte. As depicted in Figure 5, the corresponding local increase in interfacial pH neutralizes the positive charges on the ammonium groups in chitosan chains reaching the cathode through electrostatic attraction. Continuous electrophoretic delivery and concomitant removal of positive charges produces chitosan thin film formation on the sensor surface, as the material's solubility falls to the point of precipitation ("sol−gel transition").

Apart from the nature of the waterborne polyelectrolyte, chitosan electrodeposition is mechanistically comparable to the familiar industrial process of electrodeposition of paint (EDP), based on water-dispersible anionic polyacrylic or cationic polyepoxy resins. Among customers the practice of EDP is also known as electrocoating, electropainting, e-coating, electrophoretic coating, or electrophoretic painting and is a proven method for applying corrosion-protective paint layers to automobile bodies and the interior of food tins.[151−155] However, in a pioneering step in sensor fabrication, EDP was established in the 1990s as a convenient, nonmanual approach for effectively insulating etched Pt/Ir and W scanning tunneling microscopy (STM) tips[156,157] and carbon fibers[158,159] in order to produce electrochemical STM probes and carbon disk microelectrodes, respectively. A subsequent study by Kurzawa et al. confirmed the suitability of commercial EDP formulations for formation of enzyme biosensor immobilization matrices when the final heat-curing step was omitted so as to preserve electrical paint conductivity.[160]

To optimize deposition, industrial EDP baths are supplemented with pigments, surfactants, antifouling agents, or (electro-)catalysts, and these additives are not intentionally optimized for biocompatibility as the end use of the paint formulations is corrosion protection of metallic products rather than biosensor applications. On the other hand, chitosan electrodeposition solutions are freshly prepared, and at least in sensor fabrication and work with sensitive biological recognition elements, use of toxic chemical additions can easily be avoided with critical awareness and proper choice of materials. This experimental freedom is one advantage of chitosan over anodic or cathodic EDP as long as commercial EDP systems are the alternative. Another is that the operational pH is closer to physiological values than that used with anodic and cathodic paints based on micellar acrylic and epoxy polyelectrolytes.

Electrodeposition of chitosan is particularly important in miniaturization of electrochemical biosensor devices and in selective placement of immobilizing biocompatible polymer deposits on the active sites of individually addressable micro- and nanoelectrode arrays that are not easily reached with other (manual) film-forming procedures. Figure 6 is a representative

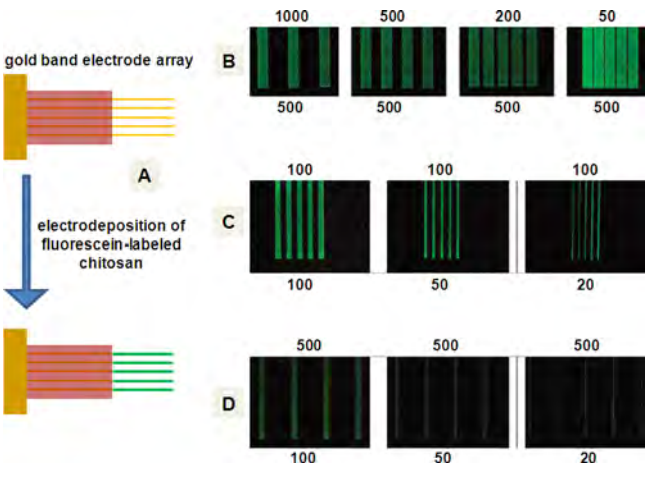

Figure 6. (A) Scheme showing electrochemically driven, pH-induced deposition of fluorescein-labeled chitosan onto the individual conductive entities of gold band electrode arrays of various band widths and separations. (B−D) Photomicrographs taken with an optical fluorescence microscope after the spatially selective chitosan electrodeposition on the patterned gold template was performed. Band widths and separations of the studied electrode test structures, in micrometers, are shown below and above the images, respectively.[161]

dx.doi.org/10.1021/cr300325r | *Chem. Rev.* XXXX, XXX, XXX−XXX

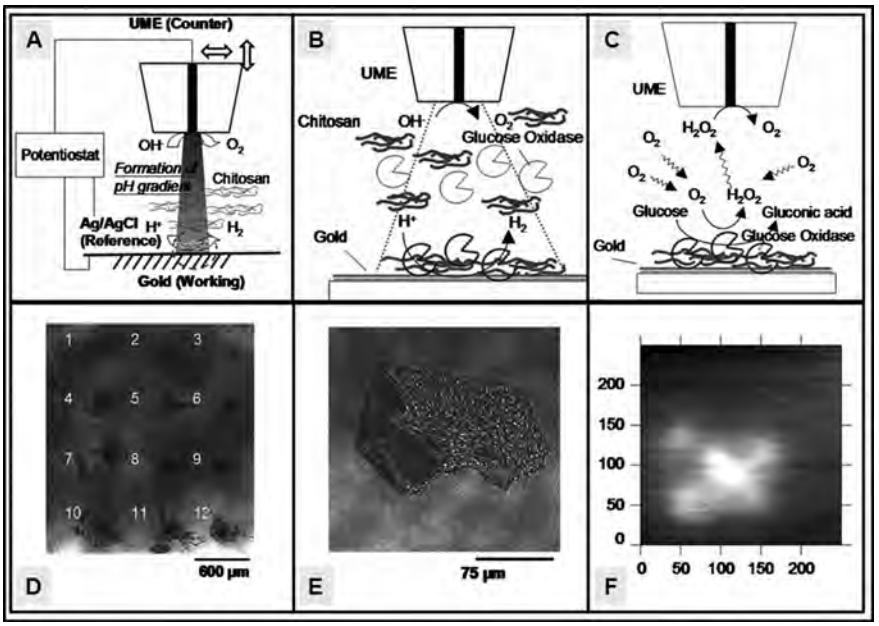

Figure 7. Generation of chitosan micropatterns in a scanning electrochemical microscope (SECM). (A) SECM arrangement for probe tip-controlled local pH elevation on a flat gold substrate electrode to be chitosan decorated. (B) Entrapment of glucose oxidase (GOD) into chitosan electrodeposits that grow in front of a positioned SECM probe tip. (C) Detection of hydrogen peroxide production in a GOD−chitosan spot upon provision of the enzyme's substrate, glucose. H_2O_2 produced in the spot diffuses to the anodic disc of the probe and there generates current through electrooxidation. Two-dimensional (x,y) plot of the SECM tip current provides a map of the spatial distribution of H_2O_2, which reflects the localization and dimension of the immobilized spot. (D) Confocal laser scanning microscope (CLSM) reflectance image of chitosan spots that have been electrodeposited by the procedure depicted in A through application of potential pulses ($E_{substrate}$ = −1.0 V vs Ag/AgCl, pulse length = 1 s) between the SECM tip (Pt microdisk electrode; radius (r) = 25.9 μm; RG factor ($radius_{glass\ insulation}$ /$radius_{Pt}$) = 4; tip-to-substrate separation (d) = 10 μm) and the gold substrate. One (spots 1, 2, and 3), two (spots 4, 5, and 6), three (spots 7, 8, and 9), and four (spots 10, 11, and 12) potential pulses were applied for spot generation. Deposition solution contained 1.5% (w/v) chitosan, pH 5.7. (E) CLSM reflectance image of GOD−chitosan spot obtained by a single localized pulse deposition from a solution containing 5 mg/mL of the enzyme and 1.5% chitosan. Other experimental conditions were as listed in D. (F) Generator-collector type of SECM image that visualizes H_2O_2 production in a tiny GOD−chitosan spot prepared by the procedure described in C on exposure to 50 mM glucose in the air-saturated surrounding electrolyte (0.1 M phosphate buffer, 0.1 M KCl, pH 7.0). Parameters for SECM image acquisition: $E_{Pt\text{-}ECM\ tip}$ = +0.6 V vs Ag/AgCl; $r_{Pt\text{-}SECM\ tip}$ = 13.2 μm, RG = 25; d = 10 μm, tip scan speed = 10 μm/s. Reprinted with permission from ref 167. Copyright 2009 John Wiley and Sons.

selection from one of the earlier studies on chitosan electrodeposition on gold band electrode arrays,[161] and the images of the chitosan-coated gold strips confirm the excellent spatial selectivity of the stimulus-responsive deposition method. As can clearly be seen, individual members of the five-band array structure could be chitosan coated with precision and neither a band separation as narrow as 20 μm nor a bandwidth as thin as 20 μm led to visible failures. The excellent precision of the chitosan electrodeposition was confirmed by the demonstration that substrate electrode edges could be constructed from electrodeposited chitosan scaffolds with an accuracy of 0.5−1 μm[162] and compared very well with that of an EDP modification of a gold microdisk structure.[160] A more recent study demonstrated that defined redox activity could be established in thin electrodeposited chitosan films through their reaction with the products of anodic catechol oxidation at the covered electrode.[163]

Many original research articles have addressed the topic of voltage-induced chitosan deposition. In the context of sensor studies, immobilization of oxidases, horseradish peroxidase, acetylcholine esterase, gelatin, albumin, and silk fibroin has been achieved using entrapment into chitosan electrode layers formed from solution by an electrochemically produced pH shift. Incorporation of nanoscale immobilization matrix modifiers such as CNTs, metal, or metal oxide nanoparticles by coentrapment into nascent chitosan electrodeposits or through chemical modifications of freshly electrodeposited chitosan films by postdeposition protein cross-linking was also successful. Space limitations preclude detailed description of individual procedures here, but many of the examples have been discussed in a set of recent comprehensive reviews on site-directed voltage-dependent protein assembly,[164−166] and these are recommended as sources of further information.

Electrodeposition of chitosan on the active sites of prefabricated electrode microarrays can generate microscopic chitosan patterns that can be further processed into spatially confined sensor entities incorporating biomolecules such as enzymes, DNA strands, antibodies, or antigens. Recently, chitosan-based BRE micropatterning was also achieved using the surface alteration capability of the tiny microelectrode tips of a scanning electrochemical microscope (SECM) for pattern formation.[167] The principle of the proposed scheme is illustrated in Figure 7. Briefly, a gold-covered microscope slide was connected in an SECM electrochemical cell as a large-area, plate-like cathode above which a disk-shaped Pt microelectrode (the "SECM tip"; diameter 10−50 μm) was positioned as a static counter-electrode (anode) at a working distance about the diameter of the insulated microelectrode metal disk. At a potential carefully adjusted to produce a steady rate of water electrolysis, cathodic proton reduction was spatially restricted to the area of the gold plate directly opposite the counter-electrode and only at this specific location

dx.doi.org/10.1021/cr300325r | Chem. Rev. XXXX, XXX, XXX−XXX

was the pH increased enough to neutralize dissolved chitosan, triggering surface precipitation and forming round patches of the material (Figure 7A). Repeated SECM tip-directed local electrodepositions at different *x*, *y* grid points on the substrate gold electrode formed regular arrays of microsopic chitosan sediments (Figure 7D). Addition of GOD to the chitosan electrolyte solution resulted in coprecipitation (Figure 7B), producing chitosan spots with firmly entrapped, fully functional enzyme (Figure 7C, E and F). Though further work is needed, this first successful demonstration of SECM-based chitosan pattern generation illustrates the power of the scanned probe technique in the fabrication of miniaturized biomimetic (sensor) devices. A future development may be extension of the methodology to the various types of noble metal and carbon nanoelectrodes that are now standard tools in electrochemical science, so as to move from the micro- to the nanoscale. Meanwhile, pattern generation with probe microscopes other than the SECM instrument remains a task for the future.

Chitin and chitosan are not the only film-forming biopolymers that may be used as natural surface modifiers of electrochemical (bio-)sensors. Polymeric arginine, lysine, glutamic acid, hyaluronic acid, and alginic acid, for instance, all have possible sensor applications, but among the many possibilities chitin and chitosan are attractive options as they are highly developed, nonhazardous, and cheaply available from commercial sources in various forms. Furthermore, the critical pH for chitosan's soluble−insoluble transition is about 6.3. Chitosan deposition on electrode surfaces can thus, in contrast to other natural polymers with similar behavior, occur under mild conditions through chemically or electrochemically induced pH changes close to physiological normality, ensuring suitably gentle conditions for immobilization of enzymes, antibodies, or nucleic acids. The amino groups in poly-L-lysine, for instance, have a pK_a of about 10.5 and transition between the protonated soluble and the neutral insoluble form of the polymer strings occurs at a highly alkaline pH, which is likely to cause denaturation of protein-based biological recognition elements and is therefore unfavorable to sensor assembly.

Recently, efficient anodic (instead of the usual cathodic) electrodeposition of chitosan hydrogels was reported.[168] The novel scheme starts with anodic oxidation of chloride ions to chlorine, which forms reactive HOCl through reaction with water. This can oxidize alcohol groups within chitosan to aldehydes, which then covalently cross-link to amine groups in other strands through Schiff base formation, creating chitosan hydrogel networks. An attractive feature of the anodic chitosan hydrogels is that they can repeatedly swell and shrink, with up to 3-fold volume changes in response to cyclic pH changes, an effect that has the potential to establish actuation functions such as valve controls in miniaturized fluidic devices. Furthermore, anodically deposited chitosan offers intrinsic aldehyde groups for covalent fixation of enzymes, antibodies, and oligonucleotides, avoiding the need for cross-linkers such as glutaraldehyde. The strategy was validated by construction of functional glucose biosensors using immobilized glucose oxidase.

4. SURVEY OF ELECTROCHEMICAL (BIO-)SENSOR DESIGNS WITH CHITIN OR CHITOSAN AS SURFACE MODIFIER

4.1. Chitin as Electrochemical (Bio-)Sensor Component

Chitosan is somewhat soluble in mildly acidic aqueous media and can thus be handled under conditions that are close to physiological, while chitin needs harsh organic solvents for dissolution and processing. Because of this difference chitosan is more frequently used than chitin in constructing electrochemical (bio-)sensors. However, chitin has been used as a tunable electrode modifier in several studies, and the following examples illustrate some possible options. Thin and flexible cast chitin membranes[169−171] or chitin dispersed in carbon/platinum pastes[172,173] proved to be suitable matrices for electrostatic immobilization of enzymes. On the surface of Clark-type oxygen or noble metal hydrogen peroxide electrodes GOD-loaded chitin films performed well as glucose biosensors, as did GOD/chitin/carbon/Pt pastes. Two other studies used the amine and hydroxyl functionalities of partially deacetylated chitin, with glyoxal, carbodiimide, or epichlorohydrin being used both to cross-link individual chitin chains and to attach enzymes to the chitin networks.[174,175] Corn or pea peroxidase was bound to the chitin matrix and the chitin added to carbon pastes to construct functional biosensors for screening for adrenaline and rosmarinic acid, respectively, in pharmaceutical formulations. Alternatively, the amino-reactive cross-linker glutaraldehyde can be used for covalent linkage of enzyme molecules to the surface of a chitin membrane. This strategy was used successfully for choline oxidase, with choline oxidase-modified chitin films placed on a Pt disk electrode as part of an electrochemical flow cell to create a choline-sensing flow-injection analysis system for measuring the cholinesterase inhibitory activities of synthetic chemicals or natural products.[176] Furthermore, chitin films can be used as immobilizing platforms not only for enzymes but also for other protein-based BRE's. This was shown by a study in which streptavidin was attached to chitin electrode coatings through electrostatic interactions; successful fixation of the biomolecule was demonstrated by pulse voltammetry measurements in solutions of biotin with daunomycin attached as an electroactive redox indicator.[177] More recently, smooth, homogeneous, ultrathin chitin films have been reported as suitable platforms for biosensor architectures.[178]

Though not directly related to biosensors it is worth mentioning that electrostatic binding of inorganic anions by protonated residual amino groups in chitin electrode coatings permits applications in an accumulation scheme in stripping voltammetry (SV), for instance, chitin films on glassy carbon disk electrodes allowed voltammetric detection of molybdate (MoO_4^{2-}) in seawater at concentrations in the nanomolar range.[179] Also, a conductometric humidity sensor was devised based on tailored chitin−polyaniline blends formed into films that changed their internal electrical resistance as a function of the water vapor content in their gas-phase environment.[180]

4.2. Chitosan-Based Electrochemical Nucleic Acid Biosensors

Biosensing with DNA chips or microarrays is used to screen biological samples for the presence of fragments of single-stranded target cDNA or short-chain oligonucleotide (OND) ladders that have been preidentified in clinical studies as markers for the onset or manifestation of a variety of common

dx.doi.org/10.1021/cr300325r | *Chem. Rev.* XXXX, XXX, XXX−XXX

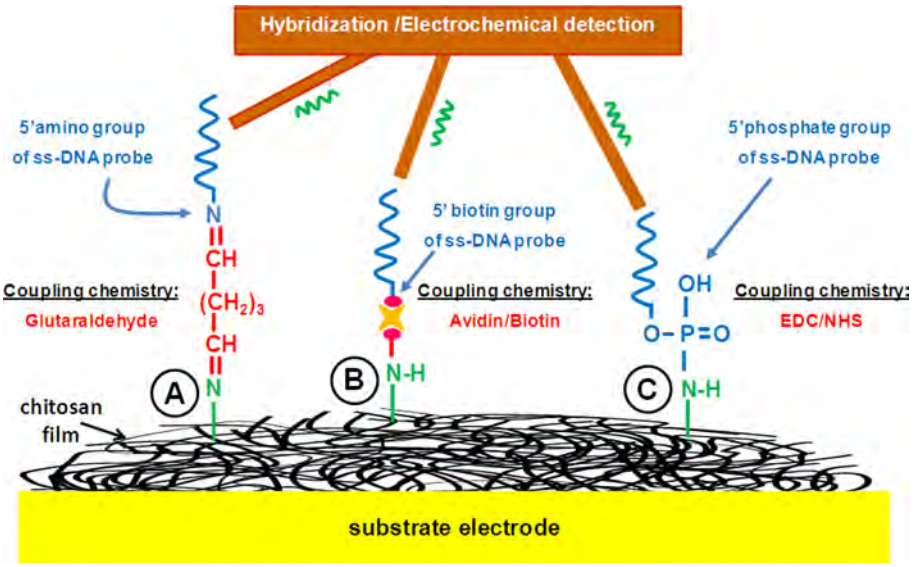

Figure 8. Chitosan-supported DNA immobilization on electrode surfaces. (A) Utilization of glutaraldehyde-based coupling chemistry. (B) Exploitation of biotin-modified chitosan and DNA and use of avidin as a high-affinity bridging molecule. (C) Coupling the phosphate groups of the DNA to the amino groups of chitosan with EDC/NHS.

diseases, indicators of infection with bacterial pathogens or as signs of contamination with other toxic biological matter.[181−190] The key issues for solving diagnostic tasks with blood, urine, or tissue extracts are production of genomic nucleotide probes (i.e., synthesis of sections of end-modified single-stranded cDNA, oligonucleotides (ONDs), or peptide nucleic acids (PNAs)), their precise microstructured assembly (immobilization) on the analytical platform, typically a solid transducer onto which high- or low-density arrangements of microscopic spots of probe DNA are placed in a regular pattern, and, finally, sensitive detection of hybridization between immobilized probe and dissolved complementary target material in some of the spots. The most widely used probe spot carrier and electrode material in electrochemical DNA chip technology is gold, although carbon and metal oxide surfaces have also been used. DNA probe immobilization on Au substrates exploits the strong affinity between Au and sulfur atoms, which produces rapid self-assembly of covalently anchored two-dimensional monolayers upon exposure of the surface to the thiol-containing organic modifier molecules. This scheme can be applied to ss-DNA probes with sulfydryl groups at one end, and this chemistry has become routine for immobilizing nucleic acid strands to Au slides by computerized DNA microspotting procedures. Since thiol-based immobilization is usually limited to gold substrates, other methods are needed for attaching DNA probes to the surfaces of transducers such as glassy carbon or screen-printed carbon and platinum electrodes. For example, covalent coupling through oxygen atoms on preactivated carbon electrodes or fixation of biotinylated DNA probes through stable complex formation, with avidin attached to a covalently premodified sensor surface, may be used. Several studies have reported the potential of chitosan for DNA probe immobilization and even hybridization detection, used either in unmodified form as a coating system or as a composite material with, for instance, carbon nanotubes (CNTs) or metal/metal oxide nanoparticles. Chitosan-based DNA surface fixation works with both covalent and electrostatic bonding to the biopolymer, the latter depending on attraction between protonated and thus cationic amino groups in the chitosan sensor coating and anionic phosphate groups in the backbone of the DNA chains.

Different schemes for DNA immobilization through attachment to chitosan are shown in Figure 8. They exploit chitosan's reactive amino groups which with a proper choice of reagents allow covalent bond formation or affinity conjugation to functional groups at, for instance, the 5′ terminals of chemically adapted probe DNA. Linkage through glutaraldehyde to 5′ amino entities,[191,192] for instance, and EDC/NHS-directed chemical cross-linking to 5′ phosphate groups[193−197] are feasible strategies for linking DNA to preformed chitosan sensor surface coatings, but other coupling procedures may also be used. Biotinylated probe DNA can be bound to chitosan on electrode surfaces by biotin−(strept)avidin coupling, which allows noncovalent but still very tight binding of the two components. An electrochemical platform for detection of gonorrhea, a widespread sexually transmitted disease, has been established using this methodology.[198]

Although not focused on biosensors, a study dealing with pH-induced capture and release of DNA by chitosan-coated polymer particles demonstrated the potency of chitosan surface modifications for controlled electrostatic DNA immobilization.[199] At slightly acidic pH values, polycationic chitosan scaffolds attracted and bound anionic nucleic acid strands; however, a change to alkaline conditions with consequent deprotonation of the chitosan allowed effective elution of the DNA from the beads. This type of ionic interaction can be used for immobilizing nucleic acid fragments on biosensor surfaces. Fish sperm ds-DNA, for instance, was immobilized electrostatically on chitosan/CNT-modified screen-printed carbon (SPCE)[200,201] and graphite[202] electrodes, and with the aid of a redox marker the arrangement allowed detection of deep DNA damage.[200] The ds-DNA capturing layer was created by dropping CNT, dispersed in a chitosan solution, onto the active discs of the SPCEs and allowing the solvent to evaporate. Condensation of chitosan with DNA segments was then achieved by exposure of the freshly formed sensor coatings to a stock solution of the target material. Likewise, cross-linked CNT−chitosan coatings were used to entrap calf thymus ds-

dx.doi.org/10.1021/cr300325r | *Chem. Rev.* XXXX, XXX, XXX−XXX

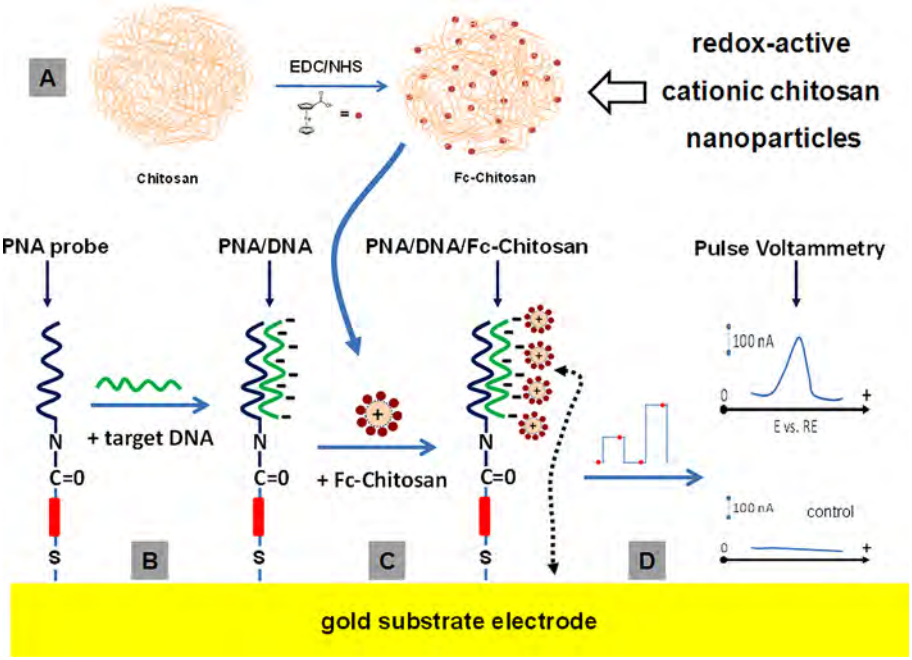

Figure 9. Chitosan-supported hybridization detection scheme for PNA/DNA biosensors. (A) Preparation of ferrocene-conjugated chitosan nanoparticles as the electroactive label. Under slightly acidic solutions amino groups are protonated, rendering the polymeric chitosan−Fc nanoparticles cationic. (B) PNA probe immobilization as self-assembled monolayers and through thiol coupling and binding of the complementary target DNA in a hybridization test. (C) Exposure of the PNA/DNA hybrid to a solution containing chitosan−Fc nanoparticles and electrostatic conjugation of the chitosan label to the nucleic acid double helix. (D) Detection of the presence of the chitosan−Fc label in particular PNA probe spots by pulse voltammetry.

DNA,[203] a synthetic 20-bp oligonucleotide sequence related to the dengue virus genome[204] was bound to drop-coated chitosan films, and the complementary oligonucleotides for DNA sequences associated with colorectal cancer were bound by a CNT-zirkonium oxide (ZrO_2) nanoparticle−chitosan matrix at the appropriate pH.[205]

These examples illustrate the practicability of using DNA/chitosan ionic interactions for probe immobilization. However, as recently shown by Kerman et al., the effect can also be used to establish an elegant chitosan-supported hybridization detection scheme.[206] For this purpose, electroactive chitosan nanoparticles were synthesized through exposure of finely dispersed nanometer chitosan beads to ferrocene carboxylic acid (Fc−COOH) and EDC/NHS as reactive chemical coupling agents (Figure 9A). Amide bond formation linked ferrocene (Fc) molecules covalently to some of the internal and external N functionalities in the chitosan nanoparticles, loading the structure with an oxidizable mediator for electroanalysis. The principle of the final hybridization detection scheme is illustrated in Figure 9B−D. Briefly, PNA probe strands, carrying no net charge, were immobilized on the surface of a gold electrode through their thiol groups. Incubation with the complementary target DNA formed a negatively charged duplex structure which, in the labeling step, bound prefabricated Fc−chitosan nanoparticles electrostatically. Anodic oxidation of surface-proximal Fc labels during differential pulse voltammetry produced typical bell-shaped current peaks, indicating the presence of PNA/DNA hybrids. As expected, no current signals were obtained when in control experiments the PNA probes were hybridized with complementary target PNA strands, because the Fc−chitosan nanoparticles had no affinity for the neutral PNA/PNA conjugates.

Ideally, signal generation with DNA biosensors should be closely coupled to the hybridization between surface-bound and dissolved target DNA strands and consequent double-helix formation or the binding of short reporter DNA strands. However, nonspecific adsorption of the target or reporter DNA strands to the sensor surface may be unavoidable and, depending on the electrochemical scheme in use for transduction, will compromise the analytical performance to a greater or lesser extent. With a chitosan-based immobilization matrix for DNA sensors there is a risk of nonspecific binding to the functional surface coating, stemming from electrostatic interaction between the DNA backbone and the residual protonated amino groups in the chitosan network. Decreasing the number of amino functionalities within the chitosan thin film sensor coating, during or after probe strand attachment, minimizes nonspecific DNA binding, and their reaction with glutaraldehyde to form imino groups is a feasible approach. Alternatively, the surface of chitosan-based DNA sensors could be treated after the hybridization step with solutions of Mg^{2+} or Ca^{2+} salts and urea. Divalent cations tend to neutralize the negative charges on DNA strands and inhibit their electrostatic binding to chitosan, while urea weakens hydrogen bonding between DNA and chitosan. A thorough wash with $MgCl_2$ and/or urea-containing buffer should therefore remove most or all of the nonspecifically bound molecules from the sensor surface and improve the quality of quantitative applications.

4.3. Chitosan-Based Electrochemical Immunosensors

Immunosensors, whether employing electrochemical or other detection schemes, take advantage of the specific recognition of antigen molecules by complementary antibodies (immunoglobulins). The basis of the outstanding analytical performance of existing immunological assays is the strong Ab−Ag binding (dissociation constants, K_D, of $\leq 10^{-7}$ M)[207] and the high

dx.doi.org/10.1021/cr300325r | Chem. Rev. XXXX, XXX, XXX−XXX

Table 1. Chitosan-Based Electrochemical Immunosensors: Target Analytes and Performance

analyte	electrode modification[a]	detection method	linear response range (ng/mL)	detection limit (ng/mL)	ref
α-1-fetoprotein (AFP)	BSA/anti-AFP/AuNPs/Thi/CS-AuNPs	CV	0.4−200.0	0.24	232
	anti-AFP/AuNP/CNT/CS	EIS and CV	1.0−55.0	0.6	233
	ITO/TiO_2/CdS/CS/anti-AFP/BSA	EIS	0.05−50	0.04	234
carcinoembryonic antigen (CEA)	anti-CEA/AuNPs/MnO_2 and CS/PB	CV	0.25−8.0; 8.0−100.0	0.083	235
	anti-CEA/AuNPs/CNT/CS	CV and EIS	0.3−2.5; 2.5−20.0	0.01	236
	Anti CEA/AuNPs/CS	CV	0.2−120.0	0.06	237
	CS/AuNPs/anti-CEA	CV and EIS	0.1−2.0; 2.0−200.0	0.04	238
	BSA/anti-CEA/CS-CNTs-AuNPs	CV	0.01−80.0	0.0034	239
	anti-CEA/Au-Gra/CS-Fc andTiO_2NPs	CV and EIS	0.2−10.0; 10.0−160	0.08	240
	BSA/anti-CEA/AuNPs/Thi/CS				
	anti-CEA/AuNPs-Nafion/Fc-CS/GCE	CV and SWV	0.01−150.0	0.003	241
	HRP-anti-CEA/CEA/Au-CS	CV	2.0−20	1.0	242
human immunoglobulin G (huIgG)	QDs/CNTs-PDDA/AuNPs-CS	ECL	0.006−150	0.001	243
	huIgG/anti-huIgG/AuNPs/	EIS	0.3−120.0	0.1	244
	CNCPE Anti-huIgG/coral-shaped AuNPs-CS	CV EIS	0.05−50.0	0.005	245
human chorionic gonadotrophin[b] (hCG)	BSA/anti-hCG/AuNPs-TiO_2/Thi/GA/ MWCNTs-CS/GCE	DPV	0.2−300.0	0.08	246
	HRP-anti-hCG/hCG/AuNPs-CS/GCE	CA	0.2−100.0	0.1	247
ochratoxin A	r-IgGs/PANI-CS	EIS	up to 10.0	0.1	248
	BSA/r-IgGs/CS-SiO_2	DPV	0.005−0.06	0.003	249
	IgGs/CS-Fe_3O_4	DPV	0.005−0.06	0.005	250
	IgGs/CS/TiO_2	EIS	up to 10	NI	251
	r-IgGs/BSA/CNT/CS		0.25−6	0.25	252
hepatitis B surface antigen (HBsAg)	CS-Fc/AuNPs/anti-HBs	DPV	0.05−305	0.016	253
	anti-HBs/CS-SiO_2NP	CV and EIS	6.85−708	3.89	254
ferritin	antiferritin/Fe_3O_4 magnetic NPs/CS	DPV	20.0−500.0	7.0	255
prostate-specific antigen (PSA)	anti/PSAAu-hydroxyapatite nanocomposite/CS	potentiometry	3.5−30	2.6	256
Shigella flexneri[c]	HRP-anti-*S. flexneri*/CNT/CS	CV	10^{04}−10^{10}	2.3×10^{03}	257
dengue virus envelope protein (DENV)	anti-DENV/CS	CA	1.0−175.0	0.94	258

[a]Abbreviations: CS, chitosan; PB, prussian blue; NPs, nanoparticles; CNT, carbon nanotube; GCE, glassy carbon electrode; Gra, graphene; QDs, quantum dots; PDDA, poly(diallydimethylammonium chloride); CsNPCE, chitosan nanoparticle entrapped-carbon paste electrode; Thi, Thionine; GA, glutaldehyde; PANI, polyaniline; Fc, ferrocene; HRP, horse radish peroxidase; r-IgG, rabbit immunoglobulin G; NI, no information; HBsAb, hepatitis B surface antibody; CV, cyclic voltammetry; DPV, differential pulse voltammetry; SWV, square wave voltammetry; EIS, electrochemical impedance spectroscopy; ECL, electrochemiluminescence; CA, chronoamperometry. [b]Units of the linear range and detection limit are mIU/mL. mIU: milli international units. [c]Units of the linear range and detection limit are cfu/mL. cfu: colony forming units.

specificity of protein complex formation. When applied in advanced configurations with optimized experimental parameter sets, detection limits of attomolar[208−210] and even subattomolar[211] concentration are possible with immunosensors. Comparable sensitivity is likewise available with DNA biosensors[212−214] as these also are affinity-based tools with responses governed by strong binding characteristics. Enzyme biosensors, on the other hand, usually do not exceed femtomolar[215] detection limits if native rather than genetically engineered[216] proteins with enhanced turnover rates are employed for signal generation. This analytical quality has led various types of immunosensing to be used not only in medical diagnostics[217] but also in food screening[218,219] and environmental analysis.[220−224] A crucial step in construction of efficient electrochemical immunosensors is electrode surface immobilization of the antibody or antigen, and many strategies have been proposed for this kind of sensor modification. As stressed in representative original[225−227] and review[228−231] articles, one condition for achievement of good sensitivity is to achieve a high loading of the active electrode area with the capturing immunochemical component, since the surface density of receptors on the transducer governs the magnitude of the electrical signal generated on analyte binding. Accordingly, strategies for simple but effective, reproducible, and stable antibody or antigen loading of electrodes at high density are intensely sought after, and among other surface preparations, various forms of chitosan films have been used as immunosensor platforms. In this context, a virtue of chitosan is that the number of amino sites available for covalent protein attachment on chitosan materials is flexible within a wide range, simply through a variation of the degree of deacetylation of the chosen variant.

Thus far, chitosan-supported EC immunosensors have been used for detection of biomarkers for hepatitis B, various cancers, pregnancy, the iron content of blood, the food-contaminant ochratoxin A, and the diarrhea-triggering bacteria *Shigella flexneri* (see Table 1). The table shows representative recent work on chitosan-supported electrochemical immunosensors with their performance characteristics (detection limits and dynamic linear ranges). In the successful cases drop-coated or electrodeposited chitosan films provided the elementary stage for surface immobilization either of antibody or of antigen and the supplementary components that with the film-forming biopolymer collectively formed the functional electrode coating.

Table 1 shows that the supplements in chitosan-based electrochemical immunosensors can be redox-active mediators

dx.doi.org/10.1021/cr300325r | *Chem. Rev.* XXXX, XXX, XXX−XXX

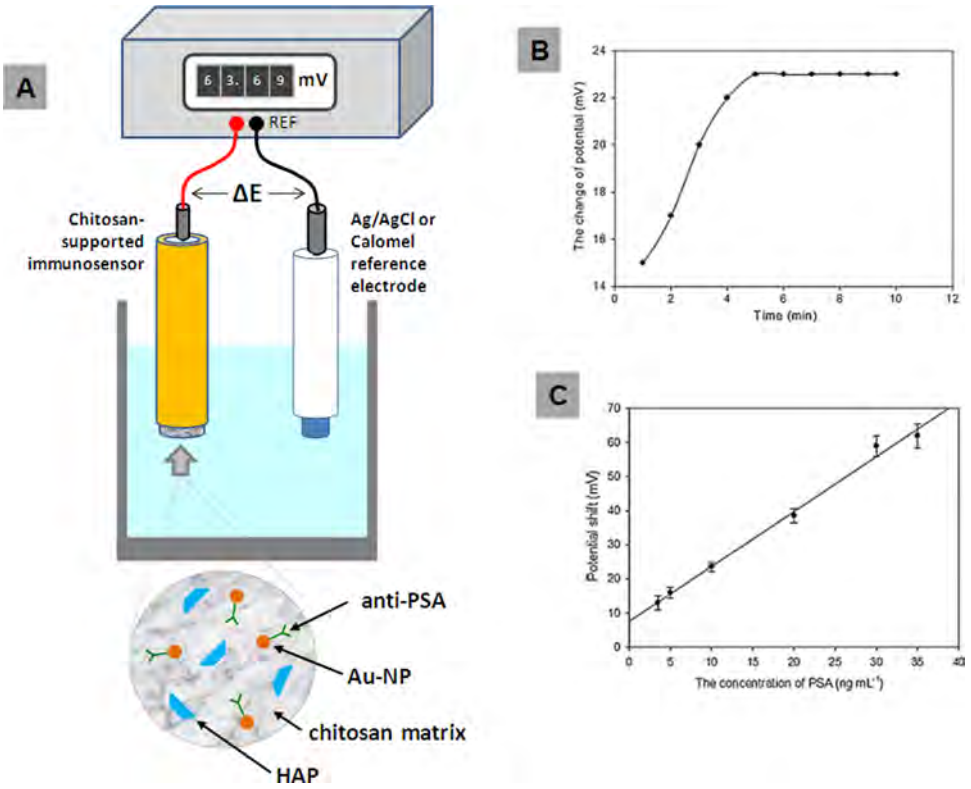

Figure 10. Potentiometric antigen quantification with chitosan-supported immunosensors. (A) Schematic representation of the experimental arrangement and sensor design. (B) Potentiometric time-dependent response of the immunosensor in phosphate buffer, pH 7.4, to addition of 10 ng/mL prostate-specific antigen. (C) Calibration plot for immunosensor. Individual data points are averages of five measurements. Abbreviations: anti-PSA, antiprostate-specific antigen (antibody); Au−NP, gold nanoparticles (anchor for antibody); HAP, biocompatible hydroxyapatite nanocrystals (porous high surface area adsorbent). Curves in B and C are reprinted with permission from ref 256. Copyright 2011 Elsevier Limited.

such as ferrocene and thionine or carbon nanotubes, graphene, conductive polymers, nanohydroxyapatite, gold nanoparticles, metal oxide, and metal sulfides. An option for antibody fixation in the chitosan matrix is covalent binding between amino groups in the biopolymer and the immunoglobins employing, for example, glutaraldehyde as cross-linking reagent. Alternatively, immobilization may be achieved with coimmobilized gold nanoparticles, which tightly adsorb antibody molecules without involvement of a covalent coupling agent. Normally the antigen/antibody interaction on chitosan-modified electrochemical platforms is translated into a signal that is detected by amperometry, voltammetry, or electrochemical impedance spectroscopy. However, as confirmed for detection of the hepatitis B surface antigen (HBsAg)[254] and prostate-specific[256] antigens, potentiometric measurements are also practicable.

Figure 10 shows the design and outcome of a typical potentiometric immunosensing procedure using a chitosan/antibody-modified gold electrode. The time course of the immunosensor potential, E_{IS}, is measured with a common reference electrode. The interaction of immobilized antibody with antigen in the measuring buffer solution and formation of the antibody/antigen conjugate affect the net electrical charge of the immunosensor/electrolyte interface, and a measurable shift in the sensor potentials is observed when the antigen concentration is raised from zero to a new level. In calibration, plots of E_{IS} against antigen concentration are linear over a certain range (see, for instance, Figure 10C) and can be used for antigen quantification.

As with DNA- and enzyme-biosensors, chitosan is an attractive immobilization material also for immunosensors because of its abundant chemically modifiable functional groups and the feasibility of nonmanual, voltage-driven electrochemical deposition. Chitosan for use in immunosensor construction may usefully be covalently modified with synthetic functional groups. For instance, in order to minimize leakage of incorporated electroactive molecules, an initial covalent coupling of the redox mediator ferrocene to chitosan chains was carried out.[253] On the other hand, prior covalent attachment of thionine to chitosan was used to increase the polymer's chemisorption affinity toward gold nanoparticles, on the electrode surface of the immunosensor.[232] Other studies have explored electrodeposition of unmodified or modified chitosan as a simple and easily controllable alternative to drop- or spin-coating procedures for creation of merged multielement immunosensor coatings.[232,238,246,247,253,254]

Most successful electrochemical immunosensors using chitosan-supported immobilization matrices avoided the problem of nonspecific adsorption by blockage of nonspecific surface binding with bovine serum albumin (BSA). Though BSA treatment successfully maintains analyte sensitivity, other blocking agents may occasionally be a better choice for priming the sensor surface, and options to try include, for instance, ovalbumin, preimmune serum, skimmed milk proteins, and surfactants/detergents such as Tween 20, all of which have previously been used in immunoassay systems to minimize the nonspecific, background response.

4.4. Chitosan-Based Electrochemical Enzyme Biosensors

The number of reports on biosensors employing chitosan/enzyme complexes is far greater than for chitosan/DNA or

dx.doi.org/10.1021/cr300325r | Chem. Rev. XXXX, XXX, XXX−XXX

chitosan/antibody systems and increased continuously during the period 2005−2011. Summarizing the almost 300 publications on this subject is beyond the scope of this review. Instead, some representative studies will be described in order to demonstrate the potential of chitosan in enzyme biosensor construction. Most of the recently proposed designs are complex multicomponent systems that combine plain or chemically premodified chitosan variants with a particular enzyme and extra functional materials such as carbon nanotubes, graphene sheets, metal/metal oxide nanoparticles, ionic liquids, and clays, to name just a few. The required analyte specificity obviously determines selection of the enzyme, and oxidases, peroxidases, acetylcholine esterases, laccases, dehydrogenases, tyrosinases, reductases, hydrolases, and phosphatases have all been used. The functional supplements mentioned above have been incorporated individually or in combination, for instance, to improve the conductivity of the immobilization matrix or create redox pathways that connect the entrapped enzyme's active sites electrically with the electrode surface.

Chitosan itself is valued as a tightly adhering and biocompatible porous polymer that provides secure fixation of the enzyme to the biosensor surface while allowing substrate and cofactor mobility for their continuous access to the enzyme. Physical entrapment in the pores and channels of the chitosan matrix and electrostatic and covalent enzyme bonding to the polycationic chitosan chains have all been shown to be feasible means of immobilizing enzymes and avoiding leakage. As described above for chitosan-based DNA immobilization on electrode surfaces, covalent coupling of enzymes to chitosan electrode coatings can be achieved using chemically reactive groups within the two sensor elements. Most published strategies for enzyme-chitosan linking have used common cross-linking reagents such as glutaraldehyde, carbodiimides, *N*-hydroxysuccinimide, epichlorohydrin, or glyoxal, but some specialized cross-linkers such as cyanuric chloride[259] have also been used successfully. There is an indication that the choice of cross-linker may affect the performance of the sensor in a recent study that used electrochemical impedance spectroscopy to evaluate the electrical properties of chitosan films prepared with different cross-linking chemistry.[260] A procedure that avoids chemical modification of the enzyme is physical entrapment within a network of chitosan cross-linked by electrostatic interaction between protonated amino groups in the chains and a multivalent anion, tripolyphosphate.[261]

Abundant functional groups and pH-dependent solubility are the most important attributes of chitosan in enzyme biosensor fabrication as they, respectively, facilitate chemical adaptation of the material and its cross-linking with other sensor components and electrochemically induced, spatially confined deposition onto a miniaturized/arrayed electrode surface. In attempts to develop advanced biosensors with interaction between the enzyme and the electrode catalyzed by a redox mediator, composites of chitosan covalently modified with redox mediators were constructed. For instance, synthesis of a special soluble Fc-modified polyaminosiloxane (Fc−PAS) was described, which after purification was covalently linked to dissolved chitosan polymer with glutaraldehyde.[262] Sensor coatings of the resulting Fc−PAS/chitosan composite and, for comparative voltammetric measurements, pure Fc−PAS, were applied to disks of glassy carbon or printed carbon electrodes by a drop-and-dry procedure. Cyclic voltammetry in phosphate buffer showed that the presence of chitosan in the immobilized Fc-labeled polymer coating significantly altered the shape of the reversible Fc redox wave and shifted the anodic and cathodic peaks toward more negative values. This improvement was attributed to an increase in the hydrophilicity and therefore in ion mobility within the polymeric Fc environment, produced by the chitosan. Loading Fc−polysiloxane/chitosan networks with glucose oxidase molecules in an additional drop-and-dry step, followed by anchoring the enzyme with glutaraldehyde, produced biosensors that were responsive to glucose, with a linear range, sensitivity, and apparent Michaelis−Menten constant (K_m) value of 0−6 mM, 0.9 μA mM^{-1} cm^{-2}, and 2.2 mM, respectively. The rather low K_m value suggests a relatively high enzyme/substrate affinity produced by the biocompatible chitosan-containing immobilization matrix. Another study reported that after reductive N-alkylation of chitosan with 4-pyridinecarboxaldehyde the anionic redox mediator pentacyaneferrate (PCF, $[Fe(CN)_5(NH_3)]^{3-}$) can be bound through a ligand-exchange reaction.[263] Immobilizing the PCF-modified chitosan in the absence or presence of supplementary carbon nanotubes together with glucose oxidase onto GC electrodes formed glucose-biosensing platforms that detected glucose at a working potential of 0.35 V vs Ag/AgCl, as expected for the mediator-supported transduction process. For sensors without and with the CNT addition the detection limits were relatively low: 110 and 30 μM, respectively. Linear ranges, however, were only 0.8−4 (without CNT) and 0.1−1.0 μM (with CNT) and need improvement before this type of sensor is suitable for analytical use. Construction of a sensitive mediator-based lactate electrode became possible by merging a network of cross-linked chitosan with polyvinylimidazole (PVI)-Os, a redox polymer familiar from its many applications in glucose sensors.[264] On the sensor surface, the positively charged biological and synthetic polymers jointly produce electrostatic attachment of negatively charged lactate oxidase (LOD). To increase the strength of the porous chitosan/PVI−Os/LOD matrix, oxidized carbon nanotubes with terminal $-COO^-$ groups have been included as tubular linkers between the two constituent polymers with the negative point charges spread along their chains. Because of the presence of the polymeric redox mediator in the immobilization layer, the system exhibited a low working electrode potential of 300 mV vs Ag/AgCl for amperometric measurements of lactate. Calibration measurements with lactate revealed fast response times (<7 s), good sensitivity (~20 μA mM^{-1} cm^{-2}), a 5 μM detection limit, and a linear response up to 1 mM. An example of the application of chemically modified chitosan variants is in a report of nitrite biosensors with good storage stability, a low detection limit (40 nM), and a linearity of response up to 11 μM.[265] These were made by immobilizing nitrite reductase into the chitosan layer with covalently attached methyl-viologen, which was trapped on the surface of a glassy carbon electrode behind a thin hydrophilic polyurethane membrane.

The principles of cathode-specific chitosan electrodeposition were introduced in an earlier section, and this nonmanual procedure for attachment of a biocompatible immobilization matrix is particularly attractive for enzyme biosensor preparation when sensor miniaturization, simplification, or automation of sensor manufacture and realization of high-density multiple-analyte micro- and nanosensor arrays are the goals. Dispersed nanoparticles can be incorporated through coentrapment in electrochemically grown chitosan films,[266] and in similar fashion, simultaneous electrodeposition of chitosan and enzyme from a solution of the two was reported as the simplest form of

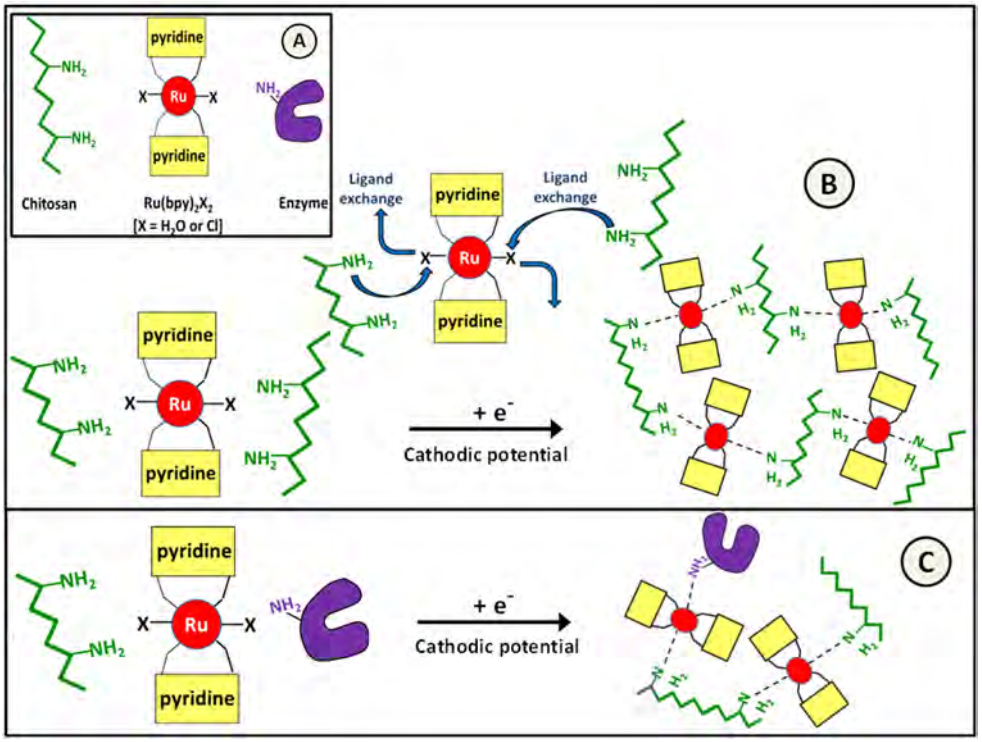

Figure 11. Enzyme immobilization on electrode surfaces through an electrochemically triggered covalent bond formation between dissolved, freely diffusible chitosan chains and between chitosan chains and macromolecules such as enzymes. (A) Simplified representations of the two components to be cross-linked, i.e., chitosan and an enzyme of choice, and the ruthenium complex that is used as molecular linker. (B) Principle of the ligand-exchange reaction that is triggered at low cathodic potentials (about −1.5 V vs reference electrode), leading to coordination of the ruthenium metal center with the nitrogen atoms from the chitosan structure. Replacement of the initial weak ruthenium ligands (water or chloride) by nitrogen from two different chitosan polymer chains forms covalent bridges and, in the course of the reaction of many chains, leads to formation of a three-dimensional chitosan network and biopolymer precipitation onto the electrode. (C) Process described in B with inclusion of enzymes in the reaction mixture forms 3D chitosan networks with covalently attached biocatalyst molecules.[280]

chitosan-mediated enzyme electroimmobilization on biosensor facades.[267−274] Alternatively, pH-shift-induced cathodic deposition of a simple chitosan sensor coating can be followed by covalent coupling of enzyme molecules to complete the biosensor configuration.[275−277] Another option is to prefabricate an enzyme-conjugated chitosan derivative, for instance, with a carbodiimide cross-linker,[278] and then perform electrodeposition of the enzyme-modified biopolymer.[279]

The local pH increase at cathodes and consequent localized precipitation of chitosan polymer through neutralization is not the only strategy for a nonmanual, site-directed deposition of chitosan immobilization matrices on sensors. In fact, the electrochemically triggered covalent cross-linking of chitosan to the surface has recently been proposed as another option for electrochemical enzyme immobilization.[280] The method exploits the change in the coordination sphere of the Ru atom within the complex $Ru(bpy)_2X_2$ (where bpy = bipyridine, X = Cl, H_2O) that occurs upon cathodic reduction, causing replacement of the weak ligands Cl or H_2O by stronger ligands, i.e., primary amino groups in chitosan and proteins. Figure 11 shows the potential-induced coordinative interaction between freely diffusing ruthenium centers and amino groups of chitosan and enzymes and exploitation of this effect for formation of a 3-dimensional chitosan network with tethered enzyme molecules.

In the original study tyrosinase was used as a model and attached to chitosan to make a sensitive phenol biosensor with a broad dynamic range; however, the methodology is easily adaptable for other enzymes used in sensing applications. Ruthenium complex-supported chitosan electrodeposition is irreversible, and the resultant electrode coatings are therefore more robust than those originating from reversible neutralization of charged amino entities. Other advantages are the lower working potential and excellent retention of the enzymes in the chitosan matrix, as a consequence of covalent bonding rather than physical or electrostatic entrapment.

A recent study, which explores in detail the behavior of Agrocybe aegerita peroxygenase at the surface of a glassy carbon electrode modified with chitosan-capped gold nanoparticles, nicely illustrates direct electron transport between chitosan-tailored electrodes and enzymes.[281]

The tips of chitosan-based enzyme biosensors normally have macroscopic dimensions and are used for substrate (analyte) determinations in the bulk phase of solutions in conventional beaker-type electrochemical cells. A case of a biosensor with a miniaturized, needle-like tip is a dopamine biosensor used for amperometric detection of localized dopamine release in the brains of rats.[282] The microbiosensor for in vivo neurotransmitter measurements was obtained by immobilizing tyrosinase in a chitosan/cerium oxide/titanium oxide composite on a 100 μm diameter carbon filament protruding from the tip of a pulled glass micropipet (see Figure 12 A). A detection limit of 1 nM, a linear range of >5 orders of magnitude (10 nM to 220 μM), and a sensitivity of about 14 nA/μM together with a good selectivity against possible interference by ascorbic acid, uric acid, 5-hydroxytryptamine, norepinephrine, and 3,4-

dx.doi.org/10.1021/cr300325r | Chem. Rev. XXXX, XXX, XXX−XXX

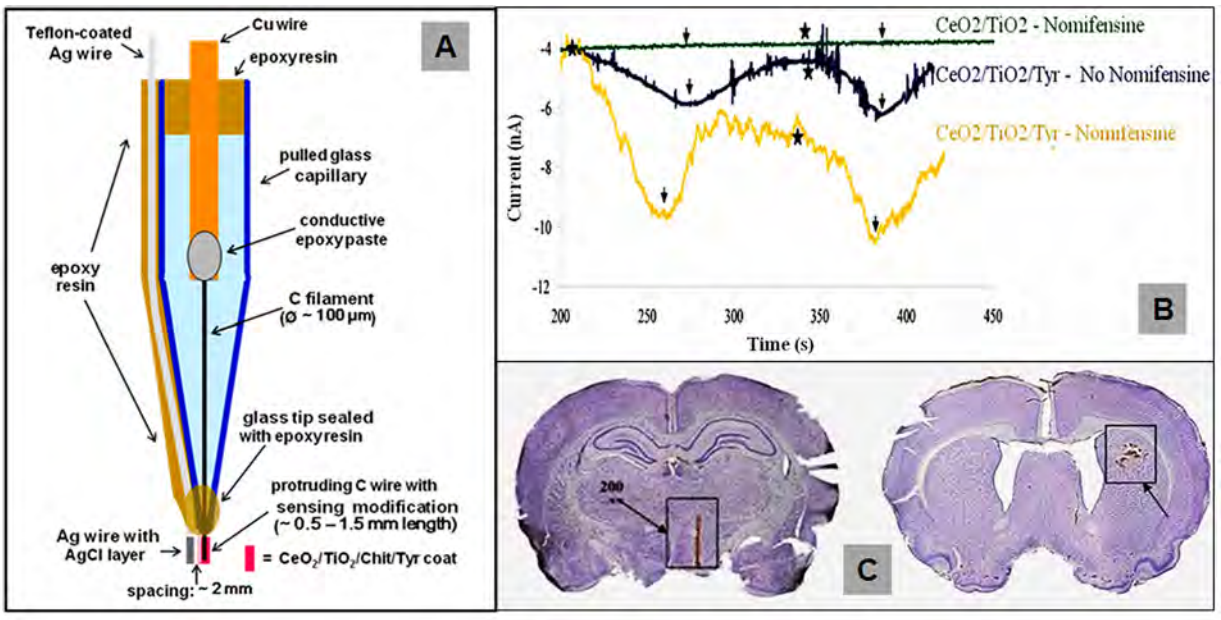

Figure 12. (A) Structural design of chitosan/metal oxide/tyrosinase-based dopamine microbiosensors developed for in vivo measurements of dopamine levels in the rat brain. (B) Histochemical images of two brain slices, showing the sites of stimulation and recording in neurochemical studies with microbiosensors as shown in A. Stimulatory electrode was placed near the median forebrain bundle (left-hand image), while dopamine release was measured with the chitosan/tyrosinase microbiosensors in the striatum (right-hand image). (C) In vivo amperometric responses of the dopamine microbiosensors in the presence (yellow trace) and absence (blue trace) of the dopamine reuptake inhibitor nomifensine. Dopamine was detected at an applied potential of −150 mV vs Ag/AgCl during electrical stimulation of the median forebrain bundle. Stars indicate the onset of electrical stimulation, while black arrows indicate when stimulation was stopped. As expected, the sensor tip reports higher levels of neurotransmitter in the presence of nomifensine because the rate of cellular reuptake is reduced. Green trace shows a control experiment with a microelectrode that was coated with immobilized chitosan and the metal oxides without tyrosinase and so was 'blind' to dopamine.[282]

dihydroxy-L-phenylalanine (L-Dopa) enabled continuous, real-time detection of dopamine release in the striatum of the rat brain, triggered by electrical stimulation of neurons near the median forebrain bundle (see Figure 12B and 12C).

More recently, a glucose microbiosensor small enough for measurements in the openings of the discharge tubing of a capillary electrophoresis device was constructed by immobilization of GOD in chitosan/CNT composite films electrodeposited on platinized Au microelectrodes.[283] Test trials with human serum were successful and confirmed the practicability of glucose analysis in clinical samples.

4.5. Chitosan-Modified Voltammetric Electrodes for Trace Analysis

Potential chelation by intrinsic oxygen and nitrogen atoms with free electron pairs makes natural or chemically modified chitosan an efficient sorbent material for heavy metals, pesticides, and dyes. In the removal of environmental pollutants from contaminated wastewater, analyte species are drawn out of solution into top layers of the material on voltammetric electrodes and analysis can be accomplished without the electrodeposition step that is used in anodic stripping voltammetry of heavy metals such as lead, cadmium, and zinc using mercury or bismuth film electrodes. Examples of trace metal electroanalysis by chitosan-supported adsorptive stripping voltammetry are the quantitation of Hg(II)[284] and Cu(II)[285] by carbon paste electrodes with chitosan additives, determination of Cd(II) using a glassy carbon electrode modified with a drop-coated nano-TiO_2/chitosan composite film,[286] determination of Hg(II)[287] and copper(II)[288] with chitosan/carbon nanotube paste electrodes, and quantification of Cd(II), Cu(II), Pb(II), and Hg(II) with chitosan-modified screen-printed carbon electrodes.[289] The feasibility of using chitosan for trace analysis of organic species is evident from a series of published studies reporting the use of glassy carbon electrodes coated with carbon nanotube/chitosan composites for detection of polyphenols,[290] paracetamol and uric acid,[291] and L-dopa and 5-hydroxytryptamine.[292] Moreover, chitosan−calcium carbonate sensor arrays were used for voltammetric organophosphate pesticide quantification,[293] an acetylene black/chitosan film electrode for methimazole voltammetry,[294] a carbon nanoparticle/chitosan-modified glassy carbon electrode for niclosamide,[295] and a multiwalled carbon nanotube/chitosan for trace bromide measurements.[296]

5. CONCLUDING REMARKS AND PERSPECTIVES

Chitin is the remarkable outcome of long evolutionary optimization of a biomaterial and occurs throughout the biosphere as an important structural component of many living species. Chitosan, on the other hand, is an industrial derivative of chitin that has been developed to high quality standards for applications in such areas as medicine, agriculture, food, and environmental technology. As abundant polysaccharides, chitin and chitosan combine the benefits of natural availability and inherent biocompatibility. Additional advantages of the two materials in their many proposed medical and technical applications are their adhesive film-forming properties and the numerous oxygen and nitrogen residues that can be used to fine tune the materials' properties to the needs of a particular application through chemical modification. A drawback of chitin in biosensor applications is its intrinsic insolubility in aqueous media, under conditions mild enough not to cause inactivation of biological recognition elements as desired; a possible way out of this problem might be suspension of

dx.doi.org/10.1021/cr300325r | Chem. Rev. XXXX, XXX, XXX−XXX

colloidal chitin into the preferred buffers for biomatrix formation on sensor surfaces. For chitosan, the chemical reversibility of hydrogel film formation may be problematic during exposure to media of low enough pH for extensive reprotonation of the amine groups, which may cause adverse internal matrix conversion and/or loss of surface adhesion and exfoliation.

In this review, attention was drawn to the dynamic field of chitin and chitosan utilization in electrochemical sensor design. The reported success cases of chitin- and chitosan-supported DNA-, enzyme-, and antibody/antigen-based biosensors are an inspiring indication of the potent role that these biopolymers can play as thin film surface modifiers of electrodes of all sorts. In particular, stable immobilization of biological recognition elements in chitosan matrices on transducer electrodes under mild conditions, such as near-physiological pH values, has proved effective and many of the early problems in chitosan electrode fabrication have been solved. The outcome of recent research has been valuable manual and nonmanual (electrochemical) procedures for placement of the functional sensor coatings, either as simple or as composite chitosan films, with additional components ranging from redox-active compounds and conductive nanoparticles to metal oxide catalysts. However, until now only the basic feasibility of chitin/chitosan biosensors has been demonstrated and their performance confirmed in proof-of-principle studies. The obvious and potentially difficult next step is extension of this work to creation of competitive chitin or chitosan biosensors that are commercially available and routinely used analytical tools for analysis of everyday samples, as handled on a daily basis in point-of-care clinical, biotechnological, and environmental control laboratories or personal health care. As the potential for this certainly exists, it will be interesting to see whether chitin- or chitosan-based biosensors will progress in a reasonable time from their current laboratory setting to claim a market share among other biosensor devices for medical diagnostics, process control, and pollutant screening and how long realization of the first viable chitin/chitosan sensor products will take. The way forward may be through a more systematic optimization and utilization of the strategy of chemical chitin/chitosan modification in advance of sensor immobilization than has so far been undertaken. Issues to be tackled in the course of design improvements include the fine details of the polymers' chemical and physical microstructure in the immobilized state, in particular their molecular attributes such as the type[297] and degree of chain cross-linking and related material characteristics such as porosity, density, rigidity, and morphology of the final chitinous surface layers. A good example of such an approach is a recently published report on the influence of salt addition to chitosan solutions on the electrodeposition of hydrogels of the material.[298] An important observation was that salt supplementation led to chitosan films that grew faster in thickness and had a greater surface roughness. Furthermore, the mechanical properties of electrodeposited hydrophilic chitosan networks varied with salt concentration: electrolysis at elevated concentrations resulted in soft hydrogel coatings, while at lower concentrations more inflexible deposits were created. This approach, it was suggested, could be used to tailor functional chitosan electrodes to the particular requirements of a given application in the life sciences or the analytical sector.

Bearing in mind trends in micro- and nanotechnology and -fabrication, there is a clear need to advance smart electrodeposition of chitosan and its derivatives from its current proof-of-principle stage to a point where prefabricated electrode micro- and even nanoarrays can reproducibly be transformed into marketable, multiple-analyte biosensor platforms for reliable and fast real sample bioanalytics. The strategies of some recent studies on production of anodic and cathodic electrodeposition paints for use as enzyme immobilization matrices[299−301] and/or the backbone structure of redox polymers for horseradish peroxidase-based biosensors[302] may also be relevant to the fine tuning of chitosan electrodeposition for (bio-)sensor applications. As for the paints, libraries of assorted chitin/chitosan derivatives of different properties might be generated and then systematically screened in a combinatorial approach for their quality as sensor components after immobilization. The near future will be an exciting period in the chitin/chitosan/biosensor research area, with novel sensor architectures to be sought and, it is hoped, many unforeseen developments to come.

AUTHOR INFORMATION

Corresponding Author

*Phone: +66-44-22-6187. Fax: +66-44-22-4185. E-mail: schulte@sut.ac.th.

Notes

The authors declare no competing financial interest.

Biographies

Wipa Suginta received her B.Sc. degree in Genetics from Chulalongkorn University, Bangkok, Thailand, in 1990 and M.Sc. degree in Biochemistry from Mahidol University, Bangkok, in 1993. After her Master's thesis (1995), which involved isolation and characterization of carbohydrate-degrading enzymes and was carried out under the supervision of Professor Dr. M. R. Jisnuson Svasti, she was granted a Royal Thai Government scholarship for doctoral studies in the Department of Biochemistry, School of Medicine, The University of Edinburgh, Scotland, under the supervision of Dr. Linda Gilmore. Her Ph.D. thesis was entitled "Structural and functional characterization of *Vibrio harveyi* chitinase". After obtaining her Ph.D. degree in 1999, she joined Dr. Richard Ashley's laboratory in the Membrane Biology Group at Edinburgh University. Her postdoctoral research was funded by the Welcome Trust and involved functional characterization of rat brain chloride intracellular ion channels (CLICs). In January 2001, she returned to her Lectureship in the School of Biochemistry, Suranaree University of Technology, Thailand. A particular theme of her past and present research is structural and functional characterization of bacterial outer membrane proteins (porins) and chitinases and chitobiases from marine bacteria to humans. Apart from promotions to Assistant (2004) and then Associate (2007) Professor, she received for her scientific achieve-

ments the L'OREAL (Thailand)/UNESCO "For Women in Science" Fellowship (2005), the Outstanding Research Award from Suranaree University of Technology (2010), and a prestigious Fellowship for Experienced Researchers from the Alexander von Humboldt Foundation, Bonn, Germany (2009–2012).

Panida Khunkaewla received her B.Sc. degree in Biochemistry and Biochemical Technology in 1997 and M.Sc. degree in Biochemistry in 2000 from Chiang Mai University, Thailand. In 2005 she received her doctoral degree in Dr. Scient. Med. (Immunology) from the Medical University of Vienna, Austria, for a thesis on identification and characterization of functional partners of the integral membrane glycoprotein molecule CD147, under the supervision of Professor Dr. Hannes Stockinger. From 2006 to 2007 she worked as a postdoctoral fellow for The National Science and Technology Development Agency, National Center for Genetic Engineering and Biotechnology (BIOTEC) at the Biomedical Research Unit, Faculty of Associated Medical Sciences, Chiang Mai University, Thailand, under the supervision of Professor Dr. Watchara Kasinrerk. In 2008 she became a lecturer at the School of Biochemistry, Institute of Science, Suranaree University of Technology. Her current research interests are focused on production of monoclonal antibodies and functional analysis of leukocytes surface molecules that are involved in regulation of the immune system.

Albert Schulte studied Chemistry at the University of Münster, Germany, and received his doctoral degree in Natural Science in 1994 for a thesis on preparation and characterization of ultramicroelectrodes and probes for electrochemical scanning tunneling microscopy under the supervision of Professor Dr. Jürgen Otto Besenhard. During postdoctoral appointments in the Department of the Molecular Biology of Neuronal Signals at the Max Planck Institute for Experimental Medicine in Göttingen, Germany, and the Department of Physiology at the University of Edinburgh, Scotland, he worked on joint patch clamp electrophysiological and electrochemical measurements of the process of vesicular chemical release from single secretory cells. A research position in the Department of Physics of Edinburgh University with scanning probe microscopy work was then followed in 2000 by employment as Senior Research Officer in Professor Dr. Wolfgang Schuhmann's electroanalysis group at Ruhr University in Bochum, Germany. His scientific activities in Bochum included development of novel modes of scanning electrochemical microscopy, biosensor miniaturization, detection of cellular action, and inspection of the local corrosion of shape memory alloys. In January 2006, he became Senior Lecturer in Physical Chemistry at the University of the West Indies in Trinidad and Tobago, and in June 2007 he was appointed Associate Professor in Physical and Analytical Chemistry at the School of Chemistry, Faculty of Science, Suranaree University of Technology in Nakhon Ratchasima, Thailand. His current research is directed toward various aspects of micro-, nano-, and bioelectrochemistry, and ongoing projects are focused on development of probes for electrochemical tunneling and scanning electrochemical microscopy, an application of microtiter plate-based robotic electroanalysis of drugs, environmental pollutants and food content, voltammetry in microliter-volume electrochemical cells, and finally enzyme biosensor advancements and electrochemical immunosensing.

ACKNOWLEDGMENTS

The authors are grateful for financial support from Suranaree University of Technology (SUT) through research grants nos. SUT1-102-54-12-14, SUT1-102-52-24-01, and SUT1-102-54-36-06. W.S. additionally received financial support from The Thailand Research Fund (grant no. RMU5380055). Furthermore, the authors express their thanks to Dr. David Apps, Biochemistry Reader (retired), Centre for Integrative Physiology, Edinburgh University, Scotland, for his critical manuscript reading and language improvements and to Miss Jiyapa Sripirom, a member of the Biochemistry-Electrochemistry Research Unit at Suranaree University, for her help with preparation of part of the graphical material.

REFERENCES

(1) Se-Kwon, K. *Chitin, chitosan, oligosaccharides and their derivatives: Biological activities and applications*; CRC Press-Taylor & Francis Group: Boca Raton, 2010.
(2) Uragami, T.; Tokura, S. *Material science of chitin and chitosan*; Springer and Kodansha Scientific Ltd.: New York and Tokyo, Japan, 2006.
(3) Khor, E. *Chitin: Fulfilling a biomaterials promise*; Elsevier: Amsterdam, The Netherlands, 2001.
(4) Muzzarelli, R. A. A; Jeuniaux, C.; Gooday, G. W. *Chitin in nature and technology*; Plenum Press: New York, 1986.
(5) Aranaz, I.; Mengibar, M.; Harris, R.; Panos, I.; Miralles, B.; Acosta, N.; Galed, G.; Heras, A. *Curr. Chem. Biol.* **2009**, *3*, 203.
(6) Rinaudo, M. *Prog. Polym. Sci.* **2006**, *31*, 603.
(7) Kurita, K. *Mar. Biotechnol.* **2006**, *8*, 203.
(8) Dutta, K. P.; Dutta, J.; Tripathi, V. S. *J. Sci. Ind. Res.* **2004**, *63*, 20.
(9) Kumar, M. N. V. R. *React. Funct. Polym.* **2000**, *46*, 1.
(10) Shepherd, R.; Reader, S.; Falshaw, A. *Glycoconjugate J.* **1997**, *14*, 535.
(11) Arakane, Y.; Taira, T.; Ohnuma, T.; Fukamizo, T. *Curr. Drug Targets* **2012**, *13*, 442.
(12) Eijsink, V.; Hoell, I.; Vaaje-Kolstada, G. *Biotechnol. Genet. Eng. Rev.* **2010**, *27*, 331.
(13) Suginta, W. *Enzyme Microb. Technol.* **2007**, *41*, 212.
(14) Bhattacharya, D.; Nagpure, A.; Gupta, R. K. *Crit. Rev. Biotechnol.* **2007**, *27*, 2.
(15) Fukamizo, T. *Curr. Protein Pept. Sci.* **2000**, *1*, 105.
(16) Suginta, W.; Chumjan, W.; Mahendran, K. R.; Janning, P.; Schulte, A.; Winterhalter, M. *PLoS One* **2013**, *8*, e55126.

(17) Meibom, K. L.; Li, X. B.; Nielsen, A. T.; Wu, C. Y.; Roseman, S.; Schoolnik, G. K. *Proc. Natl. Acad. Sci. U.S.A.* **2004**, *101*, 2524.
(18) Keyhani, N. O.; Li, X. B.; Roseman, S. *J. Biol. Chem.* **2000**, *275*, 33068.
(19) Liu, S.; Sun, J.; Yu, L.; Zhang, C.; Bi, J.; Zhu, F.; Qu, M.; Jiang, C.; Yang, Q. *Molecules* **2012**, *17*, 4604.
(20) Sajomsang, W.; Gonil, P. *Mater. Sci. Eng., C* **2010**, *30*, 357.
(21) Ai, H.; Wang, F.; Yang, Q.; Zhu, F.; Lei, C. *Carbohydr. Polym.* **2008**, *72*, 419.
(22) Majtan, J.; Bilikova, K.; Markovic, O.; Grof, J.; Kogan, G.; Simuth, J. *Int. J. Biol. Macromol.* **2007**, *40*, 237.
(23) Paulino, A. T.; Simionato, J. I.; Garcia, J. C.; Nozaki, J. *Carbohydr. Polym.* **2006**, *64*, 98.
(24) Enescu, D.; Olteanu, C. E. *Chem. Eng. Commun.* **2008**, *195*, 1269.
(25) Mendes, A. A.; de Oliveira, P. C.; de Castro, H. F.; Giordano, R. D. C. *Quim. Nova* **2011**, *34*, 831.
(26) Guibal, E. *Prog. Polym. Sci.* **2005**, *30*, 71.
(27) Krajewska, B. *Enzyme Microb. Technol.* **2004**, *35*, 126.
(28) Hirano, S. *Biotechnol. Annu. Rev.* **1996**, *2*, 237.
(29) Balakrishnan, B.; Banerjee, R. *Chem. Rev.* **2011**, *111*, 4453.
(30) Alves, N. M; Mano, J. F. *Int. J. Biol. Macromol.* **2008**, *43*, 401.
(31) Peireira, P.; Carvalho, V.; Ramos, R.; Gama, M. *Chitosan Nanoparticles for Biomedical Applications. Biotechnology in Agriculture, Industry and Medicine Nanotechnology Science and Technology series*; Nova Science Publishers, Inc.: New York, 2010.
(32) Jayakumar, R.; Prabaharan, M.; Nair, S. V.; Tamura, H. *Biotechnol. Adv.* **2010**, *28*, 42.
(33) Ueno, H.; Mori, T.; Fujinaga, T. *Adv. Drug Delivery Rev.* **2001**, *52*, 105.
(34) Sahhiwa, H.; Aiba, S. *Prog. Polym. Sci.* **2004**, *29*, 887.
(35) Laranjeira, M. C. M.; de Favere, V. T. *Quim. Nova* **2009**, *32*, 672.
(36) Khor, E. *Curr. Opin. Solid State Mater. Sci.* **2002**, *6*, 313.
(37) Park, B. K.; Kim, M. M. *Int. J. Mol. Sci.* **2010**, *11*, 5153.
(38) Khor, E.; Lim, L. Y. *Biomaterials* **2003**, *24*, 2339.
(39) Di Martino, A.; Sittinger, M.; Risbud, M. V. *Biomaterials* **2005**, *26*, 5983.
(40) Dash, M.; Chiellini, F.; Ottenbrite, R. M.; Chiellini, E. *Prog. Polym. Sci.* **2011**, *36*, 981.
(41) Hein, S.; Wang, K.; Stevens, W. F.; Kjems. *J. Mater. Sci. Technol.* **2008**, *24*, 1053.
(42) Saranya, N.; Moorthi, A.; Saravanan, S.; Devi, M. P.; Selvamurugan, N. *Int. J. Biol. Macromol.* **2011**, *48*, 234.
(43) Senel, S.; McClure, S. J. *Adv. Drug Delivery Rev.* **2004**, *56*, 1467.
(44) Minami, S.; Okamoto, Y.; Hamada, K.; Fukumoto, Y.; Shigemasa, Y. *EXS* **1999**, *87*, 265.
(45) Zhang, J. L.; Xia, W. S.; Liu, P.; Cheng, Q. Y.; Tahirou, T.; Gu, W. X.; Li, B. *Mar. Drugs* **2010**, *8*, 1962.
(46) Laurienzo, P. *Mar. Drugs* **2010**, *8*, 2435.
(47) Muzzarelli, R. A. A. *Carbohydr. Polym.* **2009**, *77*, 1.
(48) Silva Helio, S. R. C.; dos Santos, K. S. C. R.; Ferreira, E. I. *Quim. Nova* **2006**, *29*, 776.
(49) Kumar, M. N. V. R; Muzzarelli, R. A. A; Muzzarelli, C.; Sashiwa, H.; Domb, A J. *Chem. Rev.* **2004**, *104*, 6017.
(50) Singla, A. K.; Chawla, M. *J. Pharm. Pharmacol.* **2001**, *53*, 1047.
(51) Muzzarelli, R. A. A.; Muzzarelli, C. *Chitosan in pharmacy and chemistry*; ATEC: Grottammare, Italy, 2002.
(52) Zhang, H. Y.; Li, R. P.; Liu, W. M. *Int. J. Mol. Sci.* **2011**, *12*, 917.
(53) El Hadrami, A.; Adam, L. R.; El Hadrami, I.; Daayf, F. *Mar. Drugs* **2010**, *8*, 968.
(54) Badawy, M. E. I.; Rabea, E. I. *Int. J. Carbohydr. Chem.* **2011**, *2011*, 460381.
(55) Nge, K. L.; New, N.; Chandrkrachang, S.; Stevens, W. F. *Plant Sci.* **2006**, *170*, 1185.
(56) Shahidi, F.; Vidana Arachchi, J. K.; Jeon, Y.-J. *Food Sci. Technol.* **1999**, *10*, 37.
(57) Porta, R.; Mariniello, L.; Di Pierro, P.; Sorrentino, A.; Giosafatto, C. V. L *Crit. Rev. Food Sci. Nutr.* **2011**, *51*, 223.
(58) Aider, M. *LWT—Food Sci. Technol.* **2010**, *43*, 837.
(59) Dutta, P. K.; Tripathi, S.; Mehrotra, G. K.; Dutta, J. *Food Chem.* **2009**, *114*, 1173.
(60) No, H. K.; Meyers, S. P.; Prinyawiwatkul, W.; Xu, Z. *J. Food Sci.* **2007**, *72*, R87.
(61) Srinivasa, P. C.; Tharanathan, R. N. *Food Rev. Int.* **2007**, *23*, 53.
(62) Miretzky, P.; Fernandez, C. A. *J. Hazard. Mater.* **2009**, *167*, 10.
(63) Elwakeel, K. Z. *J. Dispersion Sci. Technol.* **2010**, *31*, 273.
(64) Miretzky, P.; Fernandez, C. A. *J. Fluorine Chem.* **2011**, *132*, 231.
(65) Gerente, C.; Lee, V. K. C.; Le Cloirec, P.; McKay, G. *Crit. Rev. Environ. Sci. Technol.* **2007**, *37*, 41.
(66) Guibal, E.; Van Vooren, M.; Dempsey, B. A.; Roussy, J. *Sep. Sci. Technol.* **2006**, *41*, 2487.
(67) Wan Ngah, W. S.; Teong, L. C.; Hanafiah, M. A. K. M. *Carbohydr. Polym.* **2011**, *83*, 1446.
(68) Enescu, D. *Rom. Biotechnol. Lett.* **2008**, *13*, 4037.
(69) Lim, S. H.; Hudson, S. M. *J. Macromol. Sci. Polym. Rev.* **2003**, *C43*, 223.
(70) Lertsutthiwong, P.; Nazhad, M. M.; Chandrkrachang, S.; Stevens, W. F. *Appita J.* **2004**, *57*, 274.
(71) Yi, H. M.; Wu, L. Q; Bentley, W. E.; Ghodssi, R.; Rubloff, G. W.; Culver, J. N.; Payne, G. F. *Biomacromolecules* **2005**, *6*, 2881.
(72) Chambers, J. P.; Arulanandam, B. P.; Matta, L. L.; Weis, W.; Valdes, J. J. *Curr. Issues Mol. Biol.* **2008**, *10*, 1.
(73) Zourob, M. *Recognition receptors in biosensors*; Springer: New York, 2010.
(74) In *Chitosan-based hydrogels: Functions and applications*; Yao, K., Li, J., Yao, F., Yin, Y., Eds.; CRC Press, Taylor & Francis Group: Boca Raton, FL, 2011.
(75) Yoo, E. H.; Lee, S. Y. *Sensors* **2010**, *10*, 4558.
(76) Oliver, N. S; Toumazou, C.; Cass, A. E; Johnston, D. G. *Diabetes Med.* **2009**, *26*, 197.
(77) Heller, A.; Feldman, B. *Chem. Rev.* **2008**, *108*, 2482.
(78) Wang, J. *Chem. Rev.* **2008**, *108*, 814.
(79) Wang, J. *Electroanalysis* **2001**, *13*, 983.
(80) Koschinsky, T.; Heinemann, L. *Diabetes/Metab. Res. Rev.* **2001**, *17*, 113.
(81) Dzyadevych, S. V.; Arkhypova, V. N.; Soldatkin, A. P.; Elskaya, A. V; Martelet, C.; Jaffrezic-Renault, N. *Ing. Res. Bioméd.* **2008**, *29*, 171.
(82) Zayats, M.; Willner, B.; Willner, I. *Electroanalysis* **2008**, *20*, 583.
(83) Mueller, A. *Mini. Rev. Med. Chem.* **2005**, *5*, 231.
(84) Yuqing, M.; Jianrong, C.; Xiaohua, W. *Trends Biotechnol.* **2004**, *22*, 227.
(85) Schuhmann, W. *J. Biotechnol.* **2002**, *82*, 425.
(86) Borgmann, S.; Schulte, A.; Neugebauer, S.; Schuhmann, W. Amperometric Biosensors. In *Advances in Electrochemical Science and Engineering*; Lipkowski, J., Alkire, R., Kolb, M. D., Eds., Wiley-VCH: Weinheim, Germany, 2012; Vol. *13* (Frontiers in Bioelectrochemistry), p 1.
(87) Mulchandani, A.; Rogers, K. *Enzyme and Microbial Biosensors: Techniques and Protocols*; Humana Press Inc.: Totowa, New Jersey, 2010.
(88) Borgmann, S.; Hartwich, G.; Schulte, A.; Schuhmann, W. Amperometric enzyme sensors based on direct and mediated electron transfer. In *Perspectives in Bioanalysis*; Palecek, E., Scheller, F., Wang, J., Eds.; Elsevier: Amsterdam, 2005; Vol. *1* (Electrochemistry of nucleic acids and proteins. Towards electrochemical sensors for genomics and proteomics), p 599.
(89) Heller, A. Redox-hydrogel based electrochemical biosensors. In *Biosensors*, 2nd ed.; Cooper, J., Cass, T., Eds.; Oxford University Press: Oxford, U.K., 2004.
(90) Hvastkovs, E. G.; Buttry, D. A. *Analyst* **2010**, *135*, 1817.
(91) Tosar, J. P.; Brañas, G.; Laíz, J. *Biosens. Bioelectron.* **2010**, *26*, 1205.
(92) Batchelor-McAuley, C.; Wildgoose, G. G.; Compton, R. G. *Biosens. Bioelectron.* **2009**, *24*, 3183.
(93) Peng, H.; Zhang, L.; Soeller, C.; Travas-Sejdic, J. *Biomaterials* **2009**, *30*, 2132.

(94) Lucarelli, F.; Tombelli, S.; Minunni, M.; Marrazza, G.; Mascini, M. *Anal. Chim. Acta* **2008**, *609*, 139.
(95) Odenthal, K. J.; Gooding, J. J. *Analyst* **2007**, *132*, 603.
(96) Ju, H.; Zhao, H. *Front. Biosci.* **2005**, *10*, 37.
(97) Lucarelli, F.; Marrazza, G.; Turner, A. P.; Mascini, M. *Biosens. Bioelectron.* **2004**, *19*, 515.
(98) Drummond, T. G.; Hill, M. G.; Barton, J. K. *Nat. Biotechnol.* **2003**, *21*, 1192.
(99) Kierny, M. R.; Cunningham, T. D.; Kay, B. K. *Nano Rev.* **2012**, *3*, 17240.
(100) Ricci, F.; Adornetto, G.; Palleschi, G. *Electrochim. Acta* **2012**, *84*, 74.
(101) Holford, T. R. J.; Davis, F.; Higson, F. P. J. *Biosens. Bioelectron.* **2012**, *34*, 12.
(102) Cosnier, S.; Holzinger, M. *Chem. Soc. Rev.* **2011**, *40*, 2146.
(103) Prodromidis, M. I. *Electrochim. Acta* **2010**, *55*, 4227.
(104) Centi, S.; Laschi, S.; Mascini, M. *Bioanalysis* **2009**, *1*, 1271.
(105) Liu, G.; Lin, Y. *Talanta* **2007**, *74*, 308.
(106) Warsinke, A.; Benkert, A.; Scheller, F. W. *Fresenius J. Anal. Chem.* **2000**, *366*, 622.
(107) Ghindilis, A. L.; Atanasov, P.; Wilkins, M.; Wilkins, E. *Biosens. Bioelectron.* **1998**, *13*, 113.
(108) Skladal, P. *Electroanalysis* **1997**, *9*, 737.
(109) Zhao, Y.; Park, R. D.; Muzzarelli, R. A. A. *Mar. Drugs* **2010**, *8*, 24.
(110) Eijsink, V.; Hoell, I.; Vaaje-Kolstada, G. *Biotechnol. Genet. Eng. Rev.* **2010**, *27*, 331.
(111) Tsigos, I.; Martinou, A.; Kafetzopoulos, D.; Bouriotis, V. *Trends Biotechnol.* **2000**, *18*, 305.
(112) Zeng, J. B.; He, Y. S.; Li, S. L.; Wang, Y. Z. *Biomacromolecules* **2012**, *13*, 1.
(113) Muzzarelli, C.; Tosi, G.; Francescangeli, O.; Muzzarelli, R. A. A. *Carbohydr. Res.* **2003**, *338*, 2247.
(114) Jayakumar, R.; Prabaharan, M.; Sudheesh Kumar, P. T.; Nair, S. V.; Tamura, H. *Biotechnol. Adv.* **2011**, *29*, 322.
(115) Baldrick, P. *Regul. Toxicol. Pharmacol.* **2010**, *56*, 290.
(116) Shi, C.; Zhu, Y.; Ran, X.; Wang, M.; Su, Y.; Cheng, T. *J. Surg. Res.* **2006**, *133*, 185.
(117) Kim, I. Y.; Seo, S. J.; Moon, H. S.; Yoo, M. K.; Park, I. Y.; Kim, B. C.; Cho, C. S. *Biotechnol. Adv.* **2008**, *26*, 1.
(118) Dang, J. M.; Leong, K. W. *Adv. Drug Delivery Rev.* **2006**, *58*, 487.
(119) Di Martino, A.; Sittinger, M.; Risbud, M. V. *Biomaterials* **2005**, *26*, 5983.
(120) Suh, J. K.; Matthew, H. W. *Biomaterials* **2000**, *21*, 2589.
(121) Venkatesan, J.; Kim, S. K. *Mar. Drugs* **2010**, *8*, 2252.
(122) Swetha, M.; Sahithi, K.; Moorthi, A.; Srinivasan, N.; Ramasamy, K.; Selvamurugan, N. *Int. J. Biol. Macromol.* **2010**, *47*, 1.
(123) Hamman, J. H. *Mar. Drugs* **2010**, *8*, 1305.
(124) Muzzarelli, R. A. A. *Mar. Drugs* **2010**, *8*, 292.
(125) Patel, M. P.; Patel, R. R.; Patel, J. K. *J. Pharm. Pharm. Sci.* **2010**, *13*, 536.
(126) Morris, G.; Kök, S.; Harding, S.; Adams, G.. *Biotechnol. Genet. Eng. Rev.* **2010**, *27*, 257.
(127) Amidi, M.; Mastrobattista, E.; Jiskoot, W.; Hennink, W. E. *Adv. Drug Delivery Rev.* **2010**, *62*, 59.
(128) Paños, I.; Acosta, N.; Heras, A. *Curr. Drug Discovery Technol.* **2008**, *5*, 333.
(129) Arca, H. C.; Günbeyaz, M.; Senel, S. *Expert Rev. Vaccines* **2009**, *8*, 937.
(130) Kang, M. L; Cho, C. S.; Yoo, H. S. *Biotechnol. Adv.* **2009**, *27*, 857.
(131) van der Lubben, I. M.; Verhoef, J. C.; Borchard, G.; Junginger, H. E. *Eur. J. Pharm. Sci.* **2001**, *14*, 201.
(132) Garcia, A.; Peniche-Covas, C.; Chico, B.; Simpson, B. K.; Villalonga, R. *Macromol. Biosci.* **2007**, *7*, 435.
(133) Mourya, V. K.; Inamdar, N. N. *React. Funct. Polym.* **2008**, *68*, 1013.
(134) Aranaz, I.; Harris, R.; Heras, A. *Curr. Org. Chem.* **2010**, *14*, 308.
(135) Jayakumar, R.; Reis, R. L.; Mano, J. F. *e-Polym.* **2006**, 035.
(136) II'ina, A. V.; Varlamov, V. P. *Appl. Biochem. Microbiol.* **2005**, *41*, 5.
(137) Bernkop-Schnürch, A.; Hornof, M.; Guggi, D. *Eur. J. Pharm. Biopharm.* **2004**, *57*, 9.
(138) Mourya, V. K.; Inamdar, N. N. *J. Mater. Sci. Mater. Med.* **2009**, *20*, 1057.
(139) d'Ayala, G. G.; Malinconico, M.; Laurienzo, P. *Molecules* **2008**, *13*, 2069.
(140) Jayakumar, R.; New, N.; Tokura, S.; Tamura, H. *Int. J. Biol. Macromol.* **2007**, *40*, 175.
(141) Kador, K. E.; Subramanian, A. *Int. J. Carbohydr. Chem.* **2011**, *2011*, 146419.
(142) Zhang, Y.; Thomas, Y.; Kim, E.; Payne, G. P. *J. Phys. Chem B* **2012**, *116*, 1579.
(143) Wu, F. C.; Tseng, R. L.; Juang, R. S. *J. Environ. Manage.* **2010**, *91*, 798.
(144) Bhatnagar, A.; Sillanpää, M. *Adv. Colloid Interface Sci.* **2009**, *152*, 26.
(145) Mack, C.; Wilhelmi, B.; Duncan, J. R.; Burgess, J. E. *Biotechnol. Adv.* **2007**, *25*, 264.
(146) Miretzky, P.; Cirelli, A. F. *J. Hazard. Mater.* **2009**, *167*, 10.
(147) Onsøyen, E.; Skaugrud, O. *J. Chem. Technol. Biotechnol.* **1990**, *49*, 395.
(148) Srinivasan, A.; Viraraghavan, T. *J. Environ. Manage.* **2010**, *91*, 1915.
(149) Crini, G. *Bioresour. Technol.* **2006**, *97*, 1061.
(150) Wu, L. Q.; Gadre, A. P.; Yi, H.; Kastantin, M. J.; Rubloff, G. W.; Bentley, W. E.; Payne, G. F.; Ghodssi, R . *Langmuir* **2002**, *18*, 8620.
(151) Streitberger, H. J.; Dössel, K.-F. Electrodeposition Coatings. In *Automotive Paints and Coatings*, 2nd ed.; Streitberger, H.-J., Dössel, K.-F., Eds.; Wiley-VCH Verlag GmbH & Co. KGaA: Weinheim, Germany, 2008; pp 89−128. doi: 10.1002/9783527622375.ch4.
(152) Krylova, I. *Prog. Org. Coat.* **2001**, *42*, 119.
(153) Lovell, G. *Prod. Fin.* **1990**, *April*, 58.
(154) Beck, F. *Electrochim. Acta* **1988**, *33*, 839.
(155) Brewer, G. E. F. Electrodeposition of Paint. In *Applied Polymer Science*; Poehlein, G. W., Ed.; ACS Symposium Series 285; American Chemical Society: Washington, DC, 1985; Chapter 34, pp 827−838.
(156) Schulte, A. Ph.D. Thesis; Westfaelische Wilhelms-Universitaet (WWU) Muenster, Muenster, Germany, 1993.
(157) Schulte, A. *Proc. SPIE* **1998**, *3512*, 353.
(158) Schulte, A.; Chow, R. H. *Anal. Chem.* **1996**, *68*, 3054.
(159) Schulte, A.; Chow, R. H. *Anal. Chem.* **1998**, *70*, 985.
(160) Kurzawa, C.; Hengstenberg, A.; Schuhmann, W. *Anal. Chem.* **2002**, *74*, 355.
(161) Wu, L. Q.; Yi, H.; Li, S.; Rubloff, G. W.; Bentley, W. E.; Ghodssi, R.; Payne, G. F. *Langmuir* **2003**, *19*, 519.
(162) Buckhout-White, S. L.; Rubloff, G. W. *Soft Matter* **2009**, *5*, 3677.
(163) Kim, E.; Liu, Y.; Shi, X. W.; Yang, X.; Bentley, W. E.; Payne, G. F. *Adv. Funct. Mater.* **2010**, *20*, 2683.
(164) Wu, L. Q.; Bentley, W. E.; Payne, G. F. *Int. J. Artif. Organs* **2011**, *34*, 215.
(165) Koev, S. T.; Dykstra, P. H.; Luo, X.; Rubloff, G. W.; Bentley, W. E.; Payne, G. F.; Ghodssi, R. *Lab Chip* **2010**, *10*, 3026.
(166) Liu, Y.; Kim, E.; Ghodssi, R.; Rubloff, G. W.; Culver, J. N.; Bentley, W. E.; Payne, G. F. *Biofabrication* **2010**, *2*, 022002.
(167) Chen, P. C.; Chen, R. L. C.; Cheng, T. J.; Wittstock, G. *Electroanalysis* **2009**, *21*, 804.
(168) Gray, K. M.; Liba, B. D.; Wang, Y.; Cheng, Y.; Rubloff, G. W.; Bentley, W. E.; Montembault, A.; Royaud, I.; David, L.; Payne, G. F. *Biomacromolecules* **2012**, *13*, 1181.
(169) Sugawara, K.; Fukushi, H.; Hoshi, S.; Akatsuka, K. *Anal. Sci.* **2000**, *16*, 1139.
(170) Ohashi, E.; Karube, I. *J. Biotechnol.* **1995**, *40*, 13.
(171) Ohashi, E.; Koriyama, T. *Anal. Chim. Acta* **1992**, *262*, 19.

(172) Sugawara, K.; Yugami, A.; Terui, N.; Kuramitz, H. *Anal. Sci.* **2009**, *25*, 1365.
(173) Sugawara, K.; Takano, T.; Fukushi, H.; Hoshi, S.; Akatsuka, K.; Kuramitz, H.; Tanaka, S. *J. Electroanal. Chem.* **2000**, *482*, 81.
(174) Brondani, D.; Dupont, J.; Spinelli, A.; Cruz Vieira, I. *Sens. Actuators, B* **2009**, *1*, 236.
(175) Brondani, D.; Zapp, E.; Vieira, I. C.; Dupont, J.; Scheeren, C. W. *Analyst* **2011**, *136*, 2495.
(176) Hsieh, B. C.; Matsumoto, K.; Cheng, T. J.; Yuu, G.; Chen, R. L. C. *J. Pharm. Biomed. Anal.* **2007**, *45*, 673.
(177) Sugawara, K.; Hirabayashi, G.; Kamiya, N.; Kuramitz, H.; Tanaka, S. *Electroanalysis* **2005**, *17*, 1659.
(178) Kittle, J. D.; Wang, C.; Qian, C.; Zang, Y. F.; Zang, M. Q.; Roman, M.; Morris, J. R.; Moore, R. B.; Esker, A. R. *Biomacromolecules* **2012**, *13*, 714.
(179) Sugawara, K.; Kuramitz, H.; Hoshi, S.; Akatsuka, K.; Tanaka, S. *Anal. Sci.* **2002**, *18*, 195.
(180) Ramaprasad, A. T.; Rao, V. *Sens. Actuators, B* **2010**, *148*, 117.
(181) Bilitewski, U. *Methods Mol. Biol.* **2009**, *509*, 1.
(182) Sassolas, A.; Leca-Bouvier, B. D.; Blum, L. J. *Chem. Rev.* **2008**, *108*, 109.
(183) Bier, F. F.; von Nickisch-Rosenegk, M.; Ehrentreich-Förster, E.; Reiss, E.; Henkel, J.; Strehlow, R.; Andresen, D. *Adv. Biochem. Eng. Biotechnol.* **2008**, *109*, 433.
(184) Stoughton, R. B. *Annu. Rev. Biochem.* **2005**, *74*, 53.
(185) Chittur, S. V. *Comb. Chem. High Throughput Screening* **2004**, *7*, 531.
(186) Vercoutere, W.; Akeson, M. *Curr. Opin. Chem. Biol.* **2002**, *6*, 816.
(187) Pirrung, M. C. *Angew. Chem., Int. Ed. Engl.* **2002**, *41*, 1276.
(188) Wang, J. *Nucleic Acids Res.* **2000**, *28*, 3011.
(189) Gabig, M.; Wegrzyn, G. *Acta Biochim. Pol.* **2001**, *48*, 615.
(190) Cuzin, M. *Transfus. Clin. Biol.* **2001**, *8*, 291.
(191) Consolandi, C.; Severgnini, M.; Castiglioni, B.; Bordoni, R.; Frosini, A.; Battaglia, C.; Bernardi, L. R.; De Bellis, G. *Bioconjugate Chem.* **2006**, *17*, 371.
(192) Wang, Q.; Zhang, B.; Lin, X.; Weng, W. *Sens. Actuators, B* **2011**, *156*, 599.
(193) Qian, P.; Ai, S.; Yin, H.; Li, J. *Microchim. Acta* **2010**, *168*, 347.
(194) Taufik, S.; Yusof, N. A.; Tee, W. T.; Ramli, I. *Int. J. Electrochem. Sci.* **2011**, *6*, 1880.
(195) Siddiquee, S.; Yusof, N. A.; Salleh, A. B.; Tan, S. G.; Abu Bakar, F. *Curr. Anal. Chem.* **2011**, *7*, 296.
(196) Bo, Y.; Wang, W.; Qi, J.; Huang, S. *Analyst* **2011**, *136*, 1946.
(197) Tran, L. D.; Nguyen, B. H.; Hieu, N. V.; Tran, H. V.; Nguyen, H. L.; Nguyen, X. P. *Mater. Sci. Eng., C* **2011**, *31*, 477.
(198) Singh, R.; Sumana, G.; Verma, R.; Sood, S.; Sood, K. N.; Gupta, R. K.; Malhotra, B. D. *Thin Solid Films* **2010**, *519*, 1135.
(199) Cao, W.; Easley, C. J.; Ferrance, J. P.; Landers, J. P. *Anal. Chem.* **2006**, *78*, 7222.
(200) Galandova, J.; Ziyatdinova, G.; Libuda, J. *Anal. Sci.* **2008**, *24*, 711.
(201) Galandova, J.; Trnkova, L.; Mikelova, R.; Libuda, J. *Electroanalysis* **2009**, *21*, 563.
(202) Li, J.; Liu, Q.; Liu, Y.; Liu, S.; Yao, S. *Anal. Biochem.* **2005**, *346*, 107.
(203) Arias, P.; Ferreyra, N. F.; Riva, G. A.; Bollo, S. *J. Electroanal. Chem.* **2009**, *634*, 123.
(204) Ribeiro Teles, F. R.; França dos Prazeres, D. M.; de Lima-Filho, J. L. *Sensors* **2007**, *7*, 2510.
(205) Yang, Y.; Wang, Z.; Yang, M.; Li, J.; Zheng, F.; Shen, G.; Yu, R. *Anal. Chim. Acta* **2007**, *584*, 268.
(206) Kerman, K.; Saito, M.; Tamiya, E. *Anal. Bioanal. Chem.* **2008**, *391*, 2759.
(207) Lin, S.; Lee, A. S.-Y.; Lin, C.-C.; Lee, C.-K. *Curr. Proteomics* **2006**, *3*, 271.
(208) Dijksma, M.; Kamp, B.; Hoogvliet, J. C.; van Bennekom, W. P. *Anal. Chem.* **2001**, *73*, 901.
(209) Truong, P. L.; Cao, C.; Park, S.; Kim, M.; Sim, S. J. *Lab Chip* **2011**, *11*, 2591.
(210) Munge, B. S.; Coffey, A. L.; Doucette, J. M.; Somba, B. K.; Malhotra, R.; Patel, V.; Gutkind, J. S.; Rusling, J. F. *Angew. Chem., Int. Ed. Engl.* **2011**, *50*, 7915.
(211) Loyprasert, S.; Hedstrom, M.; Thavarungkul, P.; Kanatharana, P.; Mattiasson, B. *Biosens. Bioelectron.* **2010**, *25*, 1977.
(212) Luang, Q. F.; Xue, Y.; Yao, X. *Sens. Actuators, B* **2010**, *147*, 561.
(213) Hu, J.; Zheng, P. C.; Jiang, J. H.; Shen, G. L.; Yu, R. Q.; Liu, G. K. *Analyst* **2010**, *135*, 1084.
(214) Zanoli, L. M.; D'Agata, R.; Spoto, G. *Anal. Bioanal. Chem.* **2012**, *402*, 1759.
(215) Yang, H. *Curr. Opin. Chem. Biol.* **2012**, *16*, 422.
(216) Sotiropoulou, S.; Fournier, D.; Chaniotakis, N. A. *Biosens. Bioelectron.* **2005**, *20*, 2347.
(217) Luppa, P. B.; Sokoll, L. J.; Chan, D. W. *Clin. Chim. Acta* **2001**, *314*, 1.
(218) Ricci, F.; Volpe, G.; Micheli, L.; Palleschi, G. *Anal. Chim. Acta* **2007**, *605*, 111.
(219) Xu, Z. X.; Gao, H. J.; Zhang, L. M.; Chen, X. Q.; Qiao, X. G. *J. Food Sci.* **2011**, *76*, R69.
(220) Jiang, X.; Li, D.; Xu, X.; Ying, Y.; Li, Y.; Ye, Z.; Wang, J. *Biosens. Bioelectron.* **2008**, *23*, 1577.
(221) Kurosawa, S.; Park, J. W.; Aizawa, H.; Wakida, S.; Tao, H.; Ishihara, K. *Biosens. Bioelectron.* **2006**, *22*, 473.
(222) Gonzalez-Martinez, M. A.; Puchades, R.; Maquieira, A. *Anal. Bioanal. Chem.* **2007**, *387*, 205.
(223) Shriver-Lake, L. C.; Charles, P. T.; Kusterbeck, A. W. *Anal. Bioanal. Chem.* **2003**, *377*, 550.
(224) Thiruppathiraja, C.; Saroja, V.; Kamatchiammal, S.; Adaikkappan, P.; Alagar, M. *J. Environ. Monit.* **2011**, *13*, 2782.
(225) Yan, W.; Chen, X.; Li, X.; Feng, X.; Zhu, J.-J. *J. Phys. Chem. B* **2008**, *112*, 1275.
(226) Feng, B.; Huang, S.; Ge, F.; Luo, Y.; Jia, D.; Dai, Y. *Biosens. Bioelectron.* **2011**, *28*, 91.
(227) Yan, W.; Chen, X.; Li, X.; Feng, X.; Zhu, J.-J. *J. Phys. Chem. B* **2012**, DOI: 10.1007/s10544012-9732-x.
(228) Vetil, J. V.; Ye, K. *Biotechnol. Prog.* **2007**, *23*, 517.
(229) Rusling, J. F.; Sotzing, G.; Papadimitrakopoulosa, F. *Bioelectrochemistry* **2009**, *76*, 189.
(230) Chikkaveeraiah, B. V.; Bhirde, A. A.; Morgan, N. Y.; Eden, H. S.; Chen, X. *ACS Nano* **2012**, *6*, 6546.
(231) Rusling, F. *Chem. Rec.* **2012**, *12*, 164.
(232) Liu, Y.; Yuan, R.; Chai, Y.; Hong, C.; Guan, S. *Bioprocess Biosyst. Eng.* **2010**, *33*, 613.
(233) Lin, J.; He, C.; Zhang, L.; Zhang, S. *Anal. Biochem.* **2009**, *384*, 130.
(234) Wang, G. L.; Xu, J. J.; Chen, H. Y.; Fu, S. Z. *Biosens. Bioelectron.* **2009**, *25*, 791.
(235) Ling, S.; Yuan, R.; Chai, Y.; Zhang, T. *Bioprocess Biosyst. Eng.* **2009**, *32*, 407.
(236) Huang, K. J.; Niu, D. J.; Xie, W. Z.; Wang, W. *Anal. Chim. Acta* **2010**, *659*, 102.
(237) He, X.; Yuan, R.; Chai, Y.; Shi, Y. *J. Biochem. Biophys. Methods* **2008**, *70*, 823.
(238) Gao, X.; Zhang, Y.; Wu, Q.; Chen, H.; Chen, Z.; Lin, X. *Talanta* **2011**, *85*, 1980.
(239) Han, J.; Zhuo, Y.; Chai, Y. Q.; Mao, L.; Yuan, Y. L.; Yuan, R. *Talanta* **2011**, *85*, 130.
(240) Chai, Y. Q.; Liu, Y. X.; Yuan, R.; Hong, C. L.; Liu, K. G.; Guan, S. *Microchim. Acta* **2009**, *167*, 217.
(241) Shi, W.; Ma, Z. *Biosens. Bioelectron.* **2011**, *26*, 3068.
(242) Lin, J.; Qu, W.; Zhang, S. *Anal. Sci.* **2007**, *23*, 1059.
(243) Zhang, S. S.; Jie, G. F.; Liu, P.; Wang, L. *Electrochem. Commun.* **2010**, *12*, 22.
(244) Huang, K. J.; Sun, J. Y.; Xu, C. X.; Niu, D. J.; Xie, W. Z. *Microchim. Acta* **2010**, *168*, 51.
(245) Tang, J.; Hu, R.; Wu, Z. S.; Shen, G. L.; Yu, R. Q. *Talanta* **2011**, *85*, 117.

(246) Yang, H.; Yuan, R.; Chai, Y.; Zhuo, Y. *Colloids Surf., B* **2011**, *82*, 463.
(247) Yang, G.; Chang, Y.; Yang, H.; Tan, L.; Wu, Z.; Lu, X.; Yang, Y. *Anal. Chim. Acta* **2009**, *644*, 72.
(248) Khan, R.; Dhayal, M. *Biosens. Bioelectron.* **2009**, *24*, 1700.
(249) Kaushik, A.; Solanki, P. R.; Sood, K. N.; Ahmad, S.; Malhotra, B. D. *Electrochem. Commun.* **2009**, *11*, 1919.
(250) Kaushik, A.; Solanki, P. R.; Ansari, A. A.; Ahmad, S.; Malhotra, B. D. *Electrochem. Commun.* **2008**, *10*, 1364.
(251) Dhayal, M.; Khan, R. *Electrochem. Commun.* **2008**, *10*, 492.
(252) Kaushik, A.; Solanki, P. R.; Pandey, M. K.; Kaneto, K.; Ahmad, S.; Malhotra, B. D. *Thin Solid Films* **2010**, *519*, 1160.
(253) Qiu, J. D.; Liang, R. P.; Wang, R.; Fan, L.; Chen, Y. W.; Xia, X. H. *Biosens. Bioelectron.* **2009**, *25*, 852.
(254) Liang, R.; Peng, H.; Qiu, J. J. *Colloid Interface Sci* **2008**, *320*, 125.
(255) Wang, S. F.; Tan, Y. M.. *Anal. Bioanal. Chem.* **2007**, *387*, 703.
(256) Shen, G.; Cai, C.; Yang, J. *Electrochim. Acta* **2011**, *56*, 8272.
(257) Zhao, G.; Zhan, X.; Dou, W. *Anal. Biochem.* **2011**, *408*, 53.
(258) Cavalcanti, I. T.; Silva, B. V. M; Peres, N. G.; Sotomayor, M. D. P. T.; Guedes, M. I. F.; Dutra, R. F. *Talanta* **2012**, *91*, 41.
(259) De Lima, F.; Lucca, B. G.; Barbosa, A. M. J.; Ferreira, V. S.; Moccelini, S. K.; Franzoni, A. C.; Vieira, V. S. *Enzyme Microbial Technol.* **2010**, *47*, 153.
(260) Pauliukaite, R.; Ghica, M. E.; Fatibello-Filho, O.; Brett, C. M. A. *Electrochim. Acta* **2010**, *55*, 6239.
(261) Fernanes, S. C.; de Oliveira, I. R. W. Z.; Fatibello-Filho, O.; Spinelli, A.; Cruz Vieira, I. *Sens. Actuators, B* **2008**, *133*, 202.
(262) Nagarale, R. K.; Lee, J. M.; Shin, W. *Electrochim. Acta* **2009**, *54*, 6508.
(263) Parra-Alfambra, A. M.; Casero, E.; Ruiz, M. A.; Vázquez, L.; Pariente, F.; Lorenzo, E. *Anal. Bioanal. Chem.* **2011**, *401*, 883.
(264) Cui, X.; Li, C. M.; Zang, J.; Yu, S. *Biosens. Bioelectron.* **2007**, *22*, 3288.
(265) Quan, D.; Shin, W. *Sensors* **2010**, *10*, 6241.
(266) Wu, L. Q.; Lee, K.; Wang, X.; English, D. S.; Losert, W.; Payne, G. F. *Langmuir* **2007**, *23*, 286.
(267) Luo, X. L.; Xu, J. J.; Du, Y.; Chen, H. Y. *Anal. Biochem.* **2004**, *334*, 284.
(268) Luo, X. L.; Xu, J. J.; Wang, J. L.; Chen, H. Y. *Chem. Commun.* **2005**, *16*, 2169.
(269) Zhou, Q.; Xie, Q.; Fu, Y.; Su, Z.; Jia, X.; Yao, S. *J. Phys. Chem. B* **2007**, *111*, 11276.
(270) Xi, F.; Liu, L.; Wu, Q.; Lin, X. *Biosens. Bioelectron.* **2008**, *24*, 29.
(271) Li, F.; Wang, Z.; Chen, W.; Zhang, S. *Biosens. Bioelectron.* **2009**, *24*, 3030.
(272) Xi, F.; Liu, L.; Chen, Z.; Lin, X. *Talanta* **2009**, *8*, 1077.
(273) Zeng, X.; Li, X.; Xing, L.; Liu, X.; Luo, S.; Wei, W.; Kong, B.; Li, Y. *Biosens. Bioelectron* **2009**, *24*, 2898.
(274) Guo, M.; Fang, H.; Wang, R.; Yang, Z.; Xu, X. *J. Mater. Sci.: Mater. Med.* **2011**, *22*, 1985.
(275) Wang, Y.; Wei, W.; Zeng, J.; Liu, X.; Zeng, X. *Microchim. Acta* **2008**, *160*, 253.
(276) Meyer, L. W.; Liu, Y.; Shi, X. W.; Yang, X.; Bentley, W. E.; Payne, G. F. *Biomacromolecules* **2009**, *10*, 858.
(277) Chawla, S.; Rawal, R.; Pundir, C. S. *J. Biotechnol.* **2011**, *156*, 39.
(278) Vazquez-Duhalt, R.; Tinoco, R.; D'Antonio, P.; Topoleski, L. D. T.; Payne, G. F. *Bioconjugate Chem.* **2001**, *12*, 301.
(279) Tan, Y.; Deng, W.; Chen, C.; Xie, Q.; Lei, L.; Li, Y.; Fang, Z.; Ma, M.; Chen, J.; Yao, S. *Biosens. Bioelectron.* **2010**, *25*, 2644.
(280) Zhang, Y.; Ji, C. *Anal. Chem.* **2010**, *82*, 5275.
(281) Wu, Y. H.; Wollenberger, U.; Hofrichter, M.; Ullrich, R.; Scheibner, K.; Scheller, F. W. *Sens. Actuators, B* **2012**, *160*, 1419.
(282) Njagi, J.; Chernov, M. M.; Leiter, J. C.; Andreescu, S. *Anal. Chem.* **2010**, *82*, 989.
(283) Wang, X.; Zhang, Y.; Cheng, C.; Dong, R.; Hao, J. *Analyst* **2011**, *136*, 1753.
(284) Marcolino, L. H.; Luiz, H.; Janegitz, B. C.; Lourencao, B. C.; Fatibello, O. *Anal. Lett.* **2007**, *40*, 3119.
(285) Janegitz, B. C.; Marcolino, L. H.; Fatibello, O. *Quim. Nova* **2007**, *30*, 1673.
(286) Xie, Z. M.; Fei, J. J.; Huang, M. H. *Austral. J. Chem.* **2008**, *61*, 1000.
(287) Deng, W.; Tan, Y.; Li, Y.; Wen, Y.; Su, Z.; Huang, Z.; Huang, S.; Meng, Y.; Xie, Q.; Luo, Y.; Yao, S. *Microchim. Acta* **2010**, *169*, 367.
(288) Janegitz, B. C.; Marcolino, L. H.; Campana, S. P.; Faria, R. C.; Fatibello, O. *Sens. Actuators, B* **2009**, *142*, 260.
(289) Khaled, E.; Hassan, H. N. A.; Habib, I. H. I.; Metelka, R. *Int. J. Electrochem. Sci.* **2010**, *5*, 158.
(290) Guo, D. Y.; Zheng, D.; Mo, G. Q.; Ye, J. S. *Electroanalysis* **2009**, *21*, 762.
(291) Babaei, A.; Babazadeh, M. *Electroanalysis* **2011**, *23*, 417.
(292) Babaei, A.; Babazadeh, M. *Electroanalysis* **2011**, *23*, 1726.
(293) Gong, J.; Zhang, W.; Liu, T.; Zhang, L. *Nanoscale* **2011**, *3*, 3123.
(294) Yazhen, W. *Bioelectrochemistry* **2011**, *81*, 86.
(295) Ghalkhani, M.; Shahrokhian, S. *Electrochem. Commun.* **2010**, *12*, 66.
(296) Zeng, Y.; Zhu, Z. H.; Wang, R. X.; Lu, G. H. *Electrochim. Acta* **2005**, *51*, 649.
(297) Berger, J.; Reist, M.; Mayer, J. M.; Felt, O.; Peppas, N. A.; Gurny, R. *Euro. J. Pharm. Biopharm.* **2004**, *57*, 19.
(298) Liu, Y.; Zhang, B.; Gray, K. M.; Cheng, Y.; Kim, E.; Rubloff, G. W.; Bentley, W. E.; Wang, Q.; Payne, G. F. *Soft Matter* **2013**, *9*, 2703.
(299) Guschin, D. A.; Castillo, J.; Dimcheva, N.; Schuhmann, W. *Anal. Bioanal. Chem.* **2010**, *398*, 1661.
(300) Guschin, D. A.; Shkil, H.; Schuhmann, W. *Anal. Bioanal. Chem.* **2009**, *395*, 1693.
(301) Ngounou, B.; Aliyev, E. H.; Guschin, D. A.; Sultanov, Y. M.; Efendiev, A. A.; Schuhmann, W. *Bioelectrochemistry* **2007**, *71*, 81.
(302) Guschin, D. A.; Sultanov, Y. M.; Efendiev, A. A.; Sharif-Zade, N. F.; Aliyev, E. H.; Schuhmann, W. *Electrochim. Acta* **2006**, *51*, 5137.